Synthesis method and characterization of doped NASICON based phosphate (LATP) solid electrolyte

By

Hassaan Bin Shahid

Reg. No.: 00000327451

Session 2020-22

Supervised by

Dr. Ghulam Ali

U.S.-Pakistan Center for Advanced Studies in Energy (USPCAS-E)

National University of Sciences and Technology (NUST)

H-12, Islamabad 44000, Pakistan

March 2023

Synthesis method and characterization of doped NASICON based phosphate (LATP) solid electrolyte

By

Hassaan Bin Shahid

Reg. No.: 00000327451

Session 2020-22

Supervised by

Dr. Ghulam Ali

A Thesis Submitted to U.S.-Pakistan Center for Advanced Studies in Energy in partial fulfillment of the requirement for the degree of

MASTERS of SCIENCE in
ENERGY SYSTEMS ENGINEERING

U.S.-Pakistan Center for Advanced Studies in Energy (USPCAS-E)

National University of Sciences and Technology (NUST)

H-12, Islamabad 44000, Pakistan

March 2023

THESIS ACCEPTANCE CERTIFICATE

Certified that the final copy of MS/MPhil thesis written by Mr. **Hassaan Bin Shahid** (Registration No. 00000327451) of U.S.-Pakistan Center for Advanced Studies in Energy has been vetted by undersigned, found complete in all respects as per NUST Statues/Regulations, is within similarity indices limit and accepted as partial fulfillment for award of MS/MPhil degree. It is further certified that necessary amendments, as GEC members of the scholar pointed out, have also been incorporated in the thesis.

Signature: _____

Name of Supervisor: Dr. Ghulam Ali_____

Date: _____

Signature (HoD): _____

Date: _____

Signature (Dean/Principle): _____

Date: _____

Certificate

This is to certify that the work in this thesis has been carried out by **Mr. Hassaan Bin Shahid** and completed under my supervision in Advance energy materials and systems lab, U.S.-Pakistan Center for Advanced Studies in Energy (USPCAS-E), National University of Sciences and Technology, H-12, Islamabad, Pakistan.

Supervisor:
                                         _____

Dr. Ghulam Ali
USPCAS-E
NUST, Islamabad

GEC member # 1
_____

Prof. Dr. Naseem Iqbal
USPCAS-E
NUST, Islamabad

GEC member # 2:
_____

Dr. Zeeshan Ali
USPCAS-E
NUST, Islamabad

GEC member # 3:
_____

Dr. Mustafa Anwar
USPCAS-E
NUST, Islamabad

HoD-ESE:
_____

Dr. Rabia Liaquat
USPCAS-E
NUST, Islamabad

Dean/Principal:
_____

Prof. Dr. Adeel Waqas
USPCAS-E
NUST, Islamabad

Acknowledgements

First and foremost, I am grateful to the Almighty ALLAH, the creator and source of knowledge, for making this monumental task possible through His blessings and guidance. Without His support, I would not have been able to accomplish this feat.

I extend my heartfelt appreciation to my supervisor, Dr. Ghulam Ali, for his exceptional guidance, unwavering encouragement, and support during my master's research and thesis phase. I feel incredibly fortunate to have had a supervisor who was deeply invested in my research progress and always available to answer my queries in a timely manner. Additionally, I would like to express my gratitude to my GEC members Prof. Dr. Naseem Iqbal, Dr. Zeeshan Ali, and Dr. Mustafa Anwar, for their advice and support at various stages of the project.

I am grateful to the staff of the Advanced Energy Materials Lab, Synthesis and Energy Storage Lab. I would also like to thank other lab staff, faculty members, and administration who have been a part of this journey. I would like to extend my heartfelt thanks to my family and friends, who have been a constant source of love, encouragement, and support. Their unwavering belief in me has been a driving force behind my success.

I am deeply grateful for the unwavering support and encouragement provided by my parents and wife, throughout my research. There constant presence and motivation have been invaluable to me.

Finally, I would like to express my appreciation to all the participants who generously gave their time and insights to contribute to this research. Without their willingness to share their experiences and perspectives, this study would not have been possible.

Dedication

My thesis is dedicated to my beloved parents, who have been my role models and taught me to persevere through life's challenges. My father has always stood by me through thick and thin, while my mother instilled in me the values of patience and hard work in pursuit of my goals. My brother has also taught me how to confront difficulties head-on. In addition, I am grateful for the guidance of my teachers, as well as the support of my colleagues, peers, and leaders who share my passion for addressing and working on energy storage devices.

Abstract

Solid-state electrolytes have emerged as a viable substitute for liquid electrolytes in lithium-ion batteries, holding promise for improved safety, energy density, and cyclic performance. Solid-state electrolytes have the potential to address the challenges associated with conventional liquid electrolytes, opening the door for high-performance batteries to become commercialized. Among the various solid-state electrolytes, the NASICON-type electrolyte $Li_{1.3}Al_{0.3}Ti_{1.7}P_3O_{12}$ (LATP) is particularly attractive due to its high ionic conductivity, excellent stability, and impressive air stability.

This research project focuses on the synthesis of a co-doped LATP electrolyte through the solid-state method, with the dopants targeted at the Titanium and Phosphate sites, respectively. The study examines the impact of cobalt and silicon on the phase composition, microstructure, and ionic conductivity of the LATP solid-state electrolyte. X-ray photoelectron spectroscopy confirms the presence of silicon and cobalt dopants, with peaks indicating Co in the +2 oxidation state and Silicon in the +4 oxidation state. The X-ray diffraction analysis confirms a highly crystalline structure. The optimal cobalt and silicon dopant content leads to an ionic conductivity of 5.45×10^{-5} S cm^{-1} at room temperature. These findings suggest that an ideal level of cobalt doping results in better ionic conductivity than pristine LATP.

Keywords: *Solid state electrolytes (SSE), lithium batteries, all solid-state batteries (ASSLBs), lithium-ion batteries (LIB), Lithium Aluminum Titanium Phosphate (LATP), NASICON, Batteries, oxide-based electrolytes, electrolytes*

Table of Contents

List of Figures

xiii

List of Tables

List of Publications

Investigation of the Effect of Cobalt and Silicon Co-Doping on the Structural and Electrochemical Properties of LATP Solid State Electrolytes

Journal (IF =) (Status)

Abbreviations

ASSLBs	All solid-state lithium batteries
CAGR	Compound annual growth rate
Co	Cobalt
EDS	Energy dispersive X-ray spectroscopy
EDX	Energy dispersive X-ray spectroscopy
EIS	Electrochemical chemical spectroscopy
EV	Electric Vehicle
FTIR	Fourier transform infrared spectroscopy
Li	Lithium
LIB	Lithium Ion Batteries
LISICON	Lithium superionic conductor
MOF	Metal organic frame work
NASICON	Sodium superionic conductor
RT	Room Temperature
SEI	Solid Electrolyte Interphase
SEM	Scanning electron microscopy
Si	Silicon
SSE	Solid-state Electrolyte
TEM	Tunneling electron microscopy
TR	Thermal runaway
USD	United State Dollar
XPS	X-ray photoelectron spectroscopy
XRD	X-ray diffraction
σ	Ionic conductivity

Chapter: 1   Introduction

1.1.   Background

Energy production is the essential process of generating power from various sources that serve different purposes like powering homes, businesses, and transportation. The most common sources of energy production are fossil fuels, nuclear energy, and renewable energy. Fossil fuels such as coal, oil, and natural gas are the widely used sources of energy production across the globe. However, the burning of fossil fuels releases significant amounts of greenhouse gases into the atmosphere, leading to various environmental hazards like global warming, air pollution, and acid rain. Conversely, nuclear energy produces large amounts of electricity with minimal greenhouse gas emissions, but accidents can pose significant environmental risks [1].

To combat the environmental hazards, renewable energy sources like solar, wind, hydro, and geothermal have emerged as an alternative to traditional energy sources. Renewable energy sources do not release greenhouse gases and have a lower environmental impact. However, they also face environmental hazards such as wind turbines posing a risk to birds and bats, and hydroelectric power affecting aquatic ecosystems. Additionally, renewable energy sources require energy storage devices like batteries to ensure a consistent supply of electricity. Green energy refers to energy generated from renewable energy sources with minimal environmental impact, and it includes solar panels, wind turbines, and hydropower plants.

Technology plays a significant role in energy production and storage. Technological advancements have made renewable energy sources more cost-effective and efficient while improving energy storage capacity and durability [2]. Energy storage devices like batteries, flywheels, and pumped hydro storage are crucial in energy production and storage. LIB are the most widely used energy storage devices due to their high energy density, long cycle life, and relatively low maintenance requirements [3]. These batteries come in different types, including cylindrical, prismatic, and pouch cells, with cylindrical cells commonly used in consumer electronics, and prismatic and pouch cells in larger applications like electric vehicles and grid-scale energy storage systems [4]. Research groups are intensely focused on LIBs, in addition to other battery systems such as lithium-air [5], lithium-sulfur [6], and redox flow batteries [7]. LIB work by storing energy in the form of chemical energy, where lithium ions move from the cathode to the anode during charging, and move back to the cathode during discharge, releasing energy in the process [8].

1.1.1. Market Estimation

The market for LIB has expanded quickly in recent years due to rising interest in electric vehicles, energy storage devices, and consumer electronics. The global LIB market was estimated to be worth USD 36.7 billion in 2020 and is anticipated to increase at a CAGR of 19.8% from 2021 to 2027 to reach USD 129.3 billion [9]. In the upcoming years, the demand for LIB is anticipated to be further fueled by the growing emphasis on renewable energy sources and energy storage technologies. LIB are becoming more appealing for a variety of applications due to improvements in battery performance, increased energy density, and lower costs brought about by technological developments [10]. China, Japan, and South Korea are the major market participants in the Asia-Pacific region, which leads the worldwide LIB industry [11].
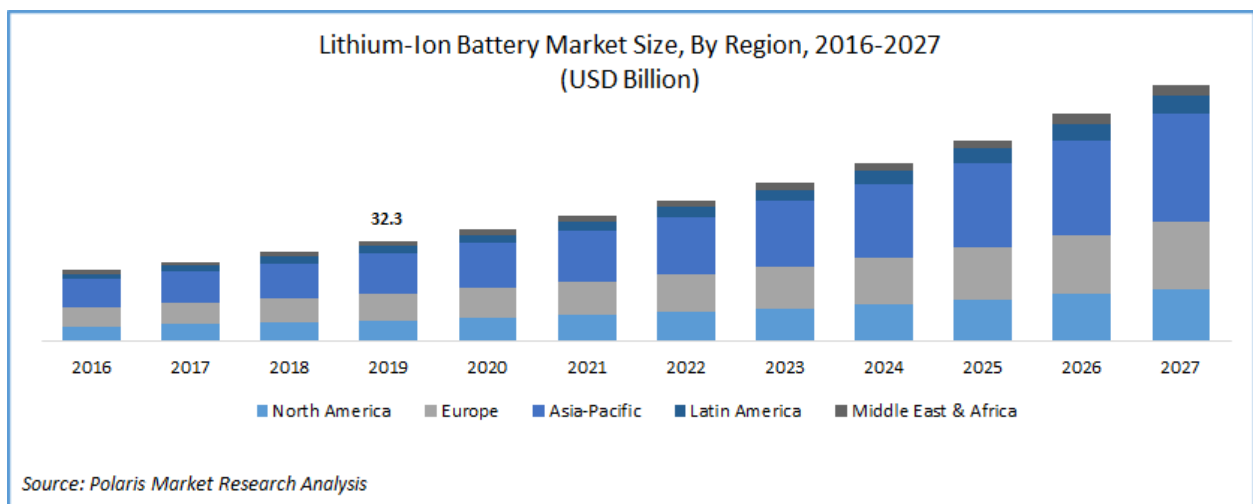
Figure 1.1: Global estimation of LIB Market from 2016 to 2027 including all continents (Polaris Market Research)

1.2. History of LIB

The first LIB was developed in the 1970s by M. Stanley Whittingham while he was employed at Exxon [12]. However, Sony unveiled the first commercial LIB in 1991, utilizing a carbon anode and a lithium cobalt oxide cathode. This is when LIB first became popular. This battery changed the electronics sector by giving portable electronics like laptops and cell phones a compact, long-lasting power source. Since then, technological developments have contributed to the development of several cathode, anode, and electrolyte types, increased energy density, prolonged cycle life, and enhanced safety. Due to its use in electric vehicles and grid-scale energy storage systems, the demand for LIB has increased significantly during the past several years [13], [14]. The development of technology and the rising need for energy storage

solutions across a variety of industries are both reflected in the history of LIB. To achieve high energy density LIBs, considerable study has recently been devoted into electrode and electrolyte materials [15]. The journey of LIB started when the UK Atomic Energy Authority published a patent demonstrating the reversibility of A_x (an alkaline metal) insertion and deintercalation in a material with the structural formula $A_xM_yO_2$, where M_y is a transition metal. In 1990, SONY used this patent to manufacture HP-211, which employed a chemistry of $LiCoO_2$ and soft carbon [16]. The mass production of HP-211 began the following year for use in the TR-1 camcorder application, but now with $LiCoO_2$ and hard carbon [17].

1.2.1. Working of LIB

LIB work by storing and releasing energy in the form of chemical energy. The battery contains a cathode, an anode, and an electrolyte, which acts as a medium for the movement of ions between the electrodes. During charging, lithium ions move from the cathode to the anode, where they are stored as potential energy. The movement of the ions is facilitated by the flow of electrons through an external circuit. When the battery is discharged, the lithium ions move back to the cathode, releasing energy in the form of electrical current. The process of charging and discharging is reversible, allowing LIB to be used multiple times. The performance of LIB depends on various factors, including the type of cathode and anode material, the composition of the electrolyte, and the manufacturing process. Advances in technology have led to the development of high-capacity LIB with longer cycle life, improved safety, and reduced cost [18].
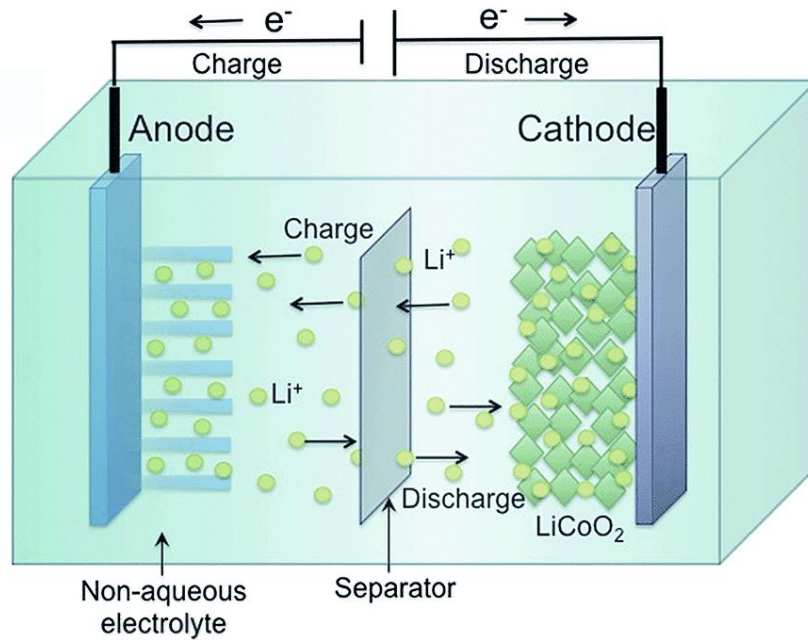
Figure 1.2: The basic concept behind the LIB involves the insertion and removal of lithium ions (represented by yellow spheres) into the anode and cathode structures during the charging and discharging processes, respectively

1.2.2. Electrochemistry of LIB

LIB operate based on electrochemical principles, specifically redox reactions. During charging, the battery undergoes an oxidation reaction at the anode, and a reduction reaction at the cathode. Conversely, during discharge, the opposite occurs, with a reduction reaction taking place at the anode and an oxidation reaction occurring at the cathode.

The anode in a LIB is typically made of graphite or other forms of carbon. During charging, lithium ions are extracted from the cathode and move through the electrolyte to the anode, where they are intercalated into the graphite structure. This process is accompanied by an oxidation reaction, where electrons are released by the graphite anode and flow through the external circuit to the cathode. The overall reaction is:

$LiCoO_2 + C_6 <=> Li_{1-x}CoO_2 + xLiC_6 + xe-$ *(eq.1)*
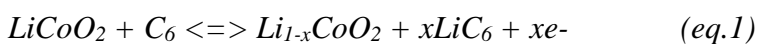
where $LiCoO_2$ represents the cathode material, C_6 represents the graphite anode, and x represents the amount of lithium ions intercalated into the graphite structure.

At the cathode, lithium ions combine with metal oxide compounds such as lithium cobalt oxide ($LiCoO_2$) to form lithium metal oxide. This process is accompanied by a reduction reaction, where electrons are accepted by the cathode material. The overall reaction is:

4

$Li_{1-x}CoO_2 + xLiC_6 + xe- <=> LiCoO_2 + xLi+ + xe-$ *(eq.2)*

where $Li_{1-x}CoO_2$ represents the partially depleted cathode material and $LiCoO_2$ represents the fully charged cathode material.

During discharge, the opposite reactions occur, with lithium ions moving from the anode to the cathode and combining with metal oxide compounds at the cathode, releasing energy in the form of electrical current. The process is reversible, allowing the battery to be charged and discharged repeatedly.

1.2.3. Types of Li-ion cells

LIB's have become an integral part of modern life, powering a wide range of electronic devices, including smartphones, laptops, electric vehicles, and energy storage systems. Different types of lithium cells are available, each with its unique characteristics that make them suitable for specific applications and usage requirements.

The cylindrical cell, also known as the 18650 cell, is the most commonly used type of LIB. It has a cylindrical shape with a diameter of 18 mm and a length of 65 mm, making it ideal for high-power applications, such as power tools, laptops, and electric vehicles [19].

Prismatic cells, also called pouch cells, have a rectangular or square shape and are available in different sizes, making them more versatile than cylindrical cells. They offer high energy density and excellent power delivery, making them suitable for electric vehicles and energy storage systems [19].

Button cells are small, flat, and round, mainly used in low-power devices like calculators and watches due to their low energy density.

Pouch cells, also known as flexible cells, have a thin and lightweight structure, making them ideal for portable devices such as smartphones and tablets. They offer a high energy density and can be arranged in various configurations to meet specific power and energy requirements [20].

In conclusion, the choice of lithium cell depends on the specific application and usage requirements. Cylindrical and prismatic cells are ideal for high-power applications, while button cells are suitable for low-power devices. Pouch cells are preferred for their thin and lightweight structure, making them ideal for portable devices. applications, and pouch cells are preferred for their thin and lightweight structure, making them ideal for portable devices.

5
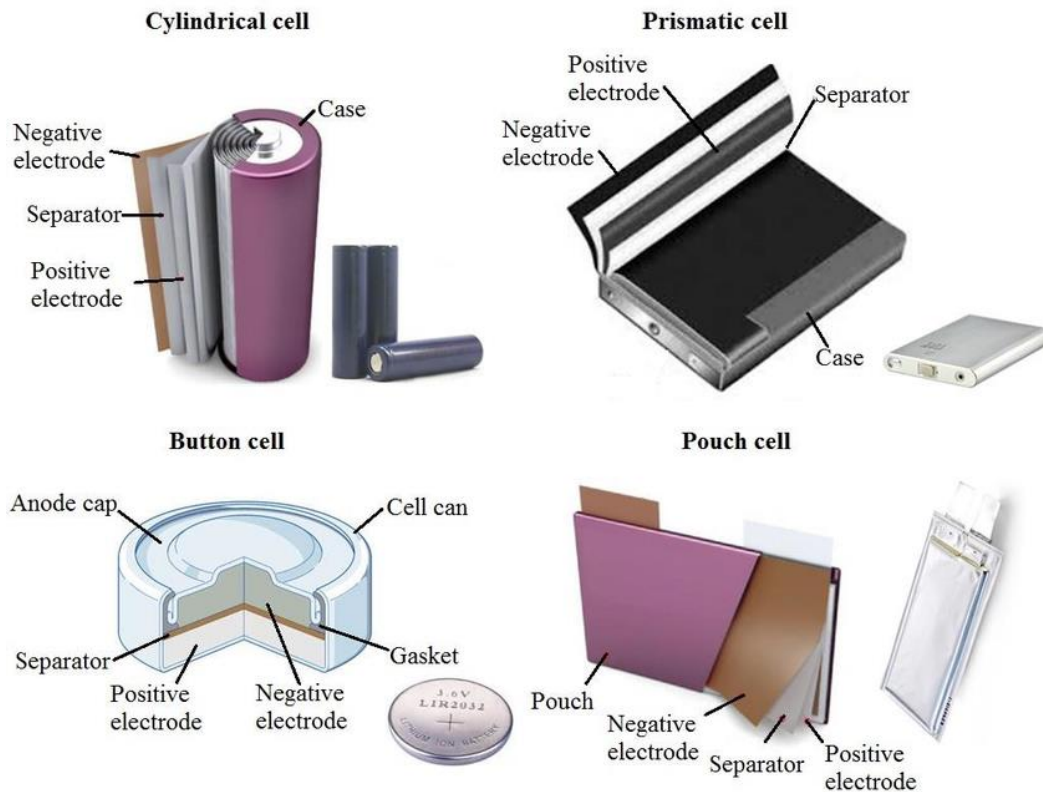
Figure 1.3: Different types of cells and components present in them

1.2.4. Advantages of LIB on other Technologies

LIB have several advantages over other battery technologies that make them one of the most popular types of rechargeable batteries used today.

The high energy density of LIB is one of their most important benefits. The amount of energy that may be stored in a battery per unit of volume or weight is known as energy density. Compared to other battery types like nickel-cadmium (NiCd) and nickel-metal hydride (NiMH) batteries, LIB have a higher energy density. This makes them perfect for portable gadgets like smartphones, tablets, laptops, and electric vehicles since they can store more energy in a smaller, lighter size. LIB' high energy density prolongs battery life and minimizes the need for frequent recharging. The increased lifespan of LIB is another benefit. LIB have a far better rechargeability than other rechargeable batteries, allowing for hundreds of recharge cycles before needing to be replaced. Because of this, LIB will eventually prove to be a more cost-effective solution. LIB also have a low self-discharge rate, allowing them to maintain their charge for longer periods of time without the need for recharging. For less commonly used gadgets, this is very helpful. The minimal maintenance required by LIB is another important benefit. LIB don't need to be discharged on a regular basis like other rechargeable batteries do.

Moreover, they are immune to the memory effect, a condition in which batteries gradually lose capacity if they are not fully depleted before recharging. LIB is more handy and dependable because they can be recharged whenever you want without the battery being harmed [21]. And lastly, compared to other battery technologies, LIB is more environmentally benign. Compared to NiCd batteries, they have fewer hazardous components and are simpler to recycle. When LIB is disposed away, the components they contain cause less damage to the environment [22].

In conclusion, LIB have several advantages over other battery technologies, including high energy density, longer lifespan, low maintenance, and environmental friendliness. These advantages have made LIB a popular choice for portable devices, electric vehicles, and renewable energy systems. As technology advances, we can expect to see even more improvements in LIB technology, making them an even more attractive option for a variety of applications.
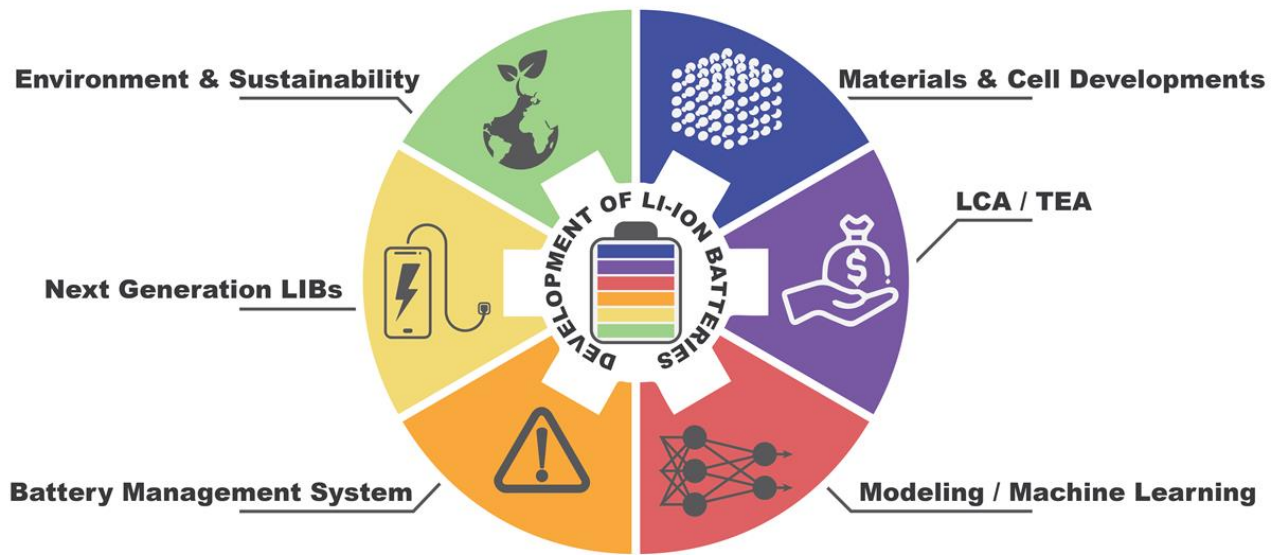
Figure 1.4: Advances taking place in the world of LIBs
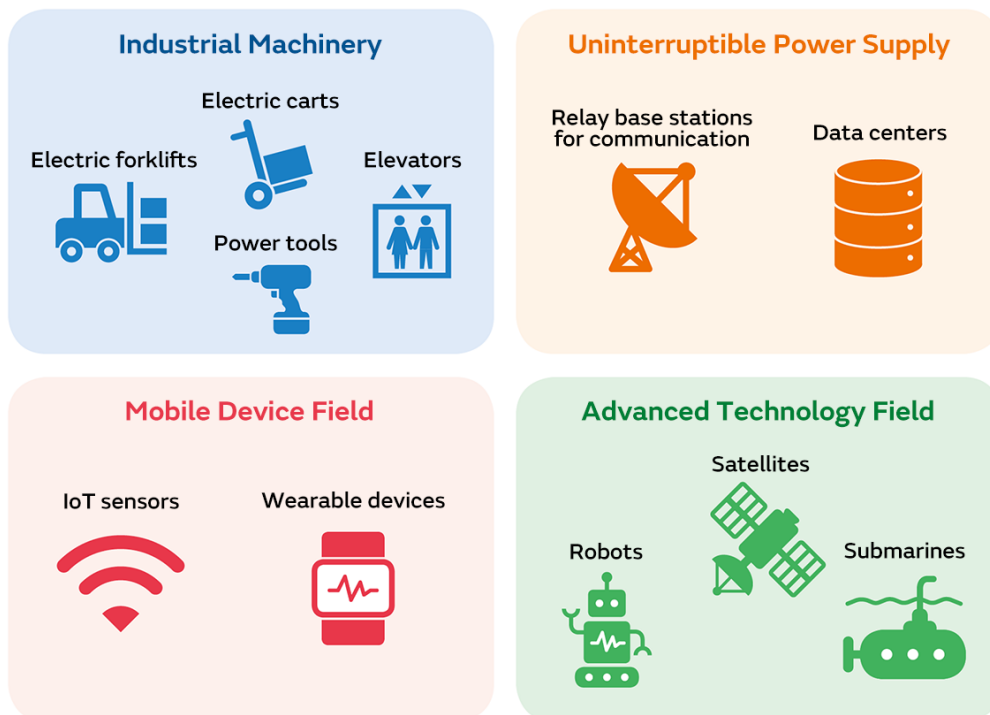
Figure 1.5: Applications and uses of LIBs in different sectors of technologies

1.2.5. Applications of LIB

LIB have a wide range of applications in various industries. One of the most significant applications is in portable electronics, including cell phones, laptops, tablets, and other devices. These batteries provide a lightweight and long-lasting power source that allows users to remain connected on the go. LIBs are also commonly used in electric vehicles, providing a high-capacity energy storage solution for long-range driving [23]. Another growing application is in grid-scale energy storage systems, where LIB can be used to store renewable energy generated from sources such as solar and wind power [24]. LIBs are also used in medical devices, aerospace, and defense applications, where high reliability and safety are critical. The versatility and performance of LIB make them a popular choice for various industries and are expected to play an increasingly important role in the transition towards a sustainable energy future [25].

1.3. Safety issues associated with LIB

Safety issues associated with LIB arise primarily due to their inherent chemical instability and the potential for thermal runaway, which can result in fires, explosions, or release of toxic gases, and gas evolution. One of the main safety concerns is related to the formation of dendrites, which are tiny filaments that can grow on the anode surface and pierce through the separator, leading to short circuits and potential thermal runaway. Another safety issue is related to overcharging, which can cause the cathode to break down and release oxygen, leading to thermal runaway and possible ignition. Furthermore, physical damage or manufacturing defects can also result in internal short circuits and potential thermal runaway. Manufacturers take various measures to mitigate these risks, including the use of high-quality materials, advanced manufacturing processes, and safety features such as protection circuits and thermal management systems. It is essential to follow proper charging and handling procedures and to use high-quality batteries from reputable manufacturers to minimize safety risks associated with LIB [26].

1.3.1. Recycling of LIB

LIBs contain toxic chemicals that can harm the environment, so recycling is essential. The process involves collection, sorting, dismantling, shredding, chemical treatment, refining, and reuse. Recycling reduces environmental impact, recovers valuable materials, and supports sustainability goals [27].
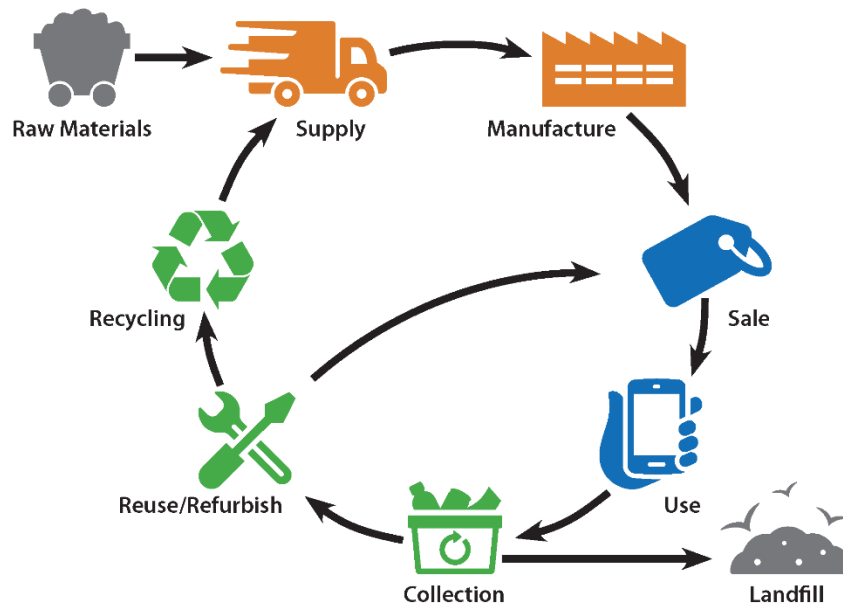
Figure 1.6: Recycling process of LIB from raw material to reuse after processing

1.3.2. Chemical Instability

Chemical instability issues in LIB arise due to the inherent properties of the materials used in their construction. The electrolyte in LIB typically contains highly flammable organic solvents, which can lead to thermal runaway if they come into contact with the high-energy materials used in the anode and cathode. Additionally, the use of certain cathode materials, such as cobalt, can lead to thermal instability due to their tendency to undergo exothermic reactions at high temperatures. LIB are also susceptible to degradation over time, leading to the formation of highly reactive materials that can trigger thermal runaway. Manufacturers take various steps to mitigate these risks, such as selecting stable materials for the anode and cathode, developing stable electrolytes, and implementing thermal management systems. However, the potential for chemical instability remains a significant concern, and ongoing research is focused on developing more stable and safer battery chemistries [28].

1.3.3. Thermal Runaway

Andrey and colleagues published a review on thermal runaway (TR) in LIB in 2018 [29]. TR, which can result in smoke, fire, or explosions, begins in one cell and can spread to neighboring cells, causing hazardous outcomes at the system level [30]. Since 1991, the safety concern related to the risk of TR has been a significant challenge for lithium batteries. In 2006, batteries manufactured by Dell, Lenovo, and Apple were recalled due to incidents of fire and explosions.

- **Abuse Condition:**

  Mechanical abuse can occur when a battery pack is involved in a vehicle collision or when it is penetrated. The volume expansion of electrode materials can also result in mechanical abuse. In the event of a vehicle accident, the battery pack may deform under the impact of an external force, as noted in references [31] and [32]. Such deformation may lead to various consequences, such as the breakage of the battery separator causing an internal short circuit or the leakage of electrolyte.

- **Electrical Abuse:**

  Feng and colleagues have reviewed that the conditions for electrical abuse include external short circuit, overcharge, and over-discharge. External short circuit can result from improper maintenance, collision, contamination, or water immersion, among other causes, as described in reference [33]. During an external short circuit event, the battery discharges rapidly and the discharge current exceeds the normal state. The use of electronic devices can help mitigate the hazards of external short circuit abuse, as noted in reference [34]. Balarkrishnan and colleagues described the use of magnetic switches, fuses, and positive thermal coefficient (PTC) devices to overcome the hazards of external short circuit.

- **Thermal Abuse:**

  Thermal abuse conditions refer to localized overheating and external high temperature. Loose contacts of the cell connector are a common cause of thermal abuse. Thermal abuse can result in the melting of the separator, the decomposition of electrodes, and, ultimately, the occurrence of thermal runaway [35], [36].
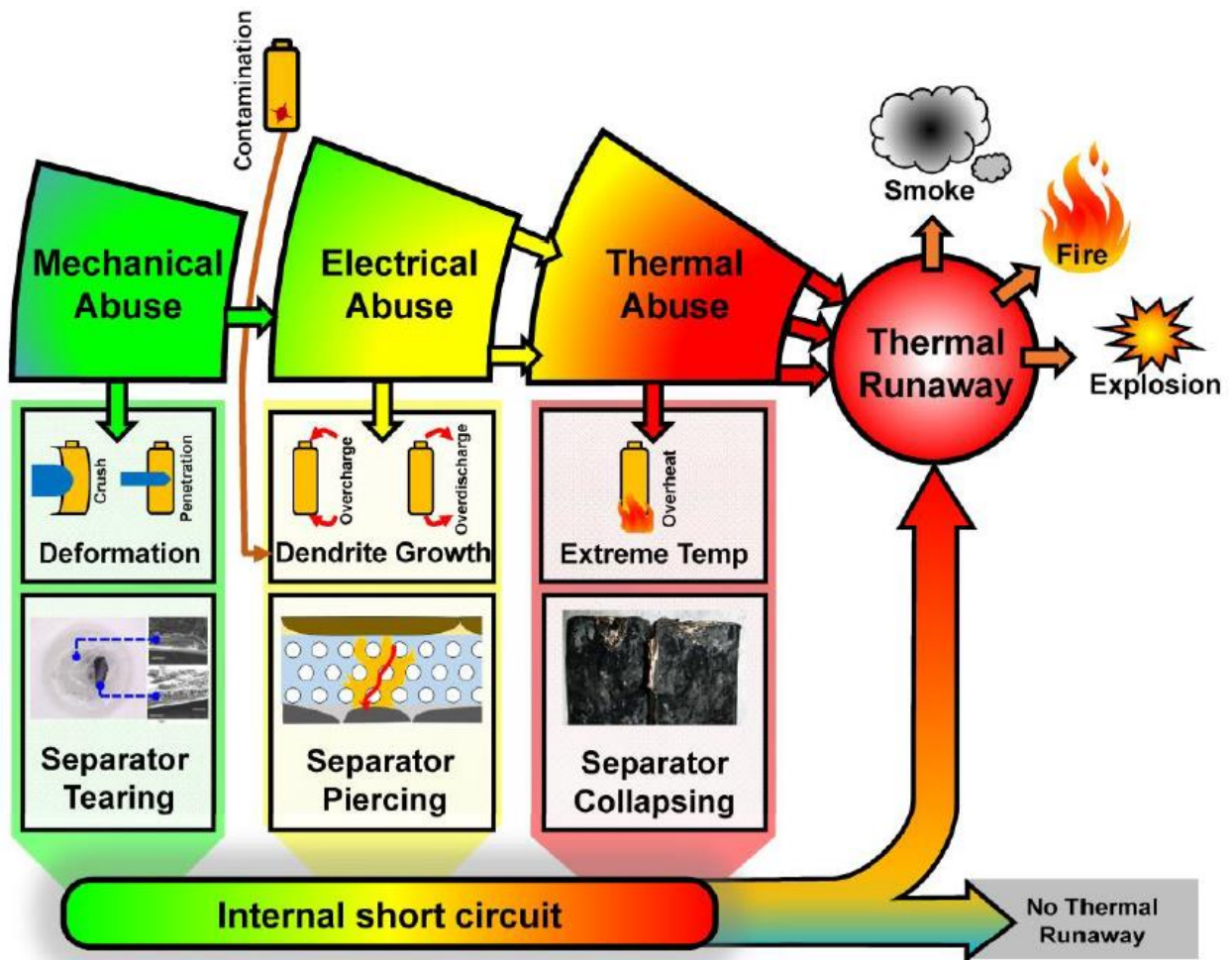
Figure 1.7: Thermal runaway process and its causes in LIB

1.4. Mitigation of TR

TR is a major safety concern in LIB, and it can lead to hazardous outcomes such as fire, explosion, and loss of life or property. To address this issue, various strategies can be employed at different levels, including material, cell, and system levels.

At the material level, intrinsic safety can be increased by modifying the materials used in the battery. For example, the use of solid electrolytes or flame-retardant additives can help reduce the risk of thermal runaway. The development of more stable electrode materials that can withstand high temperatures and pressure can also improve battery safety.

At the cell level, battery management systems can be improved to protect the system before abuse conditions occur. For example, advanced monitoring systems can detect signs of overheating or overcharging and take appropriate action to prevent TR. The use of protective coatings or barriers can also prevent the spread of thermal runaway to neighboring cells.

Finally, at the system level, mitigation strategies can be implemented after abuse conditions have occurred. These strategies can include the use of cooling systems, such as liquid or air cooling, to reduce the temperature of the battery pack. The use of fire suppression systems, such as fire-retardant chemicals or automatic extinguishers, can also help prevent the spread of fire and reduce damage to the battery and surrounding structures [37].

Overall, the mitigation of TR in LIB requires a comprehensive approach that involves the use of various strategies at different levels to improve battery safety and prevent catastrophic outcomes [38].

1.5. Gas Evolution

The electrolyte in LIBs is unstable at high voltage level and reacts with electrode materials at the interface, leading to gas evolution. This occurs during normal cycling, overcharge, high temperatures, and the first charge process [39]. During the first charge process, carbon monoxide, hydrogen, and ethylene are mainly evolved. During normal cycling, carbon dioxide, carbon monoxide, ethylene, methane, and ethane are released. The gases are generated during the oxidation and reduction of electrolyte at the electrode surface. Overcharge conditions lead to higher gas release than normal cycling, with O_2 and H_2 gases being generated at the cathode and anode surfaces, respectively. The gases released during storage under high temperatures include carbon dioxide at the cathode surface and carbon monoxide at both electrode surfaces [40].

1.6. Dendrite Growth

Dendrite growth is a common problem in LIB, which occurs when lithium ions build up and form needle-like structures on the surface of the anode. These dendrites can pierce the separator, leading to short circuits and potentially catastrophic failure of the battery [41]. Researchers are exploring various ways to mitigate dendrite growth, including modifying the electrolyte composition, using additives to the electrolyte, and developing new anode materials. One promising approach involves using solid-state electrolytes, which could prevent dendrite growth by eliminating the liquid electrolyte that allows lithium ions to move freely. Overall, addressing dendrite growth is an important area of research for improving the safety and performance of LIB [42].

1.7. Overcharging Issue

Overcharging is a critical issue in LIB that can lead to serious safety hazards. When a LIB is overcharged, it can cause the battery to overheat and even catch fire or explode. Overcharging

occurs when the battery is charged beyond its maximum voltage limit, which causes the lithium ions to react with the electrolyte and produce excessive heat. To prevent overcharging, LIB are typically equipped with protection circuits that detect when the battery is fully charged and stop the charging process. However, these circuits are not foolproof, and overcharging can still occur due to faulty circuits, poor battery design, or user error. Therefore, it is important to handle LIB with care and follow manufacturer recommendations to avoid overcharging and ensure safe and reliable operation.

1.8. Battery Management System (BMS)

A BMS is a sophisticated electrical device used to control and keep track of rechargeable batteries' performance. This is crucial for high-power applications, like electric cars, where the battery must function effectively and securely under a variety of circumstances. The BMS functions by continuously tracking a number of battery-related variables, including voltage, temperature, and state of charge. The battery's voltage is kept under observation to make sure that it remains within a safe range when being charged and discharged. In order to avoid overheating, which could harm the battery or possibly be dangerous, the temperature of the battery is also monitored. To guarantee that the battery is charged and drained appropriately and to avoid overcharging or over-discharging, the state of charge (SOC) is tracked [43]. Based on this data, the BMS may regulate the battery's charging and discharging to make sure it functions effectively and safely. For instance, the BMS can limit the charging current to prevent overcharging if the battery voltage rises too high during charging. Similar to this, the BMS can limit the load on the battery to prevent over-discharging if the battery's SOC drops too low while discharging. The BMS can also give useful details about the battery's functioning, like its capacity, overall health, and remaining life. The battery may be charged and discharged more efficiently with the use of this information, which can also be used to determine when the battery needs to be replaced [44].

Overall, a rechargeable battery's performance and lifespan are greatly enhanced by the battery management system. It assures the battery functions safely and effectively and offers helpful data about its functionality and state of health. As a result, it plays a crucial role in a variety of high-power applications, including electric cars, renewable energy sources, and portable devices [45].

1.9. Electrolytes

LIB utilize lithium ions to store and release energy and rely on electrolytes to conduct these ions between the anode and the cathode during charging and discharging. There are four main

types of electrolytes used in these batteries, including liquid electrolytes, solid-state electrolytes, solid polymer electrolytes, and inorganic ceramic electrolytes.

Liquid electrolytes, which are the most widely used type, are typically composed of lithium hexafluorophosphate ($LiPF_6$) and an organic solvent such as ethylene carbonate (EC). They offer high ionic conductivity, low resistance, and compatibility with a variety of electrode materials. Solid-state electrolytes, on the other hand, are a newer type of electrolyte gaining popularity due to their potential to improve battery safety and performance. They consist of lithium-ion conducting ceramic materials like lithium phosphate (Li_3PO_4) or lithium garnet ($Li_7La_3Zr_2O_{12}$) and offer higher safety, improved energy density, and higher stability at high temperatures [46]. Solid polymer electrolytes are a type of solid-state electrolyte made up of a polymer matrix, such as polyethylene oxide (PEO), and a lithium salt, providing high ionic conductivity, good mechanical properties, and improved safety compared to liquid electrolytes [47], [48]. Inorganic ceramic electrolytes, made up of an inorganic compound, such as lithium aluminum titanium phosphate (LATP), and a lithium salt, offer high ionic conductivity, good thermal stability, excellent chemical stability, and less flammability than liquid electrolytes [49].

Lastly, hybrid electrolytes combine the advantages of both liquid and solid-state electrolytes and consist of a solid-state electrolyte coated with a thin layer of a liquid electrolyte. This design offers both the safety and stability of solid-state electrolytes and the high conductivity of liquid electrolytes [50].

In conclusion, the type of electrolyte used in LIB plays a significant role in the performance and safety of the batteries. Liquid electrolytes are the most commonly used type of electrolyte and offer high ionic conductivity and low resistance. Solid-state electrolytes are a newer type of electrolyte that is gaining popularity due to their potential to improve battery safety and performance which can overcome the main problems of liquid electrolytes that will allow us to manufacture safe and high energy density All solid-state batteries.

1.10. Problem Statement

In recent years, the development of NASICON-based solid-state electrolytes such as lithium aluminum titanium phosphate (LATP) has gained significant attention due to their potential use in high-performance LIB. However, a major challenge in the development of LATP is the formation of impurity phases during the sintering process, particularly the common formation of $AlPO_4$ phases. The presence of impurities like $LiTiPO_5$ can also significantly reduce the

ionic conductivity of the electrolyte. The ideal function of an electrolyte is to provide a smooth pathway for the diffusion of Li ions between the cathode and anode, without any electron conductivity. Unfortunately, impurity phases, cracks, voids, and narrow lithium channels can hinder the flow of Li ions, reducing the overall efficiency of the battery. Moreover, impurities present at the grain boundaries can also act as barriers to the movement of Li ions. Therefore, understanding the factors that influence the formation of impurities and optimizing the sintering conditions is essential for the successful development of high-performance LATP electrolytes.

1.11. Objectives

Synthesize of a pristine and co-doped LATP ($Li_{1.3+2x+y}Al_{0.3}Co_xTi_{1.7-x}Si_yP_{3-y}O_{12}$) with a cost effective and simple synthesis method. Co-doping to improve the ionic conductivity and provide larger channel paths for the diffusion of Li ion. The physiochemical properties were studied by X-ray diffraction (XRD), Scanning electron microscopy (SEM), Tunneling electron microscopy (TEM), Fourier-transform infrared spectroscopy (FTIR), X-ray photoelectron spectroscopy (XPS), and electrochemical properties by Electrochemical impedance spectroscopy (EIS), and battery analyzer.

Summary

This section provides an overview of LIB as a means of storing energy, including its history and uses. Additionally, safety concerns related to using LIB in high-energy applications are explored. Specifically, the phenomenon of thermal runaway is examined, and potential methods for mitigating its effects are mentioned. The chapter also delves into the various types of electrolytes used in LIB, explaining their functionality and performance metrics.

List Of References

[1]   P. Moriarty and D. Honnery, "What is the global potential for renewable energy?," *Renewable and Sustainable Energy Reviews*, vol. 16, no. 1, pp. 244–252, Jan. 2012, doi: 10.1016/J.RSER.2011.07.151.

[2]   F. Jia, K. Soucie, S. Alisat, D. Curtin, and M. Pratt, "Are environmental issues moral issues? Moral identity in relation to protecting the natural world," *J Environ Psychol*, vol. 52, pp. 104–113, Oct. 2017, doi: 10.1016/J.JENVP.2017.06.004.

[3]   B. Diouf and R. Pode, "Potential of lithium-ion batteries in renewable energy," *Renew Energy*, vol. 76, pp. 375–380, Apr. 2015, doi: 10.1016/J.RENENE.2014.11.058.

[4]   T. H. Kim, J. S. Park, S. K. Chang, S. Choi, J. H. Ryu, and H. K. Song, "The Current Move of Lithium Ion Batteries Towards the Next Phase," *Adv Energy Mater*, vol. 2, no. 7, pp. 860–872, Jul. 2012, doi: 10.1002/AENM.201200028.

[5]   Y. Sun, "Lithium ion conducting membranes for lithium-air batteries," *Nano Energy*, vol. 2, no. 5, pp. 801–816, Sep. 2013, doi: 10.1016/J.NANOEN.2013.02.003.

[6]   J. Scheers, S. Fantini, and P. Johansson, "A review of electrolytes for lithium–sulphur batteries," *J Power Sources*, vol. 255, pp. 204–218, Jun. 2014, doi: 10.1016/J.JPOWSOUR.2014.01.023.

[7]   T. Kojima, T. Ishizu, T. Horiba, and M. Yoshikawa, "Development of lithium-ion battery for fuel cell hybrid electric vehicle application," *J Power Sources*, vol. 189, no. 1, pp. 859–863, Apr. 2009, doi: 10.1016/J.JPOWSOUR.2008.10.082.

[8]   G. E. Blomgren, "The Development and Future of Lithium Ion Batteries," *J Electrochem Soc*, vol. 164, no. 1, pp. A5019–A5025, Dec. 2017, doi: 10.1149/2.0251701JES/XML.

[9]   P. Greim, A. A. Solomon, and C. Breyer, "Assessment of lithium criticality in the global energy transition and addressing policy gaps in transportation," *Nature Communications 2020 11:1*, vol. 11, no. 1, pp. 1–11, Sep. 2020, doi: 10.1038/s41467-020-18402-y.

[10]   F. H. Gandoman, E. M. Ahmed, Z. M. Ali, M. Berecibar, A. F. Zobaa, and S. H. E. Abdel Aleem, "Reliability Evaluation of Lithium-Ion Batteries for E-Mobility Applications from Practical and Technical Perspectives: A Case Study," *Sustainability 2021, Vol. 13, Page 11688*, vol. 13, no. 21, p. 11688, Oct. 2021, doi: 10.3390/SU132111688.

[11] S. Wang and J. Yu, "A comparative life cycle assessment on lithium-ion battery: Case study on electric vehicle battery in China considering battery evolution," *Waste Management and Research*, vol. 39, no. 1, pp. 156–164, Jan. 2021, doi: 10.1177/0734242X20966637.

[12] M. v. Reddy, A. Mauger, C. M. Julien, A. Paolella, and K. Zaghib, "Brief History of Early Lithium-Battery Development," *Materials 2020, Vol. 13, Page 1884*, vol. 13, no. 8, p. 1884, Apr. 2020, doi: 10.3390/MA13081884.

[13] W. van Schalkwijk and B. Scrosati, "Advances in Lithium Ion Batteries Introduction," *Advances in Lithium-Ion Batteries*, pp. 1–5, 2002, doi: 10.1007/0-306-47508-1_1.

[14] G. E. Blomgren, "The Development and Future of Lithium Ion Batteries," *J Electrochem Soc*, vol. 164, no. 1, pp. A5019–A5025, Dec. 2017, doi: 10.1149/2.0251701JES/XML.

[15] C. M. Costa, J. C. Barbosa, R. Gonçalves, H. Castro, F. J. D. Campo, and S. Lanceros-Méndez, "Recycling and environmental issues of lithium-ion batteries: Advances, challenges and opportunities," *Energy Storage Mater*, vol. 37, pp. 433–465, May 2021, doi: 10.1016/J.ENSM.2021.02.032.

[16] A. Eftekhari, "Lithium-Ion Batteries with High Rate Capabilities," *ACS Sustain Chem Eng*, vol. 5, no. 4, pp. 2799–2816, Apr. 2017, doi: 10.1021/ACSSUSCHEMENG.7B00046/ASSET/IMAGES/LARGE/SC-2017-00046B_0009.JPEG.

[17] R. Moshtev and B. Johnson, "State of the art of commercial Li ion batteries," *J Power Sources*, vol. 91, no. 2, pp. 86–91, Dec. 2000, doi: 10.1016/S0378-7753(00)00458-4.

[18] Z. Yang, Y. Luo, X. Gao, and R. Wang, "High-Safety All-Solid-State Lithium-Ion Battery Working at Ambient Temperature with In Situ UV-Curing Polymer Electrolyte on the Electrode," *ChemElectroChem*, vol. 7, no. 12, pp. 2599–2607, Jun. 2020, doi: 10.1002/CELC.202000411.

[19] T. D. Hatchard, D. D. MacNeil, A. Basu, and J. R. Dahn, "Thermal Model of Cylindrical and Prismatic Lithium-Ion Cells," *J Electrochem Soc*, vol. 148, no. 7, p. A755, Jun. 2001, doi: 10.1149/1.1377592/XML.

[20] R. P. Ramasamy, R. E. White, and B. N. Popov, "Calendar life performance of pouch lithium-ion cells," *J Power Sources*, vol. 141, no. 2, pp. 298–306, Mar. 2005, doi: 10.1016/J.JPOWSOUR.2004.09.024.

[21] B. Diouf and R. Pode, "Potential of lithium-ion batteries in renewable energy," *Renew Energy*, vol. 76, pp. 375–380, Apr. 2015, doi: 10.1016/J.RENENE.2014.11.058.

[22] D. Deng, "Li-ion batteries: basics, progress, and challenges," *Energy Sci Eng*, vol. 3, no. 5, pp. 385–418, Sep. 2015, doi: 10.1002/ESE3.95.

[23] "Lithium-Ion Batteries: Basics and Applications - Google Books." https://books.google.com.pk/books?hl=en&lr=&id=ll1oDwAAQBAJ&oi=fnd&pg=PA 4&dq=applications+of+lithium+ion+batteries&ots=s2TQFFuTL-&sig=l3PVa1g_H-- W3UvyhPbcLF0HjTo&redir_esc=y#v=onepage&q=applications%20of%20lithium%2 0ion%20batteries&f=false (accessed Mar. 03, 2023).

[24] T. Chen *et al.*, "Applications of Lithium-Ion Batteries in Grid-Scale Energy Storage Systems," *Transactions of Tianjin University*, vol. 26, no. 3, pp. 208–217, Jun. 2020, doi: 10.1007/S12209-020-00236-W/FIGURES/4.

[25] A. Ritchie and W. Howard, "Recent developments and likely advances in lithium-ion batteries," *J Power Sources*, vol. 162, no. 2, pp. 809–812, Nov. 2006, doi: 10.1016/J.JPOWSOUR.2005.07.014.

[26] J. Wen, Y. Yu, and C. Chen, "A review on lithium-ion batteries safety issues: Existing problems and possible solutions," *Materials Express*, vol. 2, no. 3, pp. 197–212, Sep. 2012, doi: 10.1166/MEX.2012.1075.

[27] B. Huang, Z. Pan, X. Su, and L. An, "Recycling of lithium-ion batteries: Recent advances and perspectives," *J Power Sources*, vol. 399, pp. 274–286, Sep. 2018, doi: 10.1016/J.JPOWSOUR.2018.07.116.

[28] R. Zhan, X. Wang, Z. Chen, Z. W. Seh, L. Wang, and Y. Sun, "Promises and Challenges of the Practical Implementation of Prelithiation in Lithium-Ion Batteries," *Adv Energy Mater*, vol. 11, no. 35, p. 2101565, Sep. 2021, doi: 10.1002/AENM.202101565.

[29] X. Feng, M. Ouyang, X. Liu, L. Lu, Y. Xia, and X. He, "Thermal runaway mechanism of lithium ion battery for electric vehicles: A review," *Energy Storage Mater*, vol. 10, pp. 246–267, Jan. 2018, doi: 10.1016/J.ENSM.2017.05.013.

[30] N. E. Galushkin, N. N. Yazvinskaya, and D. N. Galushkin, "Mechanism of Thermal Runaway in Lithium-Ion Cells," *J Electrochem Soc*, vol. 165, no. 7, pp. A1303–A1308, May 2018, doi: 10.1149/2.0611807JES/XML.

[31] R. Saada, D. Patel, and B. Saha, "Causes and consequences of thermal runaway incidents - Will they ever be avoided?," *Process Safety and Environmental Protection*, vol. 97, pp. 109–115, Sep. 2015, doi: 10.1016/J.PSEP.2015.02.005.

[32] S. Xie, Y. Gong, X. Ping, J. Sun, X. Chen, and Y. He, "Effect of overcharge on the electrochemical and thermal safety behaviors of LiNi0.5Mn0.3Co0.2O2/graphite lithium-ion batteries," *J Energy Storage*, vol. 46, p. 103829, Feb. 2022, doi: 10.1016/J.EST.2021.103829.

[33] D. Kong, G. Wang, P. Ping, and J. Wen, "Numerical investigation of thermal runaway behavior of lithium-ion batteries with different battery materials and heating conditions," *Appl Therm Eng*, vol. 189, p. 116661, May 2021, doi: 10.1016/J.APPLTHERMALENG.2021.116661.

[34] X. Feng *et al.*, "Investigating the thermal runaway mechanisms of lithium-ion batteries based on thermal analysis database," *Appl Energy*, vol. 246, pp. 53–64, Jul. 2019, doi: 10.1016/J.APENERGY.2019.04.009.

[35] P. Ping, Q. Wang, P. Huang, J. Sun, and C. Chen, "Thermal behaviour analysis of lithium-ion battery at elevated temperature using deconvolution method," *Appl Energy*, vol. 129, pp. 261–273, Sep. 2014, doi: 10.1016/J.APENERGY.2014.04.092.

[36] D. Ren *et al.*, "A comparative investigation of aging effects on thermal runaway behavior of lithium-ion batteries," *eTransportation*, vol. 2, Nov. 2019, doi: 10.1016/J.ETRAN.2019.100034.

[37] S. Wilke, B. Schweitzer, S. Khateeb, and S. Al-Hallaj, "Preventing thermal runaway propagation in lithium ion battery packs using a phase change composite material: An experimental study," *JPS*, vol. 340, pp. 51–59, Feb. 2017, doi: 10.1016/J.JPOWSOUR.2016.11.018.

[38] X. Feng, D. Ren, X. He, and M. Ouyang, "Mitigating Thermal Runaway of Lithium-Ion Batteries," *Joule*, vol. 4, no. 4, pp. 743–770, Apr. 2020, doi: 10.1016/J.JOULE.2020.02.010.

[39] D. Ren, X. Feng, L. Lu, X. He, and M. Ouyang, "Overcharge behaviors and failure mechanism of lithium-ion batteries under different test conditions," *Appl Energy*, vol. 250, pp. 323–332, Sep. 2019, doi: 10.1016/J.APENERGY.2019.05.015.

[40] D. Ouyang, J. Liu, M. Chen, and J. Wang, "Investigation into the Fire Hazards of Lithium-Ion Batteries under Overcharging," *Applied Sciences 2017, Vol. 7, Page 1314*, vol. 7, no. 12, p. 1314, Dec. 2017, doi: 10.3390/APP7121314.

[41] L. A. Selis and J. M. Seminario, "Dendrite formation in silicon anodes of lithium-ion batteries," *RSC Adv*, vol. 8, no. 10, pp. 5255–5267, Jan. 2018, doi: 10.1039/C7RA12690E.

[42] X. Gao *et al.*, "Thermodynamic Understanding of Li-Dendrite Formation," *Joule*, vol. 4, no. 9. Cell Press, pp. 1864–1879, Sep. 16, 2020. doi: 10.1016/j.joule.2020.06.016.

[43] Y. Wang *et al.*, "A comprehensive review of battery modeling and state estimation approaches for advanced battery management systems," *Renewable and Sustainable Energy Reviews*, vol. 131, p. 110015, Oct. 2020, doi: 10.1016/J.RSER.2020.110015.

[44] A. Szumanowski and Y. Chang, "Battery management system based on battery nonlinear dynamics modeling," *IEEE Trans Veh Technol*, vol. 57, no. 3, pp. 1425–1432, May 2008, doi: 10.1109/TVT.2007.912176.

[45] M. Shen and Q. Gao, "A review on battery management system from the modeling efforts to its multiapplication and integration," *Int J Energy Res*, vol. 43, no. 10, pp. 5042–5075, Aug. 2019, doi: 10.1002/ER.4433.

[46] W. Xiao, J. Wang, L. Fan, J. Zhang, and X. Li, "Recent advances in Li1+xAlxTi2−x(PO4)3 solid-state electrolyte for safe lithium batteries," *Energy Storage Materials*, vol. 19. Elsevier B.V., pp. 379–400, May 01, 2019. doi: 10.1016/j.ensm.2018.10.012.

[47] F. Croce, L. Persi, F. Ronci, and B. Scrosati, "Nanocomposite polymer electrolytes and their impact on the lithium battery technology," *Solid State Ion*, vol. 135, no. 1–4, pp. 47–52, Nov. 2000, doi: 10.1016/S0167-2738(00)00329-5.

[48] F. B. Dias, L. Plomp, and J. B. J. Veldhuis, "Trends in polymer electrolytes for secondary lithium batteries," *J Power Sources*, vol. 88, no. 2, pp. 169–191, Jun. 2000, doi: 10.1016/S0378-7753(99)00529-7.

[49]   V. Aravindan, J. Gnanaraj, S. Madhavi, and H. K. Liu, "Lithium-Ion Conducting Electrolyte Salts for Lithium Batteries," *Chemistry – A European Journal*, vol. 17, no. 51, pp. 14326–14346, Dec. 2011, doi: 10.1002/CHEM.201101486.

[50]   J. Liang, J. Luo, Q. Sun, X. Yang, R. Li, and X. Sun, "Recent progress on solid-state hybrid electrolytes for solid-state lithium batteries," *Energy Storage Mater*, vol. 21, pp. 308–334, Sep. 2019, doi: 10.1016/J.ENSM.2019.06.021.

Chapter 2:   Literature Review

2.1. Solid state Electrolytes

The exceptional properties of solid electrolytes, which are often referred to as superfast ionic conductors due to their high ionic conductivity comparable to that of liquid electrolytes ($> 10^{-2}$ S cm^{-1} at room temperature), have led to a surge of interest in solid-state batteries as a safer and more efficient alternative to traditional LIB [1].

LIB with liquid electrolyte pose significant safety risks due to the highly flammable organic liquid or polymer electrolytes they use, which have low thermal stability and are easily ignited, leading to fire accidents and explosions if handled improperly. To mitigate these safety concerns, it is crucial to avoid using highly flammable organic liquid electrolytes altogether. All-solid-state batteries (ASSBs) present a viable alternative as they utilize inorganic solid electrolytes that exhibit high thermal stability [2]. Additionally, ASSBs offer several other benefits, including simplified packaging due to the absence of a liquid electrolyte, resulting in reduced weight and increased energy density. Inorganic solid electrolytes are also highly electrochemically stable and can accommodate high-potential cathode materials to further increase energy density. Lastly, ASSBs possess excellent mechanical properties [3]–[6].

2.2. Brief History

All-solid-state lithium batteries (ASSLBs) are a type of rechargeable battery that use a solid electrolyte instead of the liquid or gel-like electrolytes used in traditional LIB. The concept of solid-state batteries was first proposed in the 1960s, but the development of suitable solid electrolytes and electrode materials was a major challenge [7].

In the early 2000s, researchers began making significant progress in the development of solid-state electrolytes, particularly lithium phosphorus oxynitride (LiPON) and lithium thiophosphate (Li_3PS_4). These electrolytes had high ionic conductivity and stability, making them suitable for use in solid-state batteries [2]. In 2011, a team of researchers at Toyota Central R&D Labs announced the development of an all-solid-state LIB using a sulfide-based electrolyte. The battery had a high energy density and a long cycle life, making it a promising candidate for use in electric vehicles. Since then, several other companies and research groups have been working on developing all-solid-state lithium batteries with improved performance and safety features. In 2018, researchers at the University of Texas at Austin announced the development of a new solid electrolyte that could potentially double the energy density of existing solid-state batteries [8].

While all-solid-state lithium batteries are still in the research and development phase, they have the potential to offer several advantages over traditional LIB, including higher energy density, faster charging times, and improved safety. As such, they are a promising technology for powering the next generation of electric vehicles and other portable electronics.

2.3. Types Of Solid State Electrolyte

Solid-state batteries are considered as a safer and more efficient alternative to traditional LIB due to the exceptional properties of solid electrolytes. In order to meet the various requirements of solid-state batteries, there are several types of Lithium solid electrolytes available in the market, such as NASICON, garnet, perovskite, LISICON, LiPON, Li_3N, sulphide, argyrodite, anti-perovskite, and others [9], [10].

Each of these types of solid electrolytes has its own unique properties, which can be utilized to address specific requirements of solid-state batteries. For example, garnet-type solid electrolytes are known for their high ionic conductivity and excellent electrochemical stability, while NASICON-type solid electrolytes are recognized for their high lithium-ion transference number and chemical stability against lithium metal [11]. Similarly, LiPON-type solid electrolytes are known for their good compatibility with lithium metal, while perovskite-type solid electrolytes are recognized for their ability to form good interfaces with lithium anodes.

this section provides a detailed analysis of the advantages and potential improvements of each type of solid electrolyte, to help researchers and industry professionals to make the right choice for their specific solid-state battery applications.

2.3.1. Solid Polymer Electrolytes

Polymer materials that include salts of lithium are known as solid polymer electrolytes. The most extensively researched and first material to incorporate lithium metal salt is Polyethylene oxide (PEO). PEO cannot be mixed with a liquid host because it may cause leakage. Despite being safe, flexible, and compatible, the ionic conductivity of these electrolytes is very low, ranging from 10^{-6}-10^{-8} S cm^{-1}, and their use in ASSLBs is limited due to poor mechanical strength and dendrite growth [12]. Researchers have reported combining polymers with other materials to enhance their performance and overcome these limitations. This new form of electrolytes is called composite solid-state electrolytes (CSSEs) and are considered as the solid electrolytes for future ASSLBs. CSSEs are divided into three types [13].

1. Inorganic- organic
2. Organic-organic

3. Inorganic-inorganic

Among these the inorganic/polymer are the most promising and widely investigated electrolytes. The following structure of CSSEs are used in LIBs:

- Polymer matrix incorporating inorganic fillers
- Polymer filled inorganic 3D framework
- Composite electrolytes with open framework
- Layered structures

2.3.2. Polymer matrix incorporating inorganic fillers

Depending on their ionic conductivities, inorganic fillers are classified as either active fillers or inert fillers. Although the actives have strong ionic conductivities and significant Li+ transference numbers, synthesising them is challenging, and they are difficult to tune using a polymer matrix. Active fillers are sensitive to CO_2 and moisture [14]. The interfacial resistance is quite high, the inert fillers have low conductivities, and they are affordable, simple to use, and tuneable in the matrix [15]. Adding inorganic fillers to the polymer matrix can enhance the ionic conductivity of solid composite electrolytes by reducing crystallinity, improving electrode-electrolyte interfacial stability, and increasing cation transfer-ence number. Inorganic fillers can be categorized into two types based on their Li ion conductivity: inert and active fillers. Inert fillers are typically oxide ceramic fillers that do not transport Li ions. In contrast, active fillers are ceramics that have high Li ion conductivity and can be involved in the ionic conduction process. The classification of fillers depends on the Li ion conductivity.

2.3.2.1. Inert Fillers

In the early 1980s, researchers Weston et al. [16] investigated the effects of adding Al_2O_3 as a filler to the PEO/Li salt electrolyte system in lithium batteries. They found that incorporating 10 vol.% of Al_2O_3 greatly improved the mechanical strength and ionic conductivity of the electrolyte system. Later on, Croce et al. [17] explored the use of both Al_2O_3 and TiO_2 as fillers in the PEO-LiClO$_4$ system. They found that these fillers could act as cross-linking centers for the PEO polymer segments, affecting the recrystallization kinetics and decreasing the crystallinity of the PEO polymer. This enhancement of ion transport within the PEO polymer chains was attributed to the increased amorphous phase and decreased crystalline phase in the presence of these fillers. The addition of these oxide ceramic fillers has also been shown to increase the electrochemical stability of the electrolyte, which is important for the safe and

reliable operation of lithium batteries. Additionally, these fillers have been found to reduce the risk of dendrite formation, which can cause short circuits and lead to battery failure. Overall, the use of inert oxide ceramic fillers such as Al_2O_3, SiO_2, and TiO_2 in lithium battery electrolytes has proven to be a promising strategy for improving the mechanical and electrochemical properties of the electrolyte system, leading to more reliable and efficient battery performance.

2.3.2.2. Active Fillers

In contrast to inert fillers, which increase the fraction ratio of filler while decreasing the ionic conductivity, active fillers offer strong ionic conductivities, allowing for the addition of additional filler material in the matrix [18]. Ga-LLZO, a garnet electrolyte based on gallium, creates a space charge area when it is submerged in a polymer matrix, leading to strong ionic conductivity. Defects already existing on the Ga-LLZO surface cause this region to form. The template solution approach is used to prepare the one- and two-dimensional active fillers. These fillers are added to polymer matrices using a variety of synthetic techniques [19]. By calcining PVP fibres that include the LLTO electrolyte precursors for perovskites, Liu et al. fabricated CSSE via the electrospinning process. The structure's vacancies encourage Li^+ ion hopping, which raises ionic conductivity [20].
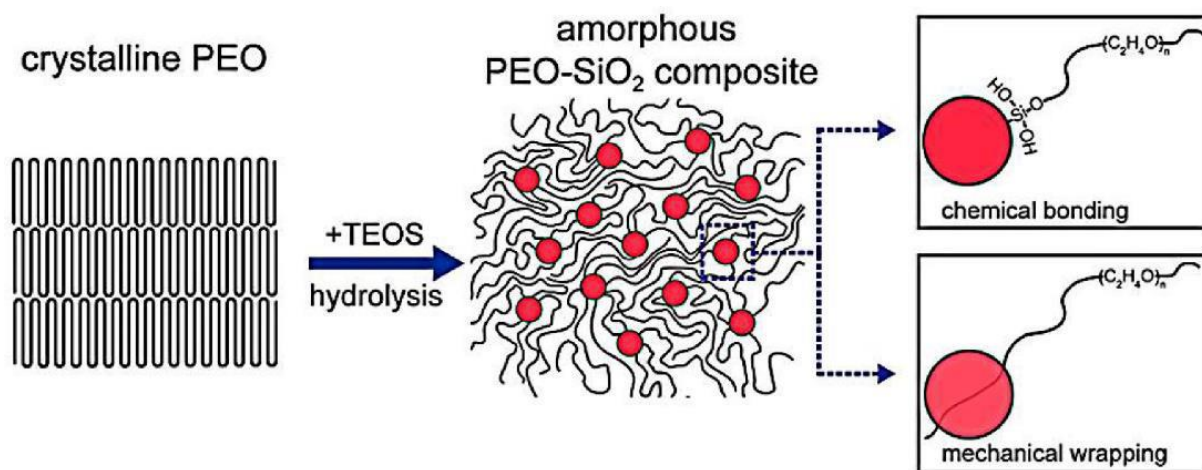
Figure 2.1: Schematic diagram of incorporation of SiO2 in PEO matrix

Ceramics of the garnet, NASICON, and perovskite types have lately been reported as active fillers. As first reported by Takahashi and Iwahara [21], [22] in 1971, perovskite-type ceramic fillers primarily have the structure of ABO_3, where A is typically a large cation of Ca, Sr, or La and B is typically a smaller cation of transition metal ions of Al or Ti. Larger A ions in particular can enhance the ionic conductivity of this type of ceramics [23]. The most significant

pervskite-type ceramic was created by Inaguma et al. [24] in 1993 and has the general formula $Li_{3x}La_{2/3}$-$xTiO_3$ (LLTO). NASICON-type ceramics are a type of active filler that have gained attention in recent years due to their ability to transport sodium ions efficiently. Some NASICON-type ceramics, such as $Li_{1+x}Al_xTi_{2-x}(PO_4)_3$ (LATP), can also transport lithium ions. LATP has been incorporated into various polymer matrices, including PEO and PVdF-HFP, to enhance their ionic conductivity and improve their electrochemical performance as solid-state electrolytes for LIB [25], [26]. Another promising type of active filler is garnet-type ceramics, such as $Li_7La_3Zr_2O_{12}$ (LLZO). Garnet-type ceramics have high Li-ion conductivity and excellent chemical stability, making them ideal for use as solid-state electrolytes in LIB. LLZO has been incorporated into polymer matrices, such as PEO and PVdF-HFP, to improve their ionic conductivity and electrochemical performance. LLZO has also been used as a coating material for lithium metal anodes to improve their stability and prevent dendrite growth. Dendrite formation is a significant problem in lithium metal anodes, and it can cause short circuits and lead to battery failure. The use of LLZO as a coating material has shown promise in addressing this issue and improving the overall performance and safety of LIB [27].
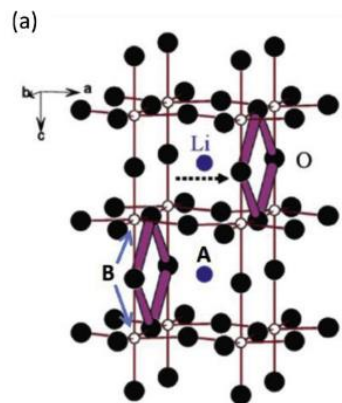
Figure 2.2: Perovskite-type structure

2.3.3. Polymer filled 3d framework

Polymer matrix can be made more conducive to high ionic conductivity by introducing fillers, which reduces crystal formation in the polymeric chain. In order to improve the electrochemical performance, numerous researchers are now focusing on inorganic fibres and rods [28]. A recent development involves 3D inorganic frameworks filled with polymers, which offer more free channels for lithium ion hopping than nanorods and wires [29]. These frameworks are created through sol-gel techniques and heat treatments. J. Bae et al. [30] have

produced a continuous 3D framework using the sol-gel method and subsequently incorporating polymer into the framework, resulting in an ionic conductivity in the range of 8.8×10^{-5} S cm^{-1} at room temperature.

2.4. Composite electrolytes with open framework:

The surface area of Metal oxide frameworks (MOFs), which consist of metal centers connected by organic linkers, can reach several thousand square meters per gram due to the development of void spaces within the coordination network of the organic molecules [31]. These materials have been employed in electrochemical systems as catalysts, electrode materials, and electrolytes [32] Fleker and colleagues have demonstrated that MOFs, due to their coordinating bonds, are nonconductive and have synthesized MOF-activated carbon compositions, where MOF nanoparticles in contact with activated carbon exhibit an interesting EPR signal [33]. In addition, the MOF's Cu^{2+}/Cu^{+} redox couple can increase the AC's double-layer capacitance by 30 %. Yaghi et al. have conducted a comprehensive study on the growth of MOF on graphene sets, where zirconium-MOF demonstrated an aerial capacitance of 5.09 μF cm^{-1} for over 10,000 charge/discharge cycles [34].

In the case of composite solid-state electrolytes (CSSEs), MOFs are typically incorporated into a polymer matrix dipped with Li salts. H. Huo et al. have developed a MOF filler-incorporated PEO with LiTFSi-based polymer matrix and a cell incorporating this SSE, which exhibited high ionic conductivity of 3.65×10^{-5} S cm^{-1}, higher than the pristine electrolyte compound. Research work has been extensively carried out on this type of CSSEs with Mg-tissue plasminogen activator (TPA) and Al-TPA-MOF [35].

2.4.1. Layered structures

CSSEs have a layered structure that consists of inorganic fillers in a polymer matrix, providing a flexible structure that can detect the advantages and disadvantages of lithium-ion hopping in each layer. These structures not only enhance the ionic conductivity and mechanical strength but also improve the interfacial contact between the electrode and electrolyte surfaces [36]. Based on the work of a group of scientists, the layered structures are mainly classified into double-layered and sandwich structures [37]

In the double-layered structure, a solid interface layer of polymer is situated between the inorganic pellet and Li metal anode, which reduces dendrite growth and interfacial resistance between the contacts, as illustrated in the figure [38].On the other hand, in the sandwich structure, the soft interface of polymer is utilized between both electrodes and the electrolyte.

For instance, W. Zhou has synthesized a CSSE comprising a ceramic layer ($L_{1.3}Al_{0.3}Ti_{1.7}(PO_4)_3$) sandwiched between two polymer layers (PEO and PEMA), which led to a decrease in interfacial contact [39].
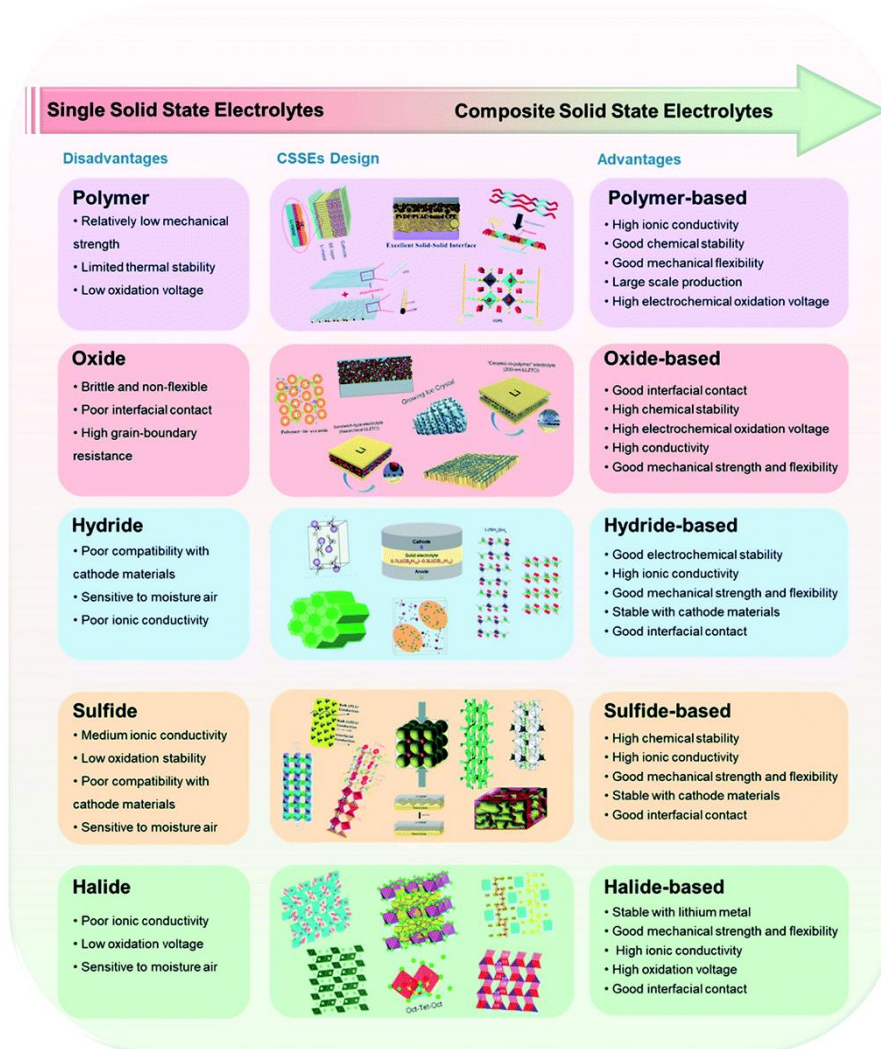
Figure 2.3: Types of solid state electrolytes and there advantages and disadvantages

2.5. Inorganic Electrolytes

Inorganic electrolytes, also known as ceramic electrolytes, have the ability to conduct lithium-ions, and they mainly consist of amorphous (glass) and crystalline structures. Among solid-state electrolytes (SSEs), inorganic electrolytes exhibit high ionic conductivities and thermal stability. Li ions' transference number in inorganic electrolytes is almost unity, making them single ion conductors. In ceramics, ion conduction occurs through vacancies and interstitial sites, as opposed to liquid electrolytes [40]. Inorganic solid electrolytes are classified into oxides and sulfides. However, some ceramics, such as lithium halides and lithium hydrides, have limitations such as poor contact with the cathode material and low ionic conductivity [41].

One of the most significant properties of ceramics is their electrochemical and thermal stability. Although ceramics possess high ionic conductivities and a wide voltage window, some of them are not stable at high temperatures, leading to dendrite growth, low electrochemical performance, and decomposition. The decomposition of the electrolyte forms a solid electrode interface (SEI) layer, which leads to an increase in the voltage window. This SEI layer also causes cell aging [42].

Research has been conducted to improve the electrochemical stability of ceramic electrolytes. For instance, a study by Minami et al. investigated the effect of adding Li_2O to $Li_{1.5}Al_{0.5}Ge_{1.5}(PO_4)_3$ (LAGP) electrolyte and demonstrated the formation of a stable SEI layer [42]. Another study by Chatterjee et al. focused on designing sulfide-based ceramic electrolytes with improved thermal stability and ionic conductivity by incorporating magnesium into the structure [43]. These studies indicate that efforts are being made to improve the stability of ceramic electrolytes, making them promising candidates for solid-state batteries [44].

2.5.1. Types of SSE's

Types of SSE (Inorganic oxide SSE)	Formula	References
Perovskite	$Li_{0.35}La_{0.55}TiO_3$	[45]–[50]
Garnet	$Li_7La_3Zr_2O_{12}$	[51]–[58]
LiPON	Li_3PO_4	[59]–[63]
LISICON	$Li_{1.4}Zn\,(GeO_4)_4$	[64]–[71]
NASICON	$Li_{1.3}Al_{0.3}Ti_{1.7}(PO_4)_3$	[72]–[81]

Table 2.1: Types of inorganic oxide SSEs

2.5.1.1. Perovskite-Type SSEs

Perovskite-type SSEs have been extensively studied due to their potential for use in solid-state batteries and fuel cells. These materials have the general formula ABX_3, where A and B represent metal ions, and X represents an anion, such as oxygen. The most widely studied perovskite-type SSEs are La-doped $BaTiO_3$, $SrTiO_3$, and $BaZrO_3$. The crystal structure of perovskite-type SSEs involves a three-dimensional network of metal-oxygen bonds formed by corner-sharing BX_6 octahedra [82]. This structure allows for the efficient transport of ions

within the material, which is critical for the high ionic conductivity of these materials. The metal ions A and B occupy different sites within the crystal structure, with A typically located at the corners of the unit cell and B at the centre. This arrangement creates a tetrahedral void in the centre of each octahedron, which can be occupied by other ions, such as lithium or sodium, to facilitate ion transport. The high chemical stability of perovskite-type SSEs is attributed to their strong metal-oxygen bonds and the absence of free anions. This stability makes them attractive candidates for use in harsh environments, such as high-temperature fuel cells [83].

Perovskite-type SSEs can be synthesized by various methods, such as solid-state reaction, sol-gel method, and hydrothermal method. Solid-state reaction involves mixing the starting materials and heating them at high temperature to form the perovskite-type SSE. The sol-gel method involves preparing a solution of the starting materials, followed by drying and heating to form the perovskite-type SSE. The hydrothermal method involves heating the starting materials in a sealed vessel under high pressure to form the perovskite-type SSE [84]. The ionic conductivity of perovskite-type SSEs can be improved by doping with rare earth elements or transition metals. Composite formation with carbon materials or metallic nanoparticles can also enhance the ionic conductivity of perovskite-type SSEs. The mechanical strength of perovskite-type SSEs can also be enhanced by the addition of dopants or sintering at high temperature.

In order to tackle this problem, Chung et al. [85] introduced substitutions of Sn^{4+}, Zr^{4+}, $Mn^{4+,}$ and Ge^{4+} for $Ti^{4+.}$ Their findings indicated that the ionic conductivity was improved by the introduction of Mn^{4+} and Ge^{4+}. However, to prevent the formation of a second phase, only a portion of the Ti^{4+} could be substituted, while the remainder could still be reduced. Thangadurai et al. [86] developed a stable perovskite-type solid electrolyte, $LiSr_{1.65}Zr_{1.3}Ta_{1.7}O_9$, which was capable of maintaining stability when in contact with lithium due to the stable oxidation states of Zr^{4+} and Ta^{5+}. However, the ionic conductivity of $LiSr_{1.65}Zr_{1.3}Ta_{1.7}O_9$ was found to be 1.3×10^{-5} S cm^{-1} at 30°C, which did not meet the requirement of 10^{-4} S cm^{-1} for solid electrolytes. In order to enhance the ionic conductivity, Chen et al. [87] investigated the composition of $Li_{2x-y}Sr_{1-x}Ta_yZr_{1-y}O_3$ and discovered that $Li_{3/8}Sr_{7/16}Ta_{3/4}Zr_{1/4}O_3$ (LSTZ) displayed the highest ionic conductivity, with bulk and grain boundary conductivities of 2×10^{-4} S cm^{-1} and 1.33×10^{-4} S cm^{-1} at 30 °C, respectively.
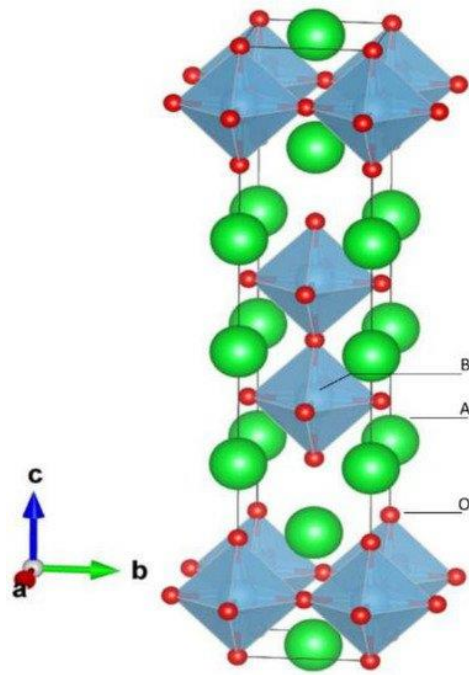
Figure 2.4: Perovskite crystal structure

2.5.1.2. Garnet-Type SSEs

Garnet-type solid-state electrolytes SSEs are a promising class of materials for use in solid-state batteries. The structure of these SSEs is composed of a three-dimensional network of corner-sharing BO_4 tetrahedra, which form the backbone of the structure. These tetrahedra are made up of a central cation, typically a metal such as aluminium or silicon, surrounded by four oxygen atoms. The A cations, which are typically smaller than the BO_4 tetrahedra, occupy the interstitial sites between the tetrahedra, creating an A-site disordered structure[88]. The high ionic conductivity of garnet-type SSEs is attributed to the presence of mobile lithium ions in the tetrahedral sites of the BO_4 framework. These lithium ions are able to move freely through the structure, hopping from one tetrahedral site to another, and are responsible for the high ionic conductivity of the material [89]. In addition to their high conductivity, garnet-type SSEs are also known for their stability, which is important for the long-term performance of solid-state batteries. Overall, the unique structure of garnet-type SSEs, with their interconnected network of BO_4 tetrahedra and mobile lithium ions, makes them an attractive material for use in solid-state batteries, which have the potential to be safer, more efficient, and longer-lasting than traditional liquid electrolyte batteries [90]. Garnet-type SSEs can be synthesized by various methods, such as solid-state reaction, sol-gel method, and hydrothermal method. Solid-state reaction involves mixing the starting materials and heating them at high temperature to form the garnet-type SSE. The sol-gel method involves preparing a solution of the starting

materials, followed by drying and heating to form the garnet-type SSE. The hydrothermal method involves heating the starting materials in a sealed vessel under high pressure to form the garnet-type SSE. The properties of garnet-type SSEs can be improved by doping with rare earth elements or transition metals. Composite formation with carbon materials or metallic nanoparticles can also enhance the ionic conductivity of garnet-type SSEs.

According to Murugan et al. [91],a new solid electrolyte with a garnet-type structure, $Li_7La_3Zr_2O_{12}$ (LLZO), was developed, demonstrating an ionic conductivity of approximately 3×10^{-4} S cm^{-1} at 25 °C. The crystal structure of LLZO was cubic, similar to $Li_5La_3M_2O_{12}$ (M = Ta, Nb) [89].The total ionic conductivity was high due to the grain boundary resistance being less than 50% of the total resistance, resulting in a similar magnitude of bulk ionic conductivity. Geiger et al. [92] discovered that the tetragonal phase of $Li_7La_3Zr_2O_{12}$ transitioned to a cubic phase at 100–150 °C, and the cubic phase showed higher ionic conductivity than the tetragonal phase. Hence, stabilization of the cubic phase at room temperature was deemed critical. Experimentally, it was found that a cubic phase could be obtained by sintering $Li_7La_3Zr_2O_{12}$ in an alumina crucible [92].
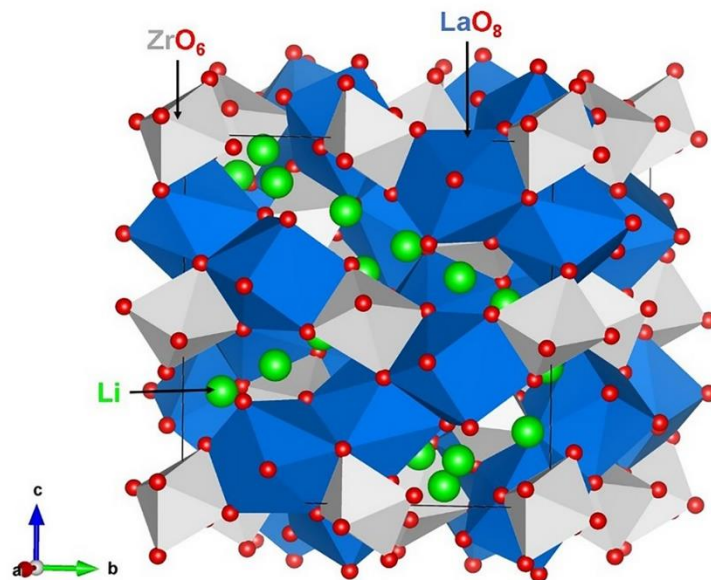
Figure 2.5: Garnet crystal structure

2.5.1.3. LiPON-type electrolytes

LiPON (Lithium Phosphorus Oxynitride) is a promising material for SSE, which can replace conventional liquid electrolytes in rechargeable batteries. The LiPON SSE has attracted significant attention due to its unique combination of excellent ionic conductivity, good thermal stability, and high electrochemical stability. The structure of LiPON SSE is an amorphous,

non-crystalline material that can be described as a random network of nitrogen, oxygen, phosphorus, and lithium atoms. The atomic arrangement of LiPON is not well-defined, and it lacks the long-range order and periodicity of crystalline materials. LiPON has a composition of $Li_{3.5}PO_{3.7}N_{0.3}$, which means that it consists of a mixture of Li, P, O, and N atoms in specific proportions. The LiPON structure is composed of a three-dimensional network of P-O and P-N bonds, with Li^+ ions occupying the interstitial sites within the network. The Li^+ ions are essential for the high ionic conductivity of LiPON, as they can easily migrate through the crystal structure and carry the charge [93].

The LiPON SSE exhibits high ionic conductivity, typically in the range of 10^{-6} to 10^{-5} S cm^{-1} at room temperature. This high ionic conductivity is due to the presence of Li^+ ions in the LiPON crystal lattice, which can easily migrate through the crystal structure. Additionally, LiPON exhibits good thermal stability, high electrochemical stability, and excellent compatibility with Li metal anodes.

LiPON films were prepared using various methods with different nitrogen doping levels and thicknesses. Li et al. [94] used ion beam assisted deposition (IBAD) to prepare LiPON films and achieved the highest ionic conductivity of 4.5×10^{-6} S cm^{-1} at room temperature when the nitrogen flow ratio was 1:8. Su et al. [95] prepared high nitrogen content LiPON films with a mean ionic conductivity of 4.9×10^{-6} S cm^{-1} at 22 °C and high transparency. Fujibayashi et al. [96] used metalorganic-chemical vapor deposition (MOCVD) to prepare LiPON films with ionic conductivities of 5.9×10^{-6} S cm^{-1} and 5.3×10^{-6} S cm^{-1} for thicknesses of 190 nm and 95 nm, respectively. Van-Jodin et al. [97] deposited LiPON films by RF sputtering in two ways: without magnetron (non-standard) and with magnetron (standard).
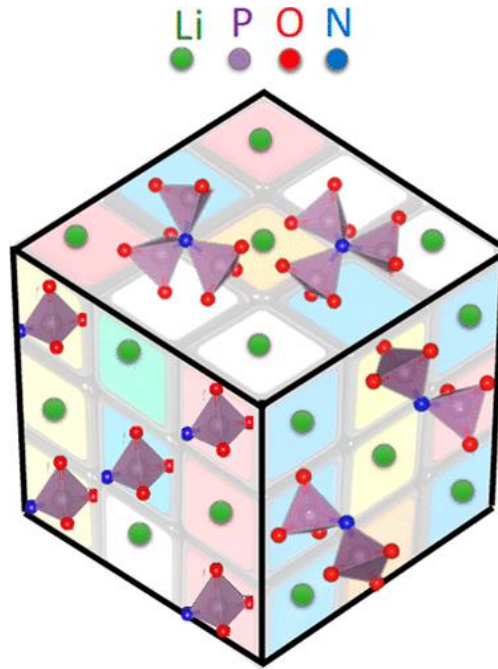
Figure 2.6: LiPON crystal structure

2.5.1.4. LISICON Electrolytes

Hong et al. reported the discovery of lithium superionic conductor (LISICON), where the electrolyte $Li_{1.4}Zn (GeO_4)_4$ displayed ionic conductivity of 1.25×10^{-1} S cm^{-1} above 100 °C, depending on bonding energy and channel size. The structure of LISICON creates weak bonds with three Li ions, allowing only two-dimensional movement of Li ions due to parallelogram-shaped channels. The introduction of interstitial atoms and vacancies improved the ionic conductivity, which was initially low [98]. Hue et al. synthesized solid solutions of lithium orthosilicate, lithium phosphate and $Li_{4-x}Si_{1-x}P_xO_4$, and found the highest ionic conductivity at x=0.5 and x=0.4 concentrations of 10^{-6} S cm^{-1}, by introducing interstitial lithium ions and substituting cation Si with phosphorus ion. However, a structural change occurred at these concentrations [99]. Song et al. partially doped oxygen O^{-1} and chlorine Cl^{-1} to synthesize $Li1_{0.42}Si_{1.5}P_{.5}Cl_{0.08}O_{11.92}$ and $Li_{10.42}Ge_{1.5}P_{.5}Cl_{0.08}O_{11.92}$ electrolytes, and achieved ionic conductivities of 1.03×10^{-5} S cm^{-1}and 3.7×10^{-5} S cm^{-1}. The large size of Cl^{-1} increases the lattice volume of channels, weakening the bonding between Li and Cl and releasing Li ions for conduction [100].

2.5.1.5. NASICON Electrolytes

NASICON-type materials LATP (Lithium Aluminum Titanium Phosphate) have been a focus of research in the world of solid-state electrolytes [101].In recent years, LATP has emerged as a highly promising SSE, attracting extensive research interest due to its exceptional properties,

including high ionic conductivity, thermal stability, and compatibility with cathodes [102]. As an ionic conductor with a rhombohedral structure, LATP facilitates lithium ion diffusion, allowing for efficient transport of lithium ions. LATP which is derived from LTP has a NASICON structure (Rhombohedral) which was first found in $NaX_2(PO_4)_3$ (X = Ti, Zr, Ge, V). The three-dimensional structure is constructed by sharing the top oxygen atom with two XO_6 octahedral and three PO_4 tetrahedral. Herein $NaX_2(PO_4)_3$ the sodium is replaced with Lithium and the X site is replaced with Titanium to form LTP, this NASICON structured rhombohedral provides a good pathway for lithium diffusion [103].Li can be found at three different sites which are arranged in an order of Alternating patterns [104].The M1 site (Li1, 6b, six-fold oxygen coordination), the M2 site (Li2, 18e, ten-fold oxygen coordination), and the M3 site (Li3, between M1 and M2, four-fold oxygen coordination) are commonly regarded as Li's three distinct sites in the NASICON structure [103].The high ionic conductivity of LATP is mainly attributed to the presence of lithium ions within the structure, enabling their free movement throughout the lattice. Despite the advancements achieved in the development of LATP, it still has a lower ionic conductivity than liquid electrolyte-based LIB [105].

$LiZr_2(PO_4)_3$ electrolyte was synthesized with Li ions instead of Na ions, resulting in a monoclinic phase at 1200 °C and an ionic conductivity of 3.3×10^{-6} S cm^{-1}, lower than its Na counterpart [106]. At high temperatures, the phase changed from monoclinic to rhombohedral, and the conductivity increased to 1.2×10^{-2} S cm^{-1}. Aono et al. reported on Ti-doped (LTP) NASICON type SSE, which showed the highest ionic conductivity among other dopants [107]. Kothari et al. reported in the concentration range of x=0.01, 0.03, 0.05, 0.07 the $Li_{1.3}Al_{0.3x}R_xTi_{1.7}(PO_4)_3$ (R=Ga^{3+}, Sc^{3+}, Y^{3+}) NASICON ceramic system demonstrated high ionic conductivity [108]. Doping trivalent cations in M^{+4} site increases the electrochemical performance in $Li_{1+x}Fe_xHf_{2-x}(PO_4)_3$, $Li_{1+x}Al_xTi_{2-x}(PO_4)_3$ (LATP), and $Li_{1+x}Al_xGe_{2-x}(PO_4)_3$ (LAGP), with ionic conductivities greater than 10^{-4} Scm^{-1} [109]. Wang et al. reported the affects of Aluminum dope LTP at different temperature ranges [110]. Among these, $Li_{1.3}Al_{0.3}Ti_{1.7}(PO_4)_3$ displayed the highest conductivity of 7×10^{-4} S cm^{-1} at room temperature, but Ti^{+4} reduces in the structure, resulting in low stability. Therefore, $Li_{1+x}Fe_xHf_2$-x$(PO_4)_3$ and $Li_{1+x}Al_xGe_{2-x}(PO_4)_3$ demonstrate good stability. Li_3PO_4 and Li_3BO_3 doping produced dense electrolytes with conductivity of 3×10^{-4} S cm^{-1} for LTP-0.2Li$_3$BO$_3$ [111].

LATP and LAGP SSEs are widely studied, but LATP suffers from incompatibility with lithium metal anode due to the reduction of Ti^{+4}. Two electrolytes were synthesized, LTP and $Li_3Ti_2(PO_4)_3$, both exhibiting rhombohedral structures, but with different lithium-ion

distribution [62]. LAGP electrolyte was developed by melt-quenching method, with an ionic conductivity of 4×10^{-4} S cm^{-1} at 25°C [63]. Adding Li$_2$O in the Li$_{1+x}$Al$_x$Ge$_{2-x}$(PO$_4$)$_3$ LAGP structure for x=0.5 increased the conductivity by forming secondary phases of lithium, improving the crystallization of glass, with grain and total conductivity values of 1.18×10^{-3} S cm^{-1} and 7.25×10^{-4} Scm^{-1} at RT [64]. The electrolyte was stable at 6 V with excellent electrochemical and thermal stability. Higher temperature sintering showed high ionic conductivities, but above 900 °C, impurity phase AlPO$_4$ was formed, decreasing the number of mobile lithium ions and affecting the conductivity [65]. LAGP shows high ionic conductivity, wide voltage window, and excellent electrochemical stability, but its application in ASSLBs is limited due to the expensive raw material GeO$_2$ used in the synthesis [66].
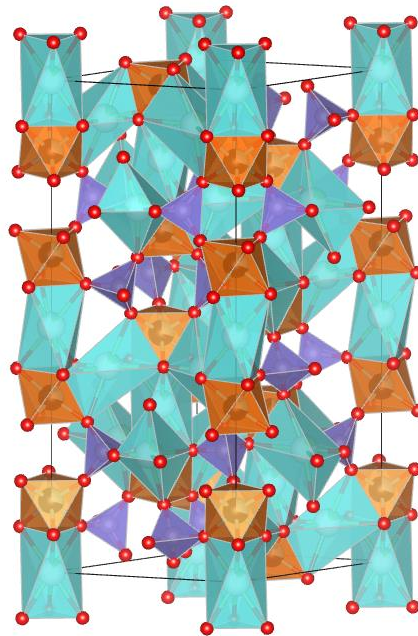
Figure 2.7: NASICON crystal structure

Summary

The present chapter presents an extensive survey of the literature on various types of solid-state electrolytes used in all-solid-state LIB (ASSLBs). The performance and other relevant characteristics of these electrolytes are thoroughly examined. The main focus of the chapter is on solid-state electrolytes, with particular attention paid to the progress made in this area. Furthermore, the limitations and benefits of oxide-based solid-state electrolytes are discussed in detail.

List of References

[1] H. H. L, W. X. M, C. S, D. Q. C, and C. S. B, "The synthesis and characterization of Li-ion solid electrolytes Li(1.3)Al(0.3)Ti(1.7)(PO4)3," *Journal of Artificial Crystal*, vol. 44, no. 01, pp. 195–199, 2015.

[2] S. C, L. J, G. Y, W. D. P, and Z. J, "Recent advances in all-solid-state rechargeable lithium batteries," *Nano Energy*, vol. 33, pp. 363–386, 2017.

[3] Y. Zhao and L. L. Daemen, "Superionic conductivity in lithium-rich anti-perovskites," *J Am Chem Soc*, vol. 134, no. 36, pp. 15042–15047, Sep. 2012, doi: 10.1021/JA305709Z/ASSET/IMAGES/LARGE/JA-2012-05709Z_0005.JPEG.

[4] B. A. Boukamp and R. A. Huggins, "Lithium ion conductivity in lithium nitride," *Phys Lett A*, vol. 58, no. 4, pp. 231–233, Sep. 1976, doi: 10.1016/0375-9601(76)90082-7.

[5] J. C. Bachman *et al.*, "Inorganic Solid-State Electrolytes for Lithium Batteries: Mechanisms and Properties Governing Ion Conduction," *Chem Rev*, vol. 116, no. 1, pp. 140–162, Jan. 2016, doi: 10.1021/ACS.CHEMREV.5B00563/ASSET/IMAGES/LARGE/CR-2015-005635_0025.JPEG.

[6] K. Takada, "Progress and prospective of solid-state lithium batteries," *Acta Mater*, vol. 61, no. 3, pp. 759–770, Feb. 2013, doi: 10.1016/J.ACTAMAT.2012.10.034.

[7] B. Scrosati, "History of lithium batteries," *Journal of Solid State Electrochemistry*, vol. 15, no. 7, pp. 1623–1630, 2011, doi: 10.1007/s10008-011-1386-8.

[8] L. Xu *et al.*, "Garnet Solid Electrolyte for Advanced All-Solid-State Li Batteries," *Adv Energy Mater*, vol. 11, no. 2, p. 2000648, Jan. 2021, doi: 10.1002/AENM.202000648.

[9] F. Zheng, M. Kotobuki, S. Song, M. O. Lai, and L. Lu, "Review on solid electrolytes for all-solid-state lithium-ion batteries," *J Power Sources*, vol. 389, pp. 198–213, Jun. 2018, doi: 10.1016/J.JPOWSOUR.2018.04.022.

[10] A. J. Samson, K. Hofstetter, S. Bag, and V. Thangadurai, "A bird's-eye view of Li-stuffed garnet-type Li7La3Zr2O12 ceramic electrolytes for advanced all-solid-state Li batteries," *Energy Environ Sci*, vol. 12, no. 10, pp. 2957–2975, Oct. 2019, doi: 10.1039/C9EE01548E.

[11] X.-B. Cheng *et al.*, "A Review of Solid Electrolyte Interphases on Lithium Metal Anode," *Advanced Science*, vol. 3, no. 3, p. 1500213, Mar. 2016, doi: 10.1002/ADVS.201500213.

[12] R. C. Agrawal and G. P. Pandey, "Solid polymer electrolytes: materials designing and all-solid-state battery applications: an overview," *J. Phys. D: Appl. Phys*, vol. 41, p. 18, 2008, doi: 10.1088/0022-3727/41/22/223001.

[13] K. Murata, S. Izuchi, and Y. Yoshihisa, "An overview of the research and development of solid polymer electrolyte batteries," *Electrochim Acta*, vol. 45, no. 8–9, pp. 1501–1508, Jan. 2000, doi: 10.1016/S0013-4686(99)00365-5.

[14] F. Deng *et al.*, "Microporous polymer electrolyte based on PVDF/PEO star polymer blends for lithium ion batteries," *J Memb Sci*, vol. 491, pp. 82–89, Oct. 2015, doi: 10.1016/J.MEMSCI.2015.05.021.

[15] M. Dirican, C. Yan, P. Zhu, and X. Zhang, "Composite solid electrolytes for all-solid-state lithium batteries," *Materials Science and Engineering R: Reports*, vol. 136. Elsevier Ltd, pp. 27–46, Apr. 01, 2019. doi: 10.1016/j.mser.2018.10.004.

[16] J. E. Weston and B. C. H. Steele, "Effects of inert fillers on the mechanical and electrochemical properties of lithium salt-poly(ethylene oxide) polymer electrolytes," *Solid State Ion*, vol. 7, no. 1, pp. 75–79, 1982, doi: 10.1016/0167-2738(82)90072-8.

[17] F. Croce *et al.*, "Physical and chemical properties of nanocomposite polymer electrolytes," *Journal of Physical Chemistry B*, vol. 103, no. 48, pp. 10632–10638, Dec. 1999, doi: 10.1021/JP992307U.

[18] S. A. Hashmi, Y. Bhat, M. K. Singh, & N. T. K. Sundaram, B. P. C. Raghupathy, and H. Tanaka, "Ionic liquid-based sodium ion-conducting composite gel polymer electrolytes: effect of active and passive fillers," *Journal of Solid State Electrochemistry*, doi: 10.1007/s10008-016-3284-6.

[19] J. Sharma and S. Hashmi, "Magnesium ion-conducting gel polymer electrolyte nanocomposites: Effect of active and passive nanofillers," *Polym Compos*, vol. 40, no. 4, pp. 1295–1306, Apr. 2019, doi: 10.1002/PC.24853.

[20]   J. Cui *et al.*, "Solid Polymer Electrolytes with Flexible Framework of SiO2 Nanofibers for Highly Safe Solid Lithium Batteries," *Polymers 2020, Vol. 12, Page 1324*, vol. 12, no. 6, p. 1324, Jun. 2020, doi: 10.3390/POLYM12061324.

[21]   V. Thangadurai and W. Weppner, "Recent progress in solid oxide and lithium ion conducting electrolytes research," *Ionics (Kiel)*, vol. 12, no. 1, pp. 81–92, 2006, doi: 10.1007/s11581-006-0013-7.

[22]   T. Takahashi and H. Iwahara, "Ionic conduction in perovskite-type oxide solid solution and its application to the solid electrolyte fuel cell," *Energy Conversion*, vol. 11, no. 3, pp. 105–111, 1971, doi: https://doi.org/10.1016/0013-7480(71)90121-5.

[23]   A. Manthiram, X. Yu, and S. Wang, "Lithium battery chemistries enabled by solid-state electrolytes," *Nat Rev Mater*, vol. 2, no. 4, 2017, doi: 10.1038/natrevmats.2016.103.

[24]   "1-s2.0-003810989390841A-main".

[25]   X. Liang, D. Han, Y. Wang, L. Lan, and J. Mao, "Preparation and performance study of a PVDF–LATP ceramic composite polymer electrolyte membrane for solid-state batteries," *RSC Adv*, vol. 8, no. 71, pp. 40498–40504, Dec. 2018, doi: 10.1039/C8RA08436J.

[26]   C. R. Mariappan, C. Yada, F. Rosciano, and B. Roling, "Correlation between micro-structural properties and ionic conductivity of Li1.5Al0.5Ge1.5(PO4)3 ceramics," *J Power Sources*, vol. 196, no. 15, pp. 6456–6464, Aug. 2011, doi: 10.1016/j.jpowsour.2011.03.065.

[27]   W. Lu, M. Xue, and C. Zhang, "Modified Li7La3Zr2O12 (LLZO) and LLZO-polymer composites for solid-state lithium batteries," *Energy Storage Mater*, vol. 39, pp. 108–129, Aug. 2021, doi: 10.1016/J.ENSM.2021.04.016.

[28]   X. Wang, M. Jiang, Z. Zhou, J. Gou, and D. Hui, "3D printing of polymer matrix composites: A review and prospective," *Compos B Eng*, vol. 110, pp. 442–458, Feb. 2017, doi: 10.1016/J.COMPOSITESB.2016.11.034.

[29]   S. sen Chi, Y. Liu, N. Zhao, X. Guo, C. W. Nan, and L. Z. Fan, "Solid polymer electrolyte soft interface layer with 3D lithium anode for all-solid-state lithium batteries," *Energy Storage Mater*, vol. 17, pp. 309–316, Feb. 2019, doi: 10.1016/J.ENSM.2018.07.004.

[30] J. Bae, Y. Li, F. Zhao, X. Zhou, Y. Ding, and G. Yu, "Designing 3D nanostructured garnet frameworks for enhancing ionic conductivity and flexibility in composite polymer electrolytes for lithium batteries," *Energy Storage Mater*, vol. 15, pp. 46–52, Nov. 2018, doi: 10.1016/J.ENSM.2018.03.016.

[31] S. Rajendran, M. Sivakumar, and R. Subadevi, "Effect of salt concentration in poly(vinyl alcohol)-based solid polymer electrolytes," *J Power Sources*, vol. 124, no. 1, pp. 225–230, Oct. 2003, doi: 10.1016/S0378-7753(03)00591-3.

[32] F. P. Nkosi *et al.*, "Garnet-Poly(ϵ-caprolactone- co-trimethylene carbonate) Polymer-in-Ceramic Composite Electrolyte for All-Solid-State Lithium-Ion Batteries," *ACS Appl Energy Mater*, vol. 4, no. 3, pp. 2531–2542, Mar. 2021, doi: 10.1021/ACSAEM.0C03098/ASSET/IMAGES/LARGE/AE0C03098_0008.JPEG.

[33] M. Yao, T. Yu, Q. Ruan, Q. Chen, H. Zhang, and S. Zhang, "High-Voltage and Wide-Temperature Lithium Metal Batteries Enabled by Ultrathin MOF-Derived Solid Polymer Electrolytes with Modulated Ion Transport," *ACS Appl Mater Interfaces*, vol. 13, no. 39, pp. 47163–47173, Oct. 2021, doi: 10.1021/ACSAMI.1C15038.

[34] M. Urgoiti-Rodriguez *et al.*, "Exploring ionic liquid-laden metal-organic framework composite materials as hybrid electrolytes in metal (ion) batteries," *Front Chem*, vol. 10, Sep. 2022, doi: 10.3389/FCHEM.2022.995063.

[35] Y. Jiang *et al.*, "Recent advances in lithium-based batteries using metal organic frameworks as electrode materials," *Electrochem commun*, vol. 122, p. 106881, Jan. 2021, doi: 10.1016/J.ELECOM.2020.106881.

[36] J. Mindemark, M. J. Lacey, T. Bowden, and D. Brandell, "Beyond PEO—Alternative host materials for Li+-conducting solid polymer electrolytes," *Prog Polym Sci*, vol. 81, pp. 114–143, Jun. 2018, doi: 10.1016/J.PROGPOLYMSCI.2017.12.004.

[37] J. Mindemark, M. J. Lacey, T. Bowden, and D. Brandell, "Beyond PEO—Alternative host materials for Li+-conducting solid polymer electrolytes," *Prog Polym Sci*, vol. 81, pp. 114–143, Jun. 2018, doi: 10.1016/J.PROGPOLYMSCI.2017.12.004.

[38] E. M. Masoud, A. A. El-Bellihi, W. A. Bayoumy, and M. A. Mousa, "Organic–inorganic composite polymer electrolyte based on PEO–LiClO4 and nano-Al2O3 filler for lithium

polymer batteries: Dielectric and transport properties," *J Alloys Compd*, vol. 575, pp. 223–228, 2013, doi: 10.1016/J.JALLCOM.2013.04.054.

[39] B. A. Abdulkadir, J. O. Dennis, M. Fadhlullah Bin Abd. Shukur, M. M. Elsayed Nasef, and F. Usman, "Preparation and characterization of gel polymer electrolyte based on PVA-K2CO3," *https://doi.org/10.1080/25740881.2020.1765380*, vol. 59, no. 15, pp. 1679–1697, Oct. 2020, doi: 10.1080/25740881.2020.1765380.

[40] R. Chen, W. Qu, X. Guo, L. Li, and F. Wu, "The pursuit of solid-state electrolytes for lithium batteries: from comprehensive insight to emerging horizons," *Mater Horiz*, vol. 3, no. 6, pp. 487–516, Oct. 2016, doi: 10.1039/C6MH00218H.

[41] E. Quartarone and P. Mustarelli, "Electrolytes for solid-state lithium rechargeable batteries: recent advances and perspectives," *Chem Soc Rev*, vol. 40, no. 5, pp. 2525–2540, Apr. 2011, doi: 10.1039/C0CS00081G.

[42] H. Yang *et al.*, "Polymer-ceramic composite electrolytes for all-solid-state lithium batteries: Ionic conductivity and chemical interaction enhanced by oxygen vacancy in ceramic nanofibers," *J Power Sources*, vol. 495, p. 229796, May 2021, doi: 10.1016/J.JPOWSOUR.2021.229796.

[43] R. Rajagopal, Y. Subramanian, and K. S. Ryu, "Improving the electrochemical performance of cathode composites using different sized solid electrolytes for all solid-state lithium batteries," *RSC Adv*, vol. 11, no. 52, pp. 32981–32987, Oct. 2021, doi: 10.1039/D1RA05897E.

[44] A. Manthiram, X. Yu, S. Wang, A. Manthiram, X. Yu, and S. Wang, "Lithium battery chemistries enabled by solid-state electrolytes," *NatRM*, vol. 2, no. 4, p. 16103, Feb. 2017, doi: 10.1038/NATREVMATS.2016.103.

[45] K. Kimura, K. Wagatsuma, T. Tojo, R. Inada, and Y. Sakurai, "Effect of composition on lithium-ion conductivity for perovskite-type lithium–strontium–tantalum–zirconium-oxide solid electrolytes," *Ceram Int*, vol. 42, no. 4, pp. 5546–5552, Mar. 2016, doi: 10.1016/J.CERAMINT.2015.12.133.

[46] R. Inada, K. Kimura, K. Kusakabe, T. Tojo, and Y. Sakurai, "Synthesis and lithium-ion conductivity for perovskite-type Li3/8Sr7/16Ta3/4Zr1/4O3 solid electrolyte by powder-

bed sintering," *Solid State Ion*, vol. 261, pp. 95–99, Aug. 2014, doi: 10.1016/J.SSI.2014.04.005.

[47] B. Huang *et al.*, "Li-Ion Conduction and Stability of Perovskite Li3/8Sr7/16Hf1/4Ta3/4O3," *ACS Appl Mater Interfaces*, vol. 8, no. 23, pp. 14552–14557, Jun. 2016, doi: 10.1021/ACSAMI.6B03070/ASSET/IMAGES/LARGE/AM-2016-03070Q_0006.JPEG.

[48] V. Thangadurai, A. K. Shukla, and J. Gopalakrishnan, "LiSr1.65□0.35B1.3B′ 1.7O9 (B = Ti, Zr; B′ = Nb, Ta): New lithium ion conductors based on the perovskite structure," *Chemistry of Materials*, vol. 11, no. 3, pp. 835–839, 1999, doi: 10.1021/CM9810382.

[49] C. H. Chen and K. Amine, "Ionic conductivity, lithium insertion and extraction of lanthanum lithium titanate," *Solid State Ion*, vol. 144, no. 1–2, pp. 51–57, Sep. 2001, doi: 10.1016/S0167-2738(01)00884-0.

[50] Y. Inaguma *et al.*, "High ionic conductivity in lithium lanthanum titanate," *Solid State Commun*, vol. 86, no. 10, pp. 689–693, Jun. 1993, doi: 10.1016/0038-1098(93)90841-A.

[51] J. F. Wu, W. K. Pang, V. K. Peterson, L. Wei, and X. Guo, "Garnet-Type Fast Li-Ion Conductors with High Ionic Conductivities for All-Solid-State Batteries," *ACS Appl Mater Interfaces*, vol. 9, no. 14, pp. 12461–12468, Apr. 2017, doi: 10.1021/ACSAMI.7B00614/ASSET/IMAGES/LARGE/AM-2017-006144_0006.JPEG.

[52] D. Rettenwander *et al.*, "Structural and Electrochemical Consequences of Al and Ga Cosubstitution in Li7La3Zr2O12 Solid Electrolytes," *Chemistry of Materials*, vol. 28, no. 7, pp. 2384–2392, Apr. 2016, doi: 10.1021/ACS.CHEMMATER.6B00579/ASSET/IMAGES/LARGE/CM-2016-00579M_0009.JPEG.

[53] D. Rettenwander *et al.*, "Structural and Electrochemical Consequences of Al and Ga Cosubstitution in Li7La3Zr2O12 Solid Electrolytes," *Chemistry of Materials*, vol. 28, no. 7, pp. 2384–2392, Apr. 2016, doi: 10.1021/ACS.CHEMMATER.6B00579/ASSET/IMAGES/LARGE/CM-2016-00579M_0009.JPEG.

[54] C. Bernuy-Lopez, W. Manalastas, J. M. Lopez Del Amo, A. Aguadero, F. Aguesse, and J. A. Kilner, "Atmosphere controlled processing of ga-substituted garnets for high li-ion conductivity ceramics," *Chemistry of Materials*, vol. 26, no. 12, pp. 3610–3617, Jun. 2014, doi: 10.1021/CM5008069/SUPPL_FILE/CM5008069_SI_001.PDF.

[55] Y. Li, J. T. Han, C. A. Wang, H. Xie, and J. B. Goodenough, "Optimizing Li+ conductivity in a garnet framework," *J Mater Chem*, vol. 22, no. 30, pp. 15357–15361, Jul. 2012, doi: 10.1039/C2JM31413D.

[56] R. Murugan, S. Ramakumar, and N. Janani, "High conductive yttrium doped Li7La3Zr2O12 cubic lithium garnet," *Electrochem commun*, vol. 13, no. 12, pp. 1373–1375, Dec. 2011, doi: 10.1016/J.ELECOM.2011.08.014.

[57] S. Ohta, T. Kobayashi, and T. Asaoka, "High lithium ionic conductivity in the garnet-type oxide Li7−X La3(Zr2−X, NbX)O12 (X = 0–2)," *J Power Sources*, vol. 196, no. 6, pp. 3342–3345, Mar. 2011, doi: 10.1016/J.JPOWSOUR.2010.11.089.

[58] R. Murugan, V. Thangadurai, W. Weppner, [R Murugan, W. Weppner, and V. Thangadurai, "Fast Lithium Ion Conduction in Garnet-Type Li7La3Zr2O12," *Angewandte Chemie International Edition*, vol. 46, no. 41, pp. 7778–7781, Oct. 2007, doi: 10.1002/ANIE.200701144.

[59] X. Yu, J. B. Bates, G. E. Jellison, and F. X. Hart, "A Stable Thin-Film Lithium Electrolyte: Lithium Phosphorus Oxynitride," *J Electrochem Soc*, vol. 144, no. 2, pp. 524–532, Feb. 1997, doi: 10.1149/1.1837443/XML.

[60] L. le Van-Jodin, A. Claudel, C. Secouard, F. Sabary, J. P. Barnes, and S. Martin, "Role of the chemical composition and structure on the electrical properties of a solid state electrolyte: Case of a highly conductive LiPON," *Electrochim Acta*, vol. 259, pp. 742–751, Jan. 2018, doi: 10.1016/J.ELECTACTA.2017.11.021.

[61] Y. Su *et al.*, "LiPON thin films with high nitrogen content for application in lithium batteries and electrochromic devices prepared by RF magnetron sputtering," *Solid State Ion*, vol. 282, pp. 63–69, Dec. 2015, doi: 10.1016/J.SSI.2015.09.022.

[62] G. Li, M. Li, L. Dong, X. Li, and D. Li, "Low energy ion beam assisted deposition of controllable solid state electrolyte LiPON with increased mechanical properties and

ionic conductivity," *Int J Hydrogen Energy*, vol. 39, no. 30, pp. 17466–17472, Oct. 2014, doi: 10.1016/J.IJHYDENE.2014.01.012.

[63]   J. B. Bates *et al.*, "Fabrication and characterization of amorphous lithium electrolyte thin films and rechargeable thin-film batteries," *J Power Sources*, vol. 43, no. 1–3, pp. 103–110, Mar. 1993, doi: 10.1016/0378-7753(93)80106-Y.

[64]   D. Mazumdar, D. N. Bose, and M. L. Mukherjee, "Transport and dielectric properties of lisicon," *Solid State Ion*, vol. 14, no. 2, pp. 143–147, Oct. 1984, doi: 10.1016/0167-2738(84)90089-4.

[65]   J. Kuwano and A. R. West, "New Li+ ion conductors in the system, Li4GeO4-Li3VO4," *Mater Res Bull*, vol. 15, no. 11, pp. 1661–1667, Nov. 1980, doi: 10.1016/0025-5408(80)90249-4.

[66]   Y. -W. Hu, I. D. Raistrick, and R. A. Huggins, "Ionic Conductivity of Lithium Orthosilicate—Lithium Phosphate Solid Solutions," *J Electrochem Soc*, vol. 124, no. 8, pp. 1240–1242, Aug. 1977, doi: 10.1149/1.2133537/XML.

[67]   S. Song, J. Lu, F. Zheng, H. M. Duong, and L. Lu, "A facile strategy to achieve high conduction and excellent chemical stability of lithium solid electrolytes," *RSC Adv*, vol. 5, no. 9, pp. 6588–6594, Dec. 2014, doi: 10.1039/C4RA11287C.

[68]   A. Khorassani, G. Izquierdo, and A. R. West, "The solid electrolyte system, Li3PO4Li4SiO4," *Mater Res Bull*, vol. 16, no. 12, pp. 1561–1567, 1981, doi: 10.1016/0025-5408(81)90029-5.

[69]   R. Kanno and M. Murayama, "Lithium Ionic Conductor Thio-LISICON: The Li[sub 2]S-GeS[sub 2]-P[sub 2]S[sub 5] System," *J Electrochem Soc*, vol. 148, no. 7, p. A742, 2001, doi: 10.1149/1.1379028.

[70]   J. L. Schaefer, Y. Lu, S. S. Moganty, P. Agarwal, N. Jayaprakash, and L. A. Archer, "Electrolytes for high-energy lithium batteries," *Applied Nanoscience (Switzerland)*, vol. 2, no. 2, pp. 91–109, Jun. 2012, doi: 10.1007/S13204-011-0044-X.

[71]   L. Suo, Y. S. Hu, H. Li, M. Armand, and L. Chen, "A new class of Solvent-in-Salt electrolyte for high-energy rechargeable metallic lithium batteries," *Nat Commun*, vol. 4, 2013, doi: 10.1038/NCOMMS2513.

[72] M. Illbeigi, A. Fazlali, M. Kazazi, and A. H. Mohammadi, "Effect of simultaneous addition of aluminum and chromium on the lithium ionic conductivity of LiGe2(PO4)3 NASICON-type glass–ceramics," *Solid State Ion*, vol. 289, pp. 180–187, Jun. 2016, doi: 10.1016/J.SSI.2016.03.012.

[73] J. S. Thokchom, N. Gupta, and B. Kumar, "Superionic Conductivity in a Lithium Aluminum Germanium Phosphate Glass–Ceramic," *J Electrochem Soc*, vol. 155, no. 12, p. A915, Oct. 2008, doi: 10.1149/1.2988731/XML.

[74] X. Xu, Z. Wen, X. Wu, X. Yang, and Z. Gu, "Lithium Ion-Conducting Glass–Ceramics of Li1.5Al0.5Ge1.5(PO4)3–xLi2O (x=0.0–0.20) with Good Electrical and Electrochemical Properties," *Journal of the American Ceramic Society*, vol. 90, no. 9, pp. 2802–2806, Sep. 2007, doi: 10.1111/J.1551-2916.2007.01827.X.

[75] J. Fu, "Fast Li+ ion conducting glass-ceramics in the system Li2O–Al2O3–GeO2–P2O5," *Solid State Ion*, vol. 104, no. 3–4, pp. 191–194, Dec. 1997, doi: 10.1016/S0167-2738(97)00434-7.

[76] H. Aono, E. Sugimoto, Y. Sadaoka, N. Imanaka, and G. Adachi, "Ionic Conductivity of Solid Electrolytes Based on Lithium Titanium Phosphate," *J Electrochem Soc*, vol. 137, no. 4, pp. 1023–1027, Apr. 1990, doi: 10.1149/1.2086597/XML.

[77] P. Goharian, B. Eftekhari Yekta, A. R. Aghaei, and S. Banijamali, "Lithium ion-conducting glass-ceramics in the system Li2O–TiO2–P2O5–Cr2O3–SiO2," *J Non Cryst Solids*, vol. 409, pp. 120–125, Feb. 2015, doi: 10.1016/J.JNONCRYSOL.2014.11.016.

[78] J. Fu, "Fast Li+ ion conduction in Li2O-Al2O3-TiO2-SiO 2-P2O5 glass-ceramics," *Journal of the American Ceramic Society*, vol. 80, no. 7, pp. 1901–1903, 1997, doi: 10.1111/J.1151-2916.1997.TB03070.X.

[79] H. Aono, N. Imanaka, and G. ya Adachi, "High Li+ Conducting Ceramics," *Acc Chem Res*, vol. 27, no. 9, pp. 265–270, Sep. 1994, doi: 10.1021/AR00045A002/ASSET/AR00045A002.FP.PNG_V03.

[80] H. Aono, E. Sugimoto, Y. Sadaoka, N. Imanaka, and G. ya Adachi, "Electrical property and sinterability of LiTi2(PO4)3 mixed with lithium salt (Li3PO4 or Li3BO3)," *Solid State Ion*, vol. 47, no. 3–4, pp. 257–264, Sep. 1991, doi: 10.1016/0167-2738(91)90247-9.

[81]   A. Aatiq, M. Ménétrier, L. Croguennec, E. Suard, and C. Delmas, "On the structure of Li3Ti2(Po4)3," *J Mater Chem*, vol. 12, no. 10, pp. 2971–2978, Oct. 2002, doi: 10.1039/B203652P.

[82]   Y. Inaguma, L. Chen, M. Itoh, and T. Nakamura, "Candidate compounds with perovskite structure for high lithium ionic conductivity," *Solid State Ion*, vol. 70–71, no. PART 1, pp. 196–202, May 1994, doi: 10.1016/0167-2738(94)90309-3.

[83]   Y. Inaguma *et al.*, "High ionic conductivity in lithium lanthanum titanate," *Solid State Commun*, vol. 86, no. 10, pp. 689–693, Jun. 1993, doi: 10.1016/0038-1098(93)90841-A.

[84]   Y. Zhao, Z. Liu, J. Xu, T. Zhang, F. Zhang, and X. Zhang, "Synthesis and characterization of a new perovskite-type solid-state electrolyte of Na1/3La1/3Sr1/3ZrO3 for all-solid-state sodium-ion batteries," *J Alloys Compd*, vol. 783, pp. 219–225, Apr. 2019, doi: 10.1016/J.JALLCOM.2018.12.289.

[85]   H. T. Chung, J. G. Kim, and H. G. Kim, "Dependence of the lithium ionic conductivity on the B-site ion substitution in (Li0.5La0.5)Ti1−xMxO3 (M=Sn, Zr, Mn, Ge)," *Solid State Ion*, vol. 107, no. 1–2, pp. 153–160, Mar. 1998, doi: 10.1016/S0167-2738(97)00525-0.

[86]   V. Thangadurai, A. K. Shukla, and J. Gopalakrishnan, "LiSr1.65□0.35B1.3B′ 1.7O9 (B = Ti, Zr; B′ = Nb, Ta): New lithium ion conductors based on the perovskite structure," *Chemistry of Materials*, vol. 11, no. 3, pp. 835–839, 1999, doi: 10.1021/CM9810382.

[87]   C. H. Chen, S. Xie, E. Sperling, A. S. Yang, G. Henriksen, and K. Amine, "Stable lithium-ion conducting perovskite lithium–strontium–tantalum–zirconium–oxide system," *Solid State Ion*, vol. 167, no. 3–4, pp. 263–272, Feb. 2004, doi: 10.1016/J.SSI.2004.01.008.

[88]   V. Thangadurai and W. Weppner, "Li6ALa2Ta2O12 (A = Sr, Ba): Novel Garnet-Like Oxides for Fast Lithium Ion Conduction," *Adv Funct Mater*, vol. 15, no. 1, pp. 107–112, Jan. 2005, doi: 10.1002/ADFM.200400044.

[89]   M. P. O'Callaghan and E. J. Cussen, "Lithium dimer formation in the Li-conducting garnets Li 5+xBaxLa3-xTa2O12 (0 < x ≤ 1.6)," *Chemical Communications*, no. 20, pp. 2048–2050, 2007, doi: 10.1039/b700369b.

[90]   F. Zheng, M. Kotobuki, S. Song, M. O. Lai, and L. Lu, "Review on solid electrolytes for all-solid-state lithium-ion batteries," *J Power Sources*, vol. 389, pp. 198–213, Jun. 2018, doi: 10.1016/j.jpowsour.2018.04.022.

[91]   R. Murugan, V. Thangadurai, W. Weppner, [R Murugan, W. Weppner, and V. Thangadurai, "Fast Lithium Ion Conduction in Garnet-Type Li7La3Zr2O12," *Angewandte Chemie International Edition*, vol. 46, no. 41, pp. 7778–7781, Oct. 2007, doi: 10.1002/ANIE.200701144.

[92]   C. A. Geiger *et al.*, "Crystal chemistry and stability of 'Li7La 3Zr2O12' garnet: A fast lithium-ion conductor," *Inorg Chem*, vol. 50, no. 3, pp. 1089–1097, Feb. 2011, doi: 10.1021/ic101914e.

[93]   N. Suzuki, T. Inaba, and T. Shiga, "Electrochemical properties of LiPON films made from a mixed powder target of Li3PO4 and Li2O," *Thin Solid Films*, vol. 520, no. 6, pp. 1821–1825, Jan. 2012, doi: 10.1016/J.TSF.2011.08.107.

[94]   G. Li, M. Li, L. Dong, X. Li, and D. Li, "Low energy ion beam assisted deposition of controllable solid state electrolyte LiPON with increased mechanical properties and ionic conductivity," *Int J Hydrogen Energy*, vol. 39, no. 30, pp. 17466–17472, Oct. 2014, doi: 10.1016/J.IJHYDENE.2014.01.012.

[95]   Y. Su *et al.*, "LiPON thin films with high nitrogen content for application in lithium batteries and electrochromic devices prepared by RF magnetron sputtering," *Solid State Ion*, vol. 282, pp. 63–69, Dec. 2015, doi: 10.1016/J.SSI.2015.09.022.

[96]   T. Fujibayashi, Y. Kubota, K. Iwabuchi, and N. Yoshii, "Highly conformal and high-ionic conductivity thin-film electrolyte for 3D-structured micro batteries: Characterization of LiPON film deposited by MOCVD method," *AIP Adv*, vol. 7, no. 8, p. 085110, Aug. 2017, doi: 10.1063/1.4999915.

[97]   L. le Van-Jodin, A. Claudel, C. Secouard, F. Sabary, J. P. Barnes, and S. Martin, "Role of the chemical composition and structure on the electrical properties of a solid state electrolyte: Case of a highly conductive LiPON," *Electrochim Acta*, vol. 259, pp. 742–751, Jan. 2018, doi: 10.1016/J.ELECTACTA.2017.11.021.

[98] H. H. Sumathipala, M. A. K. L. Dissanayake, and A. R. West, "Novel LISICON mixed conductors, Li4 − 2xCoxGeO4," *Solid State Ion*, vol. 86–88, no. PART 2, pp. 719–724, Jul. 1996, doi: 10.1016/0167-2738(96)00157-9.

[99] L. Chen *et al.*, "Bicontinuous Structure of Li3V2(PO4)3 Clustered via Carbon Nanofiber as High-Performance Cathode Material of Li-Ion Batteries," *ACS Appl Mater Interfaces*, vol. 7, no. 25, pp. 13934–13943, Jul. 2015, doi: 10.1021/ACSAMI.5B02618.

[100] M. Murayama, N. Sonoyama, A. Yamada, and R. Kanno, "Material design of new lithium ionic conductor, thio-LISICON, in the Li2S-P2S5 system," *Solid State Ion*, vol. 170, no. 3–4, pp. 173–180, May 2004, doi: 10.1016/J.SSI.2004.02.025.

[101] W. Xiao, J. Wang, L. Fan, J. Zhang, and X. Li, "Recent advances in Li1+xAlxTi2−x(PO4)3 solid-state electrolyte for safe lithium batteries," *Energy Storage Materials*, vol. 19. Elsevier B.V., pp. 379–400, May 01, 2019. doi: 10.1016/j.ensm.2018.10.012.

[102] V. Epp, Q. Ma, E.-M. Hammer, F. Tietz, and M. Wilkening, "Very fast bulk Li ion diffusivity in crystalline Li1.5Al0.5Ti1.5(PO4)3 as seen using NMR relaxometry," *Physical Chemistry Chemical Physics*, vol. 17, no. 48, pp. 32115–32121, Dec. 2015, doi: 10.1039/C5CP05337D.

[103] J. Zhu *et al.*, "Insights into the local structure, microstructure and ionic conductivity of silicon doped NASICON-type solid electrolyte Li1.3Al0.3Ti1.7P3O12," *Energy Storage Mater*, vol. 44, pp. 190–196, Jan. 2022, doi: 10.1016/j.ensm.2021.10.003.

[104] B. Zhang, Z. Lin, H. Dong, L. W. Wang, and F. Pan, "Revealing cooperative Li-ion migration in Li1+: XAlxTi2- x(PO4)3 solid state electrolytes with high Al doping," *J Mater Chem A Mater*, vol. 8, no. 1, pp. 342–348, Jan. 2020, doi: 10.1039/c9ta09770h.

[105] M. Fan, X. Deng, A. Zheng, and S. Yuan, "Solvothermal synthesis high lithium ionic conductivity of Gd-doped Li 1. 3 Al 0. 3 Ti 1. 7 (PO 4) 3 solid electrolyte," *Functional Materials Letters*, vol. 14, no. 3, Apr. 2021, doi: 10.1142/S1793604721400026/SUPPL_FILE/S1793604721400026_SM03.AVI.

[106] B. Yan *et al.*, "NASICON-structured solid-state electrolyte Li 1.5 Al 0.5-x Ga x Ge 1.5 (PO 4) 3 prepared by microwave sintering," *Materials Technology*, vol. 34, no. 6, pp. 356–360, May 2019, doi: 10.1080/10667857.2018.1563964.

[107] M. Giarola *et al.*, "Structure and Vibrational Dynamics of NASICON-Type LiTi2(PO4)3," 2017, doi: 10.1021/ACS.JPCC.6B11067.

[108] D. H. Kothari and D. K. Kanchan, "Effect of doping of trivalent cations Ga3+, Sc3+, Y3+ in Li1.3Al0.3Ti1.7 (PO4)3 (LATP) system on Li+ ion conductivity," *Physica B Condens Matter*, vol. 501, pp. 90–94, Nov. 2016, doi: 10.1016/J.PHYSB.2016.08.020.

[109] M. Monchak *et al.*, "Lithium Diffusion Pathway in Li1.3Al0.3Ti1.7(PO4)3 (LATP) Superionic Conductor," 2016, doi: 10.1021/ACS.INORGCHEM.5B02821.

[110] S. Wang, L. Ben, H. Li, and L. Chen, "Identifying Li+ Ion Transport Properties of Aluminum Doped Lithium Titanium Phosphate Solid Electrolyte at Wide Temperature Range," *Solid State Ion*, vol. 268, pp. 110–116, Dec. 2014, doi: 10.1016/j.ssi.2014.10.004.

[111] R. Wang *et al.*, "Preparation, Microstructure and Electrical Conductivity of LATP/LB Glass Ceramic Solid Electrolytes," *J Phys Conf Ser*, vol. 2101, no. 1, p. 012081, Nov. 2021, doi: 10.1088/1742-6596/2101/1/012081.

Chapter 3: Review on Experimentation and Characterization Methods

3.1. Synthesis Method

For the proper synthesis of the electrolyte material in the lab, many methods have been devised. Among them, some methods require special equipment while others can be performed without them. Choice of the synthesis process to form mainly rests on the preferred size, suitable properties of the surface, and the kind of material that is concerned such as semiconductors, metals, polymers, ceramics, etc. These methods have been researched and improved to increase the yield of SSEs, obtain better structural properties and purity. Some of these methods have been discussed below:

3.2. Solid-state method

Solid-state synthesis is a well-established method for preparing inorganic solid electrolytes. The process involves mixing chemical precursors and ball milling, followed by solid-state reaction and densification through calcination and sintering at high temperatures (700-1200 °C) for extended periods (>12 hours). The high-temperature treatment is necessary to achieve maximum densification and reduce grain boundary resistance, resulting in samples with large grains, less grain boundaries, high density, and great ionic conductivity. However, this process may cause lithium loss and secondary phase formation, leading to a negative impact on Li-ion conductivity [1]. The sintering temperature and time affect the final product's cell volume, phase purity, relative density, and ionic conductivity.

During the solid-state reaction, the chemical precursors react to form the desired LATP phase, which is a complex, three-dimensional network of Li^+, Al^{3+}, Ti^{4+}, and $(PO_4)^{3-}$ ions [2] .The precise reaction pathway and product composition depend on the specific conditions of the synthesis process, including the type and amount of precursor materials used, the sintering temperature and duration, and the atmosphere in which the reaction takes place.

Based on the experimental observations, this thesis proposes that the solid-state method of synthesizing SSEs results in finely ground powders with improved properties, including good interfacial contact, phase homogeneity, and low sintering temperatures. In particular, the study found that the grain resistance of LTP samples synthesized using this method remained unchanged, but the activation energy decreased and the grain boundary resistance was altered

[3]. These results suggest that the solid-state method may be a promising approach for fabricating SSEs with enhanced performance in lithium-ion batteries.

Overall, the solid-state method is a well-established and widely used technique for synthesizing LATP and other solid-state electrolyte materials. While the process can be time-consuming and require high temperatures, it offers precise control over the material's composition and properties, and can produce highly crystalline, defect-free samples with excellent ionic conductivity.

The solid-state method of material synthesis can be broken down into several key steps, including:

- Selection of suitable material
- Mixing of the selected materials
- Formation of pellets from the mixture
- Thermal treatment of the pellets
- Analysis of the resulting material

These steps are essential for achieving the desired material properties and ensuring the quality and performance of the final product.
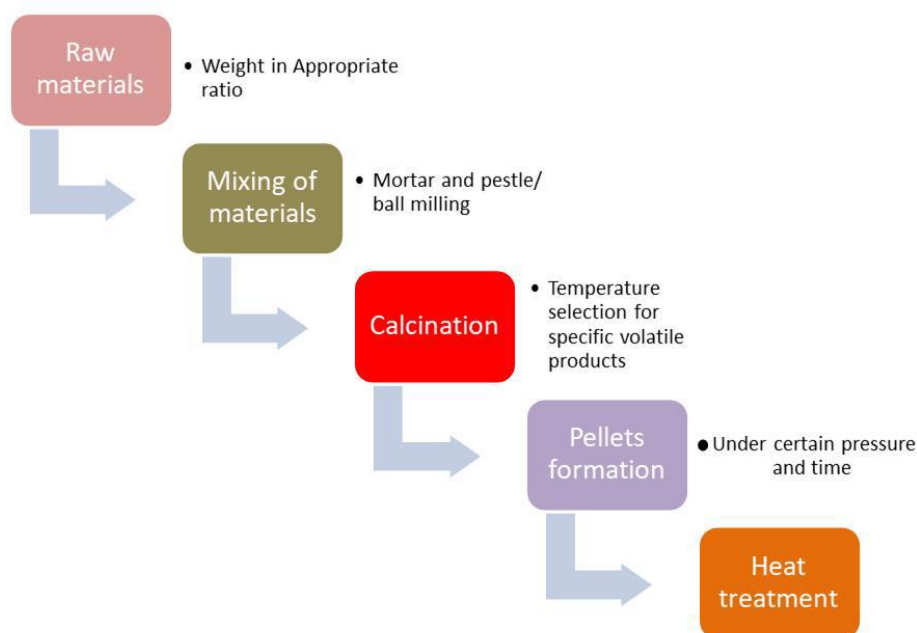
Figure 3.1: Flow chart of solid-state synthesis method

3.2.1. Appropriate material selection:

To maximize the surface area and promote effective particle contact, the solid-state method typically involves the use of fine powders as starting materials. These materials should be highly reactive rather than inert, and their composition must be precisely defined from the outset. In the case of lithium aluminum titanium phosphate (LATP) solid-state electrolytes (SSEs), the starting materials typically consist of lithium hydroxide monohydrate ($LiOH.H_2O$), aluminum oxide (Al_2O_3), titanium oxide (TiO_2), and ammonium dihydrogen phosphate ($NH_2H_2PO_4$) [4].

3.2.2. Mixing

Typically, the fine ground materials are mixed thoroughly using a mortar and pestle for a duration of 15-20 minutes. However, in the case of oxide materials, a planetary ball milling process is used for the mixing step. This technique allows for the creation of a homogeneous mixture by subjecting the materials to mechanical grinding and milling within a sealed container, which helps to prevent contamination and ensures a consistent particle size distribution throughout the mixture.

3.2.3. Calcination

The solid-state method involves subjecting the starting materials to a heat treatment process in order to decompose certain compounds, form the desired starting material, and produce the final product. For example, in the case of LATP solid-state electrolytes, the starting materials

are subjected to a heat treatment process that causes the decomposition of volatile products such as carbon dioxide (CO_2), water (H_2O), and ammonia (NH_3). Additionally, the ammonium dihydrogen phosphate ($NH_2H_2PO_4$) undergoes decomposition to produce phosphate ions $(PO_4)^{3-}$, which are necessary for the formation of the final product.

3.2.4. Pellets formation

In order to enhance the contact between the reagents and minimize contact with the sample crucible, the solid-state method involves the formation of pellets under a specific pressure. To hold the materials together in pellet form, an organic binder may be used. This process helps to ensure a uniform distribution of the starting materials and promotes the formation of the desired product with optimal properties [5].

3.2.5. Thermal treatment

to obtain the desired product from the oxide reaction, the sample is subjected to a sintering process at a specific temperature. The temperature chosen is influenced by various factors such as Tamman's rule and the potential for volatilization. According to Tamman's rule, the reaction will not take place until the temperature reaches two-thirds of the melting point of one of the reagents. Additionally, the reaction atmosphere is crucial to the process.

3.3. Sol-gel synthesis

Sol-gel method offers an efficient synthetic path for crystalline LATP solid electrolytes using a solvent intermediate step to form a colloidal solution and then a gel network, followed by the heat treatment for crystallization With the sol-gel method, it is possible to obtain pure materials at lower heat treatment temperatures and shorter times compared to solid-state synthesis and melt-quenching method. In addition, the solgel method also enables for a large-scale synthesis of LATP solid electrolytes [6]. During the sol-gel process, the precursors, the solvents, as well as the heat treatment all affect the crystal structure, composition and the conductivity of produced solid electrolytes To obtain pure phase and high ion-conduction, these synthetic parameters. Pechini process, a modified sol-gel method, is defined by the introduction of an alpha-hydroxycarboxylic acid, such as citric acid, to the mixed precursors in aqueous solution, which results in the chelation of the solution- i.e. a large and crosslinked network is formed. After the polymerization and decomposition in the following heat treatment processes, nanosized LATP particles are obtained- typically 20-50 nm [7].

Wu et al. synthesized the LATP electrolyte by sol-gel method using organic compounds, the conductivity obtained was 1.2×10^{-4} S cm^{-1} which is higher than solid-state reaction prepared LATP. The extensive and sensitive method of gel formation limits its use in large scale

production of ASSLBs [8]. The phosphate ion was not soluble in alcohol solutions therefor, Schroeder et al. synthesized the LATP electrolyte by using water and ethanol as solvents for gel formation and addition of nitric acid helped in the solubility of phosphate group. The detail synthesis procedure by sol-gel method is discussed in figure below.
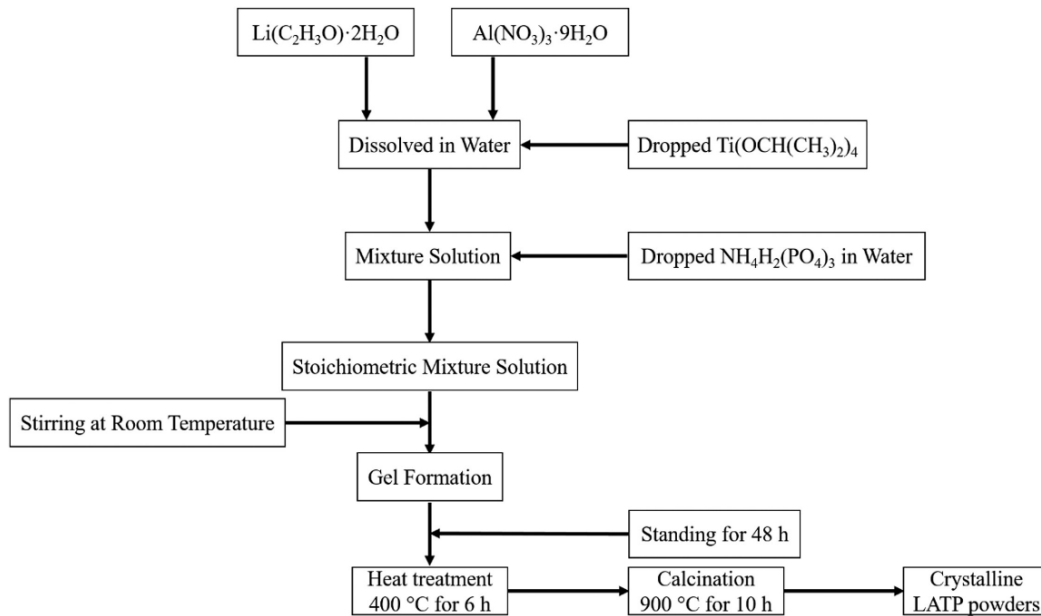
Figure 3.2: Process Sol-gel method for synthesis of LATP SSE

3.4. Co-precipitation

The co-precipitation method is a commonly used technique for the synthesis of fine crystallites of desired oxides. It involves dissolving salt compounds of two desired precursors in an aqueous solution and then precipitating them through pH adjustment. Subsequently, the resulting powders undergo intermediate to high-temperature calcination to produce the desired oxides. Although co-precipitation is good for mass production, it is associated with high costs due to the required chemicals and secondary phases that can plague the resulting product [9]conducted a study that investigated the effects of sintering temperature and holding time on the phase purity and ionic conductivity of produced LATP. They found that a sample sintered at 900 ℃ for 6 hours exhibited the maximum relative density of 97% and the highest Li-ion conductivity of 1.83×10^{-3} S cm^{-1}. This suggests that controlling sintering temperature and holding time can significantly improve the quality and performance of the resulting product. However, further research is needed to optimize the co-precipitation method and mitigate the associated costs and potential issues with secondary phases.

Figure 3.3: Process for Co-precipitation method for synthesis of SSE

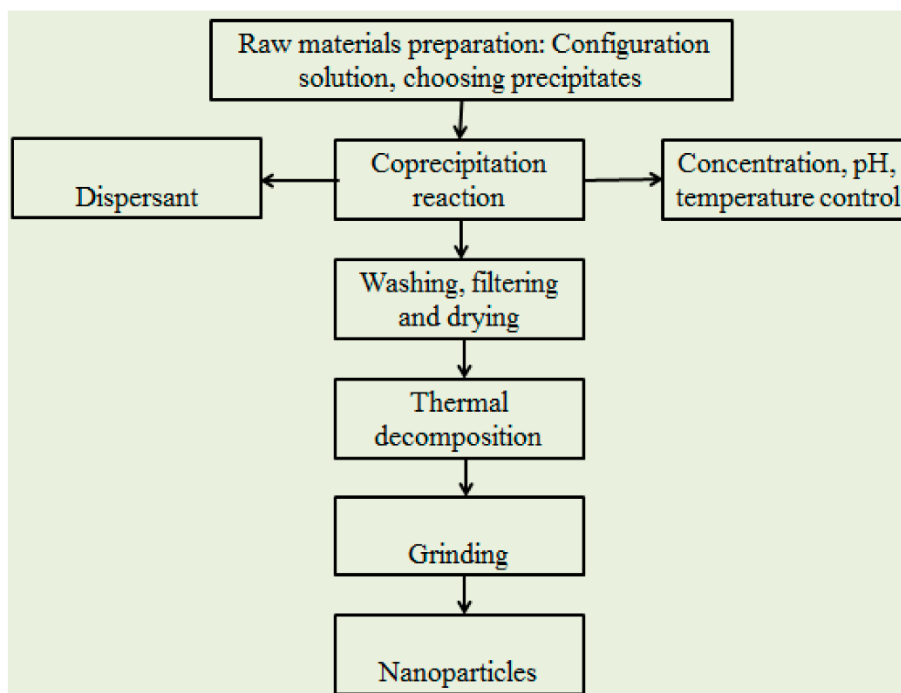## 3.5. Solvothermal Synthesis

The synthesis of materials, such as semiconductors, metals, polymers, and ceramics, is achieved through various methods, including the solvent-based process. The solvent-based process involves using a solvent under moderate to high pressure (between 1 atm and 10,000 atm) and temperature (from 100 °C to 1000 °C) to facilitate the interaction of precursors during synthesis. The hydrothermal process is a specific type of solvent-based process that uses water as the solvent, and the conditions are usually kept at the supercritical temperature of water (374 °C) [10].

This method can be used to produce a wide range of material geometries, such as thin films, single crystals, bulk powders, and nanocrystals. Additionally, the formation of crystals in various shapes such as rods (2D), spheres (3D), and wires (1D) can be controlled through the manipulation of the concentration of the chemical of interest, solvent supersaturation, and kinetic control. The solvent-based process is a versatile technique that can be used to form novel elements that are not easily constructed using other synthetic paths, and it can produce stagnant and thermodynamically stable forms [11].

Recent advances in the solvent-based process, such as the solvothermal process and the production of nanocrystals, have gained significant attention in the last decade. In fact, 80% of the literature on the solvent-based process in the past ten years has focused on nanocrystals.

This review will emphasize recent advances in the solvent-based process, with a particular focus on the solvothermal process and nanocrystalline production. By exploring the latest research, this review aims to highlight the potential of the solvent-based process in producing novel materials with unique properties and applications.

3.6. Hydrothermal Synthesis

The synthesis of materials that require special conditions can be achieved using a specific method that allows for control of their structure, morphology, and other properties. This method is known as the hydrothermal synthesis and is particularly useful for synthesizing metal oxides, halides, and composites that require specific temperature and pressure conditions [12], [13]. This method is also effective for producing nanoparticles with characteristic properties.

Typically, hydrothermal synthesis requires the use of an autoclave device, which allows for simultaneous control of temperature and pressure. The significance of this method lies in its ability to synthesize a wide range of nanoparticles with upgraded composition, size, structure, and chemistry of the surface [13]. Additionally, hydrothermal synthesis is an affordable method for synthesizing a wide variety of materials.

hydrothermal synthesis is a versatile and cost-effective method for synthesizing materials with specific properties. This method has proven useful in the synthesis of nanoparticles with unique characteristics, such as high surface area and antibacterial activity. Future research in this area could focus on expanding the range of materials that can be synthesized using hydrothermal synthesis and optimizing the process for specific applications.
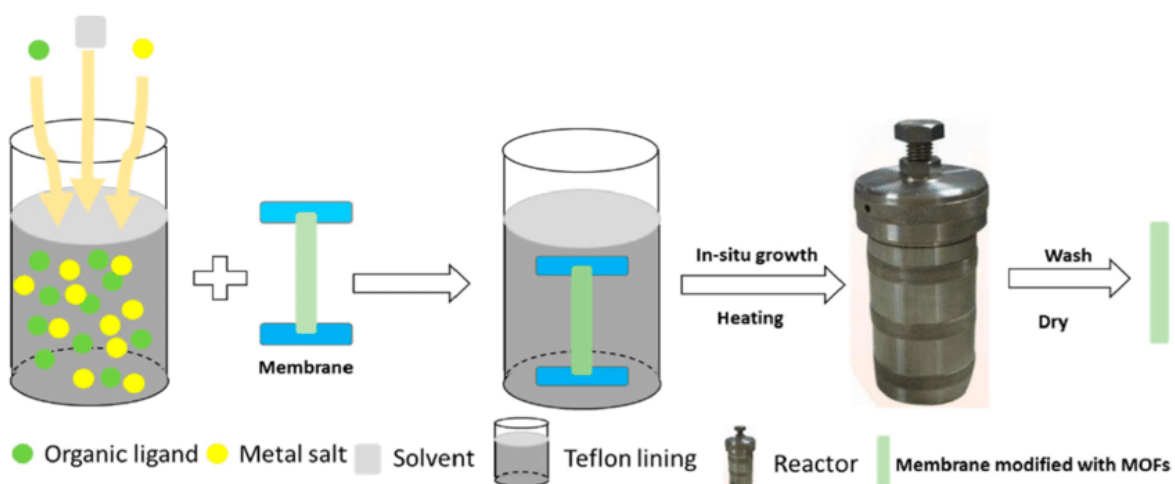

Figure 3.4: Solvothermal/Hydrothermal synthesis of SSE

3.7. Pyrolysis

Pyrolysis is a process that involves the thermal decomposition of organic matter in an oxygen-free environment, resulting in the production of non-condensable gases, condensable liquids, and biochar or charcoal as a residual solid product. This process has been increasingly utilized in the synthesis of solid-state electrolytes, which are critical components in a wide range of energy storage and conversion devices, such as batteries, fuel cells, and supercapacitors.

The use of pyrolysis in the production of solid-state electrolytes has several advantages over other synthesis methods. First, pyrolysis allows for the production of highly pure and homogeneous electrolytes with well-defined chemical and structural properties Additionally, pyrolysis can be used to produce solid-state electrolytes with a wide range of compositions and morphologies, including nanostructured materials that exhibit improved ion transport properties [14].

3.8. Characterization Techniques
3.8.1. X-Ray Diffraction (XRD)

X-ray diffraction (XRD) is a crucial characterization tool in the field of solid-state chemistry and materials science. This method offers valuable information regarding the structural properties of materials, including interatomic distances, bond angles, and crystallinity. The fundamental principle of XRD is based on the interaction of X-rays with a crystal lattice, which allows for the determination of atomic structural arrangements. It uses X-ray radiations that pass through the material at an angle to the source. The diffraction angle is calculated, and the intensity is recorded. At an angle how many radiations deflect from a specific plane on the material gives information regarding its structure morphology [15]. The effectiveness of X-rays for analyzing atomic structural arrangements is attributed to their wavelength, which falls in the 1×10^{-10} m range, similar to the order of magnitude of atomic spacings in crystalline solids. When X-rays interact with a crystal lattice, a simple model known as Bragg's law is used to understand the necessary conditions for diffraction. Bragg's law states that:
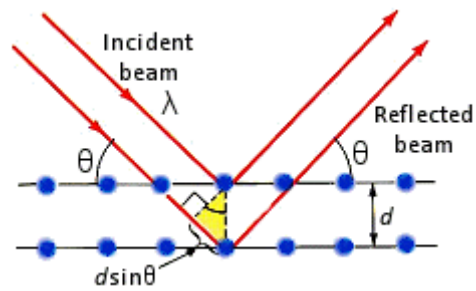
$n\lambda = 2dsin\theta$ $\qquad$ (eq. 3)

Figure 3.5: The Bragg's Law.

where λ represents the wavelength of the X-ray, d is the spacing between layers of atoms, θ is the angle between the incident X-ray beam and the scattering plane, and n is an integer. Consequently, when atoms are arranged in a periodic fashion in crystals, the diffracted waves will exhibit sharp interference maxima, or peaks, with the same symmetry as the distribution of atoms [16]. Therefore, the diffraction peaks can be utilized to reveal the structural information of the crystals.

The shape and size of the materials unit cell determine directions of likely diffractions [17]. The atom's arrangement in the crystal structure affects the diffracted wave intensities. Many materials are not one crystal rather are comprised of little, small crystallites in all likely directions which are called polycrystalline powder or aggregate. When a material with casually focused crystallites is put in an X-ray, the beam will view all available interatomic planes. If the experimental angle is scientifically altered, then all the available diffraction peaks from the substance will be identified [18].

3.8.2. Scanning Electron Microscopy
A scanning electron microscope (SEM) is a tool used to make images of solid samples and determine their elemental composition. The magnification range of an SEM is typically 20X to 50X at the low end and up to one million at the high end. SEM images generally show the topography of a sample. Backscattered electrons (BSE) can also be used to create images that show the composition of a sample, as the number of BSEs emitted is a function of the atomic number of the sample. X-rays generated by an SEM can be analyzed to determine the elements present in a sample, and if the X-ray data is mapped as a function of spatial position, an X-ray map showing the distribution of the elements can be created. However, it is not possible to determine the roughness of a sample from a plane view image, as roughness can only be determined from a cross-section of the sample. The detection limit for EDS X-ray data is typically 0.5% by weight within the X-ray generation volume [18].

The information of the substance like chemical composition, crystalline structure, external morphology (texture), and materials orientation will be revealed signals of the electron beam and sample interactions. In various applications, a 2-dimensional image is created that shows spatial variations in these properties, and numbers are collected over a particular choice area of the sample surface[19].

This method is exclusively valuable in semi quantitatively or qualitatively identifying chemical contents (by EDS), crystal orientations (using electron backscatter diffraction EBSD), and crystalline structure. The SEM is proficient in executing analyses of a specific area or point locations on the sample object.

Its design and function are quite comparable to the electron probe micro-analyzer (EPMA) and significant connections in abilities remain between the two devices [20].
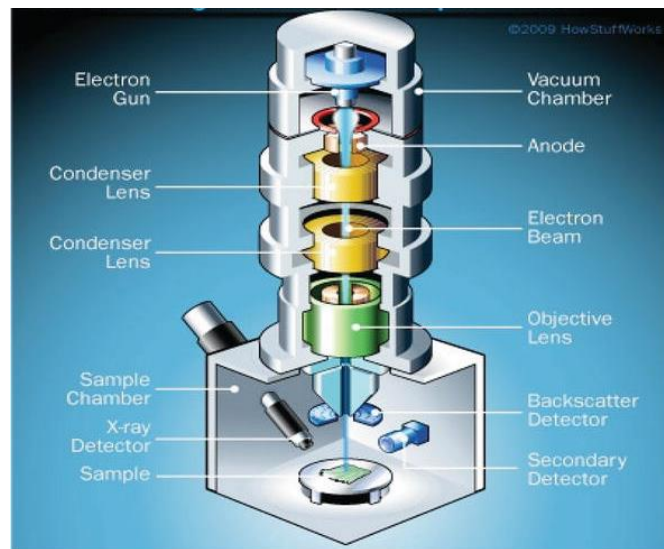
Figure 3.6: Working principle of SEM

3.8.3. Transmission Electron Microscopy (TEM)

Transmission Electron Microscopy (TEM) is an invaluable technique for characterizing materials at the atomic level with high spatial resolution. It offers a wide range of capabilities, including the ability to examine morphology, size distribution, crystal structure, defects, strain, and even chemical information. All the information provided by TEM is obtained through electron-sample interactions. TEM is a highly effective technique for investigating solid-state electrolytes like LATP at the atomic level. With TEM, researchers can obtain critical insights into the crystal structure, morphology, and chemical composition of the material, as well as the spatial distribution of constituent atoms. Moreover, TEM can provide information on defects

and other nanoscale phenomena that may have a direct influence on the performance of LATP as a solid-state electrolyte.[21]

In order to obtain TEM images, the LATP sample must be ultrathin, typically less than 200 nm in thickness, to enable the transmission of electrons through the sample. Utilizing TEM imaging and analysis, researchers can optimize the synthesis and processing of LATP to achieve desirable atomic-scale properties, leading to an enhanced performance of LATP as a solid-state electrolyte for advanced battery technologies. Overall, TEM plays a crucial role as an analytical tool in the development and optimization of solid-state electrolytes, which have the potential to revolutionize the next generation of battery applications.
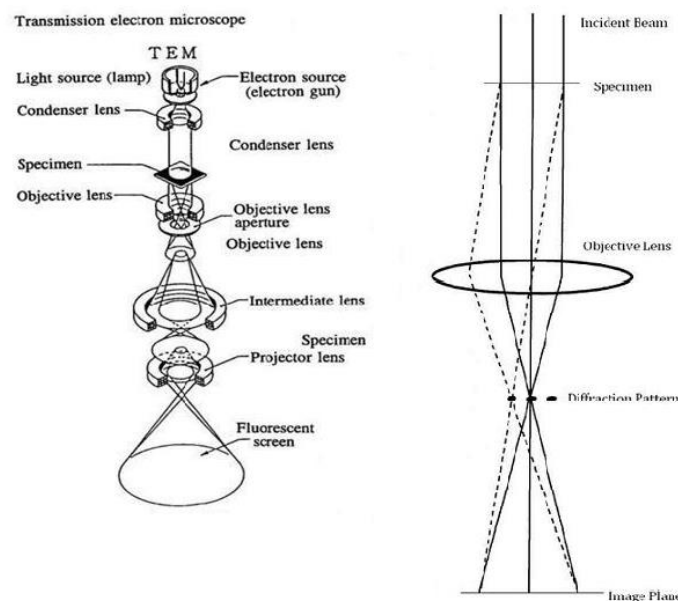
Figure 3.7: The working principle of TEM

3.8.4. Energy Dispersive X-ray Spectroscopy (EDX):

EDS, or energy-dispersive X-ray spectroscopy, is a commonly used elemental analysis technique that enables the quantification of individual elements present in a nanoparticle. Although EDS provides information on the number of substances present at a specific point, it does not give the overall quantity of each element. Typically, EDS is combined with SEM or TEM to obtain a nanoscale image of particles, and EDS performs the analysis of that nanostructure.

In the 1970s, EDS rapidly gained popularity and became a commercial product, surpassing Wavelength-dispersive spectroscopy (WDS) in terms of usage [22]. The EDS system's overall

structure is relatively simple as it does not have moving parts such as the rotation detector in WDS. Instead, the sensor gathers the X-ray energy signals from all series elements in a sample simultaneously, making EDS systems relatively fast [23]. The characteristic energy dispersion resolution of EDS is typically around 150–200 eV, which is lower than WDS resolve. It is worth noting that the lightest component that can be identified using EDS is not carbon (Z=6) but oxygen (Z=8). However, the significant benefits of low cost and fast analysis make these limitations relatively insignificant.

An EDS band is a graph that shows the relationship between the power of X-rays and the corresponding energies. This graph can capture both light and heavy elements in a spectrum ranging from 0.1 to 10-20 keV because both the M or L lines of heavy elements and K lines of light elements are visible in this range[24].
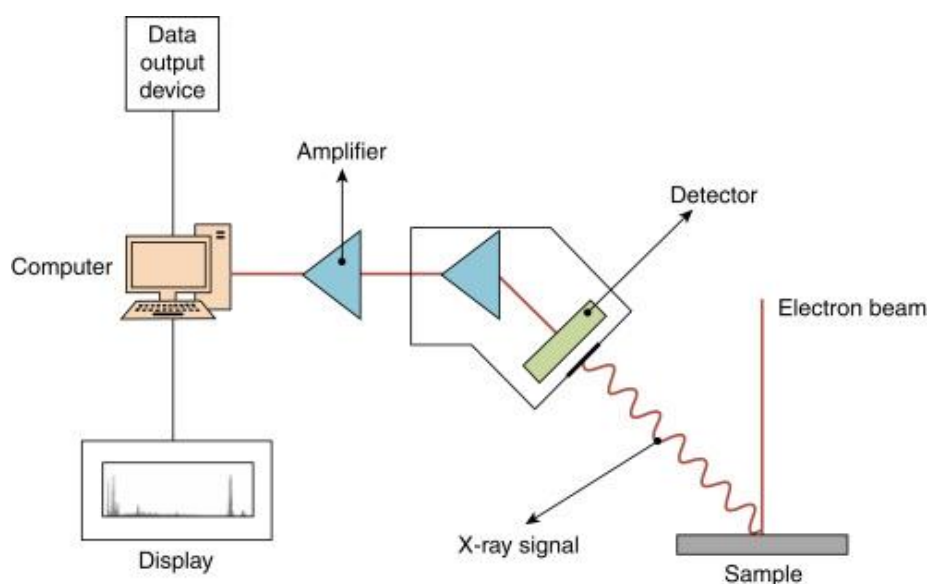
Figure 3.8: The working principle of EDX

3.8.5. Fourier Transform Infrared Spectroscopy (FTIR)

In the field of lignin chemistry, infrared (IR) spectroscopy has been a commonly used analytical tool since the 1950s. While dispersive instruments were previously used to record spectra, FTIR spectrometers have become more readily available in recent years. FTIR spectroscopy is advantageous in various specialized areas such as microanalysis, analysis of aqueous solutions or dark solid-state samples, quantitative evaluation, and process or quality control measurements due to its high sensitivity and fast analysis time[25].

In FTIR spectroscopy, an interference wave interacts with the sample as opposed to a dispersive instrument where the interacting energy has a well-defined wavelength range. The most

common type of interferometer used is the Michelson interferometer. A computer controls the interferometer, collects and stores data, and performs Fourier transformation as well as post-spectroscopic operations such as spectral presentation and resolution enhancement. In FTIR spectroscopy, a collimated light beam from the IR source is divided by a beam splitter in the Michelson interferometer, with one half of the beam being reflected from a fixed mirror and the other half from a moving mirror. The two light beams recombine after returning from the mirrors to form an interference wave, which then passes through the sample and is modified by its interaction with the sample. The modified light is received by a pyroelectric detector, and the analog signals are digitized by an analog-digital converter (ADC) and stored in the computer. Laser technology is used to provide a reference for the mirror's position during the scan and to govern the collection of data points as a function of the mirror's movement.[26]
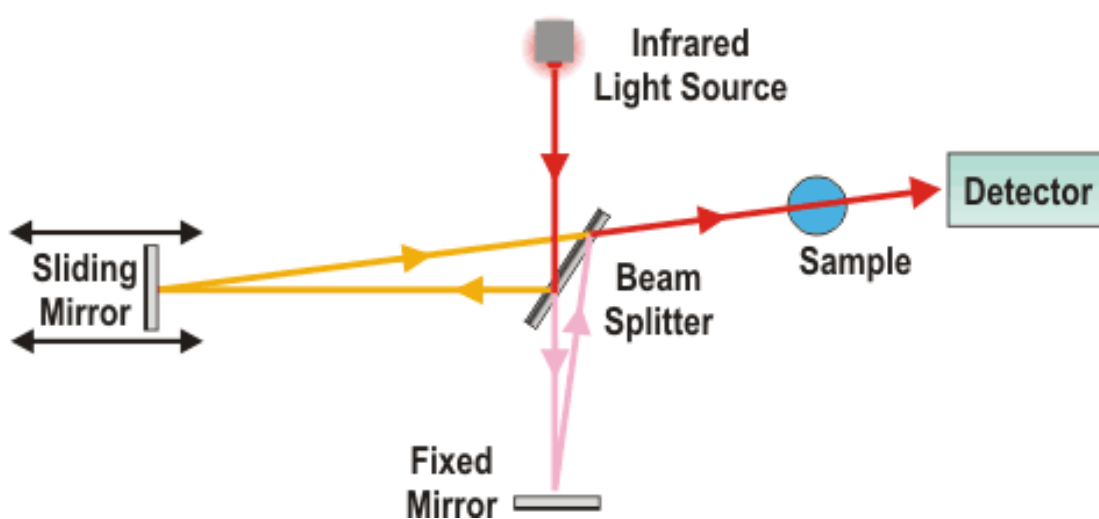
Figure 3.9: The Working principle of FTIR

3.8.6. Xray Photoelectron Spectroscopy (XPS):

Understanding the surface chemical composition, structure, and interface is critical in evaluating the corrosion properties of materials in different environments. To probe nanoscale surface layers, tools like XPS are necessary [27]. XPS provides chemical composition and elemental information for surfaces within 10 nm, with detection sensitivity of 0.1-1 at.% for all elements except H and He, making it a unique tool for surface characterization, particularly for corrosion evaluation. XPS is useful in studying surface reactions under vacuum, including the passivity of films at surfaces and their breakdown in an aqueous environment, their adhesion, mass transport, and selective oxidation phenomenon. XPS has helped understand the role of Cr and Mo elements in stainless steels and the mechanism of passivity [28]. However, XPS has limitations in analyzing films with a thickness greater than 10 nm, leading to artifacts

like preferential element etching, oxidation state modification, ion doping, and atom mixing during ion beam sputtering used to measure film thickness. Additionally, surface charging in insulating specimens may cause peak shift, broadening, and asymmetry, resulting in complex or inaccurate analysis.[29]

Combining XPS with ion-beam etching enables detailed depth profiling and line profiling elemental composition analysis [30]. XPS uses the quantity and kinetic energy of electrons to measure the chemical states of elements, requiring high vacuum (10^6 Pa) or ultra-high vacuum (10^7 Pa), while ambient pressures (ten millibars) can also be used [31]. XPS is often used to construct empirical formulas due to its good quantitative precision for homogeneous solid-state materials[32]. However, absolute quantification requires the use of certified reference samples, which is more challenging and less common. The computed atomic percent values from the primary XPS peaks have a quantitative accuracy of 90-95% for each peak under ideal conditions, making quantitative accuracy critical for proper reporting of data [33].

Figure 3.10: The Working principle of XPS

3.8.7. Electrochemical Techniques

Electrochemical Impedance Spectroscopy (EIS) is a highly sensitive and non-destructive characterization technique that is used to determine the electrical response of chemical systems. EIS systems use low amplitude alternating current (AC) voltages over a range of frequencies to establish the time response of chemical systems. The technique is performed using an electrode setup consisting of a working, reference, and counter electrodes, where a known voltage is passed from the working electrode through an electrolytic solution and into the counter electrode. EIS produces quantitative measurements that enable the evaluation of small scale chemical mechanisms at the electrode interface and within the electrolytic solution, making it useful in various research fields such as batteries and corrosion.

To obtain the electrical response of an electrolytic solution, an electrochemical cell is utilized and connected to an electrochemical spectrometer. EIS systems require specific computer

programs designed for EIS testing and all system components should be acquired before conducting an EIS experiment. Typically, EIS studies utilize a three-electrode mode consisting of a working electrode (sample material), a counter electrode (commonly graphite or platinum), and a reference electrode. Although electrode geometries may differ, the experimental setup generally follows a similar procedure.

The three electrodes are placed on an electrode stage and secured, and the electrolytic solution is prepared and transferred to the sample container. The sample container should be composed of an insulating material, such as glass or plastic, to prevent the interference of additional electron pathways during experimentation that may lead to a reduction in the EIS current response. The electrode mount is then placed on the sample container so that a portion of each electrode is submerged in the electrolytic solution [34].
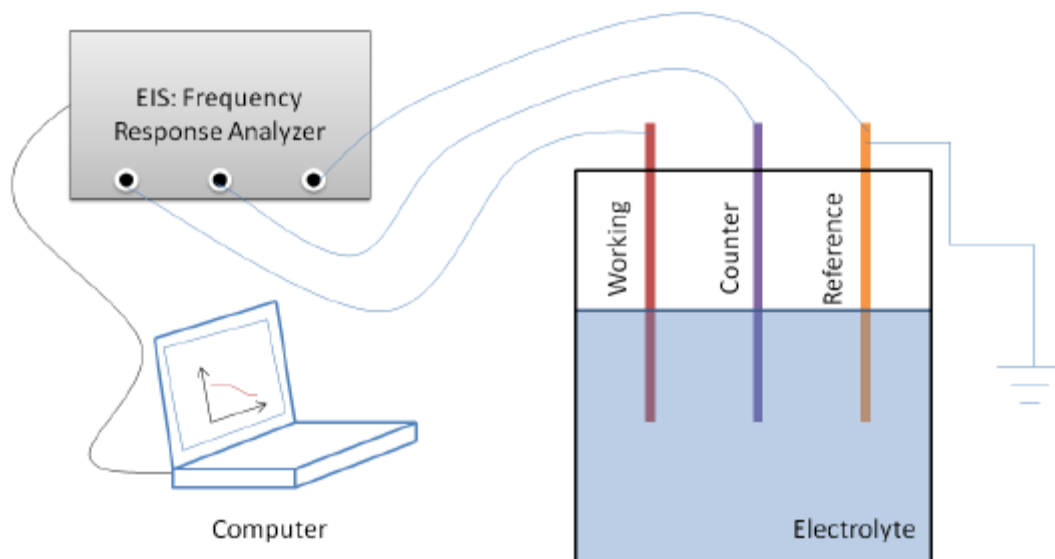
Figure 3.11: Schematic of EIS working

This technique of electrochemical workstation allows us to measure the resistivity of our system. This includes resistance of electrolyte, ohmic loss and or activation losses. Electrical resistance is the measure of the of a circuit element that resists current flow.

R=E/I   (eq. 4)

According to Ohm's law, R is the resistance which is defined as the ratio of voltage (V), and current (I) [35]. This known law use is limited to only one circuit element, the ideal resistor. An ideal resistor has several simplifying properties:

65

- Ohm's Law is followed at every range of current and voltage.

- Resistance is not dependent on the frequency.

- The voltage passing through a resistor and the AC current are in a single phase.

Figure 3.12: Image of a complex number in the complex plane
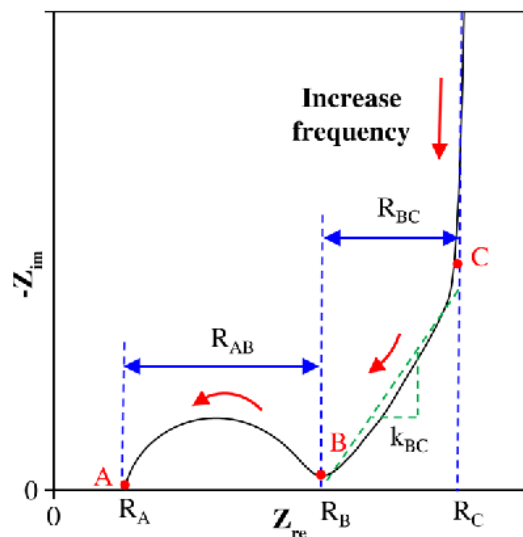
Figure 3.13: EIS Profile (Nyquist Plot)

Summary

In this chapter, the different chemical synthesis methods used for material synthesis are discussed in detail. The solvothermal method involves the use of a solvent at high temperature

66

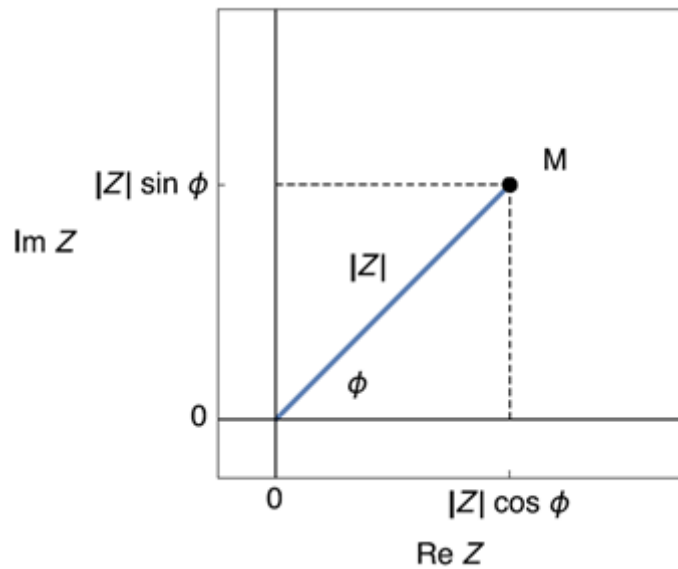and pressure to promote chemical reactions and crystallization of the material. On the other hand, the hydrothermal method involves the use of water as a solvent under high temperature and pressure to form materials with unique properties.

Following the discussion of synthesis methods, the chapter dives into the various material characterization techniques employed in this study. XRD is used to determine the crystal structure and phase of the material, while SEM and TEM provides information on the surface morphology and microstructure. EDS is used to determine the elemental composition of the material, and FTIR to identify functional groups present in the material.

Moreover, the chapter provides a comprehensive explanation of the electrochemical testing process implemented in this study. The electrochemical performance of the material is then determined using a three-electrode system. Overall, this chapter provides a detailed understanding of the experimental methodology used in this study, which helps to establish a foundation for the subsequent analysis and interpretation of the results.

List of References

[1]   R. DeWees and H. Wang, "Synthesis and Properties of NaSICON-type LATP and LAGP Solid Electrolytes," *ChemSusChem*, vol. 12, no. 16, pp. 3713–3725, Aug. 2019, doi: 10.1002/CSSC.201900725.

[2]   R. DeWees and H. Wang, "Synthesis and Properties of NaSICON-type LATP and LAGP Solid Electrolytes," *ChemSusChem*, vol. 12, no. 16, pp. 3713–3725, Aug. 2019, doi: 10.1002/CSSC.201900725.

[3]   H. Rusdi, N. S. Mohamed, R. H. Y. Subban, and R. Rusdi, "Enhancement of electrical properties of NASICON-type solid electrolytes (LiSn2P3O12) via aluminium substitution," *Journal of Science: Advanced Materials and Devices*, vol. 5, no. 3, pp. 368–377, Sep. 2020, doi: 10.1016/J.JSAMD.2020.06.003.

[4]   H. Rusdi, N. S. Mohamed, R. H. Y. Subban, and R. Rusdi, "Enhancement of electrical properties of NASICON-type solid electrolytes (LiSn2P3O12) via aluminium substitution," *Journal of Science: Advanced Materials and Devices*, vol. 5, no. 3, pp. 368–377, Sep. 2020, doi: 10.1016/J.JSAMD.2020.06.003.

[5]   F. Zheng, M. Kotobuki, S. Song, M. O. Lai, and L. Lu, "Review on solid electrolytes for all-solid-state lithium-ion batteries," *J Power Sources*, vol. 389, pp. 198–213, Jun. 2018, doi: 10.1016/J.JPOWSOUR.2018.04.022.

[6]   "Preparation of Li1.5Al0.5Ti1.5(PO4)3 solid electrolyte via a sol–gel route using various Al sources." https://www.infona.pl/resource/bwmeta1.element.elsevier-28f1cf12-7b31-3b76-adda-6842c102a689 (accessed Mar. 03, 2023).

[7]   Q. Ma, Q. Xu, C. L. Tsai, F. Tietz, and O. Guillon, "A Novel Sol-Gel Method for Large-Scale Production of Nanopowders: Preparation of Li1.5Al0.5Ti1.5(PO4)3 as an Example," *Journal of the American Ceramic Society*, vol. 99, no. 2, pp. 410–414, Feb. 2016, doi: 10.1111/JACE.13997.

[8]   S. D. Lee *et al.*, "Composite Electrolyte for All-Solid-State Lithium Batteries: Low-Temperature Fabrication and Conductivity Enhancement," *ChemSusChem*, vol. 10, no. 10, pp. 2175–2181, May 2017, doi: 10.1002/CSSC.201700104.

[9]   L. Huang, Z. Wen, M. Wu, X. Wu, Y. Liu, and X. Wang, "Electrochemical properties of Li1.4Al0.4Ti1.6(PO4)3 synthesized by a co-precipitation method," *J Power Sources*, vol. 196, no. 16, pp. 6943–6946, Aug. 2011, doi: 10.1016/J.JPOWSOUR.2010.11.140.

[10]   J. Pinkas, J. Sopoušek, P. Brož, V. Vykoukal, J. Buršík, and J. Vřešťál, "Synthesis, structure, stability and phase diagrams of selected bimetallic silver- and nickel-based nanoparticles," 2018, Accessed: Mar. 03, 2023. [Online]. Available: https://www.sciencedirect.com/science/article/pii/S0364591618301251

[11]   V. S. Bhugra, G. V. M. Williams, S. v. Chong, and T. Nann, "Electrospun, Oriented, Ferromagnetic Ni1-xFex Nanofibers," *Front Chem*, vol. 8, Feb. 2020, doi: 10.3389/FCHEM.2020.00047.

[12]   S. So -Miya and R. Roy, "Hydrothermal synthesis of fine oxide powders," *Bull. Mater. Sci*, vol. 23, no. 6, pp. 453–460, 2000.

[13]   S. Feng and R. Xu, "New materials in hydrothermal synthesis," *Acc Chem Res*, vol. 34, no. 3, pp. 239–247, 2001, doi: 10.1021/AR0000105.

[14]   D. Perednis and L. J. Gauckler, "Solid oxide fuel cells with electrolytes prepared via spray pyrolysis," *Solid State Ion*, vol. 166, no. 3–4, pp. 229–239, Jan. 2004, doi: 10.1016/J.SSI.2003.11.011.

[15]   M. Y. A. Mollah, F. Lu, and D. L. Cocke, "An X-ray diffraction (XRD) and Fourier transform infrared spectroscopic (FT-IR) characterization of the speciation of arsenic (V) in Portland cement type-V," *Science of the Total Environment*, vol. 224, no. 1–3, pp. 57–68, Dec. 1998, doi: 10.1016/S0048-9697(98)00318-0.

[16]   "Material Characterization Techniques – Analytical Instrumentation Facility (AIF)." https://www.aif.ncsu.edu/mct/ (accessed Mar. 03, 2023).

[17]   J. Kacher, C. Landon, B. L. Adams, and D. Fullwood, "Bragg's Law diffraction simulations for electron backscatter diffraction analysis," *Ultramicroscopy*, vol. 109, no. 9, pp. 1148–1156, Aug. 2009, doi: 10.1016/J.ULTRAMIC.2009.04.007.

[18]   Y. Leng, "Materials characterization: Introduction to microscopic and spectroscopic methods: Second edition," *Materials Characterization: Introduction to Microscopic and Spectroscopic Methods :Second Edition*, pp. 1–376, Aug. 2013, doi: 10.1002/9783527670772.

[19] W. Zhou, R. Apkarian, Z. L. Wang, and D. Joy, "Fundamentals of scanning electron microscopy (SEM)," *Scanning Microscopy for Nanotechnology: Techniques and Applications*, pp. 1–40, 2007, doi: 10.1007/978-0-387-39620-0_1.

[20] A. Grover, R. Sinha, D. Jyoti, and C. Faggio, "Imperative role of electron microscopy in toxicity assessment: A review," *Microsc Res Tech*, vol. 85, no. 5, pp. 1976–1989, May 2022, doi: 10.1002/JEMT.24029.

[21] S. Ebnesajjad, "Surface and Material Characterization Techniques," *Surface Treatment of Materials for Adhesive Bonding*, pp. 39–75, 2014, doi: 10.1016/B978-0-323-26435-8.00004-6.

[22] L. J. Allen, A. J. D'Alfonso, B. Freitag, and D. O. Klenov, "Chemical mapping at atomic resolution using energy-dispersive X-ray spectroscopy," *MRS Bull*, vol. 37, no. 1, pp. 47–52, Jan. 2012, doi: 10.1557/MRS.2011.331.

[23] H. Kariem, T. Kiefer, C. Hellmich, W. Gaggl, A. Steiger-Thirsfeld, and J. Füssl, "EDX/XRD-based identification of micrometer-sized domains in scanning electron micrographs of fired clay," *Materials and Structures/Materiaux et Constructions*, vol. 53, no. 4, Aug. 2020, doi: 10.1617/S11527-020-01531-7.

[24] D. E. Newbury and N. W. M. Ritchie, "Is scanning electron microscopy/energy dispersive X-ray spectrometry (SEM/EDS) quantitative?," *Scanning*, vol. 35, no. 3, pp. 141–168, May 2013, doi: 10.1002/SCA.21041.

[25] B. A. Boukamp, "Fourier transform distribution function of relaxation times; application and limitations," *Electrochim Acta*, vol. 154, pp. 35–46, Feb. 2015, doi: 10.1016/J.ELECTACTA.2014.12.059.

[26] O. Faix, "Fourier Transform Infrared Spectroscopy," pp. 83–109, 1992, doi: 10.1007/978-3-642-74065-7_7.

[27] V. Jain, M. C. Biesinger, and M. R. Linford, "The Gaussian-Lorentzian Sum, Product, and Convolution (Voigt) functions in the context of peak fitting X-ray photoelectron spectroscopy (XPS) narrow scans," *Appl Surf Sci*, vol. 447, pp. 548–553, Jul. 2018, doi: 10.1016/J.APSUSC.2018.03.190.

[28] A. v. Lubenchenko, A. A. Batrakov, A. B. Pavolotsky, O. I. Lubenchenko, and D. A. Ivanov, "XPS study of multilayer multicomponent films," *Appl Surf Sci*, vol. 427, pp. 711–721, Jan. 2018, doi: 10.1016/J.APSUSC.2017.07.256.

[29] J. B. Metson, M. M. Hyland, A. Gillespie, and M. Hemmingsen-Jensen, "X-ray photoelectron spectroscopy applications to corrosion and adhesion at metal oxide surfaces," *Colloids Surf A Physicochem Eng Asp*, vol. 93, no. C, pp. 173–180, Dec. 1994, doi: 10.1016/0927-7757(94)02974-1.

[30] D. M. Hercules, "Electron spectroscopy: Applications for chemical analysis," *J Chem Educ*, vol. 81, no. 12, pp. 1751–1766, 2004, doi: 10.1021/ED081P1751.

[31] J. M. Hollander and W. L. Jolly, "X-ray photoelectron spectroscopy," *Acc Chem Res*, vol. 3, no. 6, pp. 193–200, Jun. 1970, doi: 10.1021/AR50030A003.

[32] C. S. Fadley, "X-ray photoelectron spectroscopy: Progress and perspectives," *J Electron Spectros Relat Phenomena*, vol. 178–179, no. C, pp. 2–32, May 2010, doi: 10.1016/J.ELSPEC.2010.01.006.

[33] A. Proctor and P. M. A. Sherwood, "Data Analysis Techniques in X-ray Photoelectron Spectroscopy," *Anal Chem*, vol. 54, no. 1, pp. 13–19, 1982, doi: 10.1021/AC00238A008.

[34] "Electrochemical Impedance Spectroscopy - Engineering LibreTexts." https://eng.libretexts.org/Bookshelves/Materials_Science/Supplemental_Modules_(Materials_Science)/Insulators/Electrochemical_Impedance_Spectroscopy (accessed Mar. 03, 2023).

[35] D. D. MacDonald, "Reflections on the history of electrochemical impedance spectroscopy," *Electrochim Acta*, vol. 51, no. 8–9, pp. 1376–1388, Jan. 2006, doi: 10.1016/J.ELECTACTA.2005.02.107.

Chapter 4: Methodology and Experimentation

4.1. Chemical procurement

Precursors were procured from different chemical companies with analytical grade purity. The precursors used for the synthesis of pristine and co-doped LATP were $LiOH.H_2O$ (98%,Scharlau), Al_2O_3(99%,Daramata), TiO_2(99%,Sigma Aldrich), and $NH_4H_2PO_4$(98%, Sigma Aldrich) Doping precursors included SiO_2(99%, Daejung) and $CoCl_2. 6H_2O$((99%, Daejung).

4.2. Material Synthesis

The synthesis process for doped LATP was a simple solid-state reaction with all precursors being oxides. included $LiOH.H_2O$ (98%,Scharlau), Al_2O_3(99%,Daramata), TiO_2(99%,Sigma Aldrich), and $NH_4H_2PO_4$(98%, Sigma Aldrich) Doping precursors included SiO_2(99%, Daejung) and $CoCl_2. 6H_2O$(99%, Daejung) . All the doping elements have a similar ionic radius $(Co^{2+}$ 0.745 Å), $(Si^{4+}$ 0.41 Å), and $(Ti^{4+}$ 0.60 Å), $(P^{5+}$ 0.34 Å), respectively. Weighted precursor stoichiometric ratios were initially combined and mashed in mortar pastel. First, the combined powder was dried for 4 hrs. at 80 °C. The dried powdered precursors were placed in a metal chamber containing 18 steel balls of 3mm – 20mm, and the powder was ball milled for 6 hrs. at 500 rpm to mechanically activate it and produce uniformly sized particles. The mixture was calcined in a muffle furnace for 3 hrs. at 500 °C with an 8 °C/min ramp rate. After allowing the powder to cool to room temperature The calcined powder was pulverized again in mortar pastel for 20 minutes. A fine powder was obtained and then calcined for 4 hrs. at 800 °C. The powder was then crushed again in a mortar and pestle and passed through a 72 µm sieved before being formed into pellets with a diameter of 10 mm and a thickness of 1.2 mm using a hydraulic press. The pallets were sintered in a muffle furnace with continual air to generate dense, compact pallets.
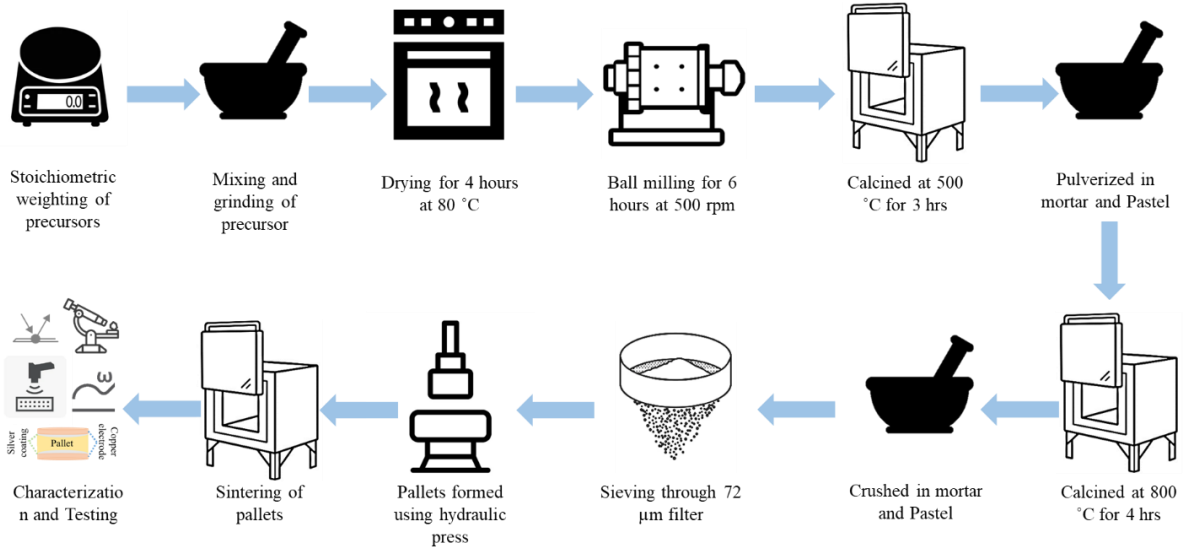
Figure 4.1: Schematic representation of methodology followed

Configuration $Li_{1.3+2x+y}Al_{0.3}Co_xTi_{1.7-x}Si_yP_{3-y}O_{12}$	Name
Pristine LATP (x = 0, y = 0)	Pristine LATP
LATP co-doped (x = 0.01, y = 0.05)	LATP-0.01
LATP co-doped (x = 0.02, y = 0.05)	LATP-0.02
LATP co-doped (x = 0.04, y = 0.05)	LATP-0.04
LATP co-doped (x = 0.06, y = 0.05)	LATP-0.06
LATP co-doped (x = 0.08, y = 0.05)	LATP-0.08

Table 4.1: **Configurations and names**

4.3. Material Characteristics
4.3.1. X-ray diffraction (XRD)

X-Ray diffraction analysis was conducted on a D8 advance Burker instrument to determine the phase and evaluate the crystallinity of the sample. The analysis utilized Cu anode K alpha radiation (lambda = 1.5406 Å) at a voltage of 40 kV and current of 30 mA, with a step size of 0.020 and a range of 10 to 70 degrees.

4.3.2. Fourier transform infrared spectroscopy (FTIR)

The covalent bond formation in the material was studied using Fourier transform infrared spectroscopy (FTIR, Agilent Cary 630) with a spectral range of 4000 to 650 cm^{-1}.

4.3.3. Scanning electron microscopy (SEM)

The electrolyte morphology was observed using Secondary electron microscopy (SEM, FE-SEM, Hitachi) with a platinum coating to enhance conductivity.

4.3.4. Transmission electron microscopy (TEM)

Transmission electron microscopy (TEM, FEI Technia G2 F20) was employed for in-depth structural analysis.

4.3.5. X-ray photon spectroscopy (XPS)

The elements present in the sample and their states were studied using X-ray photon spectroscopy (XPS, PHI 5000 VersaProbe Ulvac-PHI, Japan) with a monochromatic Al-Kα source.

4.4. Electrochemical impedance spectroscopy

To investigate the AC impedance of the pallets formed, chemical instruments CHI660E potentiostate (Shanghai Chenhua Co., Ltd.) was employed. Prior to the characterization, a thin layer of silver was coated on the pallets using a vacuum sputter coater. To avoid short-circuiting, the sides of the pallets were covered with carbon tape during the deposition. The pallets were then secured using a spring and four screws in a swag-lock. For testing the pallets, a two-electrode system was employed with a frequency range between 0.01 Hz to 1 MHz and an amplitude of 70 mV. The solid-state electrolyte resistance was determined by analyzing the data obtained from the electrochemical impedance spectroscopy (EIS) and constructing an equivalent circuit. The ionic conductivity was then calculated using Equation 1.

$$\sigma = \frac{4t}{\pi d^2 R} \qquad (eq.\,5)$$

Where "t" is thickness of the electrolyte pallet (cm), "R(ohms)" donates the total resistance in the electrolyte, and "d" is the diameter of the pallet (cm).

Summary

The current chapter presents a comprehensive account of the experimental methodology employed during the research. The chapter elaborates on the synthesis procedure for pristine and co-doped lithium aluminum titanium phosphate (LATP), as well as the various techniques used for their characterization. Furthermore, the chapter provides detailed information about

the electrochemical testing techniques utilized, including the parameters involved and the electrochemical workstation used for the testing.

Chapter 5: Results and Discussion

5.1. Structural Analysis

The prepared samples with silicon doping and different cobalt doping were synthesized using solid-state route. XRD was applied to analyze the phase developed and crystallinity of the series. Figure 1 illustrates the pristine LATP as well as the cobalt/silicon doped series. Our analysis of the pristine LATP indicates that we have successfully obtained a rhombohedral structure that matches perfectly with the JCPDS of LTP. This finding suggests that our synthesis method was successful in producing LATP, which is a critical component for the performance of our material The XRD pattern of Co-doped LATP in the range of 20.5° to 21.1° and 23.5° to 25.5° was examined. The results showed that in Fig. 1 (b), LATP-0.01 shifted slightly to the left in the investigated plane, indicating Co incorporation, while LATP-0.02 did not shift, indicating no Co incorporation. In Fig. 1 (c), LATP-0.02 shifted to the right, indicating Co incorporation, while no shift was observed in LATP-0.01. The results suggest that Co incorporation in LATP affects its lattice structure in a plane-specific manner. The peaks of the pattern shifted gradually towards the left with an increase in Co content, indicating that the Co doping causes the expansion of the crystalline lattice due to its larger radius. However, as the doping concentration exceeded 0.04, the peaks shifted towards the right, suggesting a decrease in the solubility of Co^{2+} in the LATP system; the lattice sites cannot accommodate all the cobalt ions, and the excess ions accumulate on the surface of the crystal. The optimal amount of Co^{2+} may provide more channels for the transfer of lithium ions, thereby enhancing the ionic conductivity of solid electrolytes. These findings highlight the importance of controlling the doping concentration of Co in LATP to improve the performance of solid electrolytes[1], [2]. Peaks associated with $LiTiPO_5$, which acts as an impurity phase, can be found in pure LATP around 27° to 28° degrees, however after silicon and cobalt doping, this impurity phase fades showing lower intensity, demonstrating that co-doping causes a decrease in the impurity phases. Herein an orthorhombic impurity phase can be observed of $AlPO_4$. These impurity phases are very common among these ceramics and are mostly unavoidable[3], [4]. These $AlPO_4$ phases have been observed to develop during the ball milling process in the solid-state method, as validated by XRD analysis of Pure LATP that has been ball milled. Simultaneously, the other is sintered without ball milling, demonstrating that ball milling promotes the formation of these $AlPO_4$ instances, which is also supported by prior research . However, ball milling is an important and obligatory step in our synthesis process to create small and uniform particle size, which will increase our ionic conductivity. Additionally, even

though the development of this amorphous impurity phase reduces total ionic conductivity, it improves the densification of the pallets [5]. As shown, the peak shift into smaller values in XRD, serve as evidence that cobalt has been impregnated into the crystal structure of LATP. It was believed that these phenomena resulted from the precipitation of too many cobalt particles into the matrix, which causes the lattice to contract as having a lower lattice constant. When sulfur was doped with a different concentration, a similar phenomena was observed, with sulfur having a lower lattice constant, causing the peaks to shift to the right [6]. After silicon doping, silicate phases have emerged have also been described in the earlier study. These silicate phases improves the compaction density of solid electrolytes by the formation of the SiO_2 second phase, which tends to form amorphous silicate at the grain boundary and can bind the grains together[7]. The binding of grain boundaries due to the formation of SiO_2 can help in the transfer of lithium between the grain boundaries which in terms decrease the grain boundary resistance.
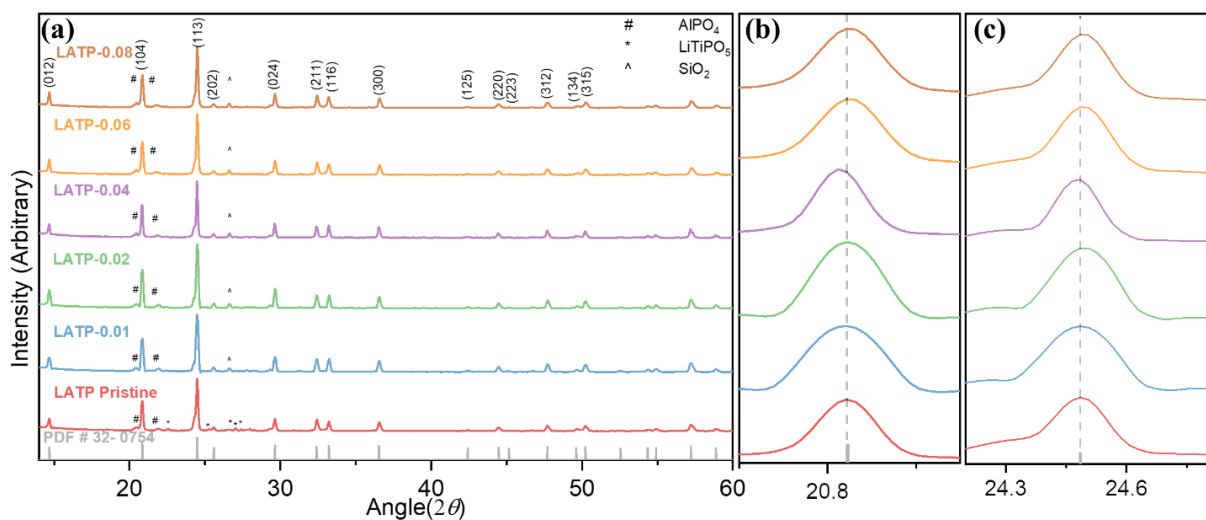

Figure 5.1: (a) XRD patterns for Pristine $Li_{1.3}Al_{0.3}Ti_{1.7}(PO_4)_3$ and doped samples of $Li_{1.3+2x+y}Al_{0.3}Co_xTi_{1.7-x}Si_yP_{3-y}O_{12}$ series at (x = 0 - 0.08) and (y = 0.05) concentration. (b) is the Partial enlargement of (a) range from 23.5º to 25.5º to investigate Cobalt doping on lattice structure of LATP

5.2. Absorption Analysis

FTIR analysis was carried out to study the bonds formed in Pristine and co-doped LATP as shown in **Error! Reference source not found.**. The P-O bond stretching vibrations in PO_4 tetrahedra are responsible for the LATP band observed at 1014 cm^{-1} and 972 cm^{-1} [8]. The peak observed at 1232 cm^{-1} is linked to the stretching of P-O bond. Additionally, a slight peak at 796

cm[-1] was discovered in samples of LATP-doped silicon that can be attributed to the symmetric stretching vibration of the Si-O-Si silanol bridge[9]. In addition, the creation of Si-O-Si bonds can also be observed by the peak between 1050 and 1200 cm[-1][10]. There are many intensity peaks near 660-721 cm^{-1} because of the Ti-O stretching vibration of the TiO_6 octahedron[11]. Peaks around 3200-3500 cm^{-1} are associated with O-H stretching vibration caused due to some moisture being observed by the material.
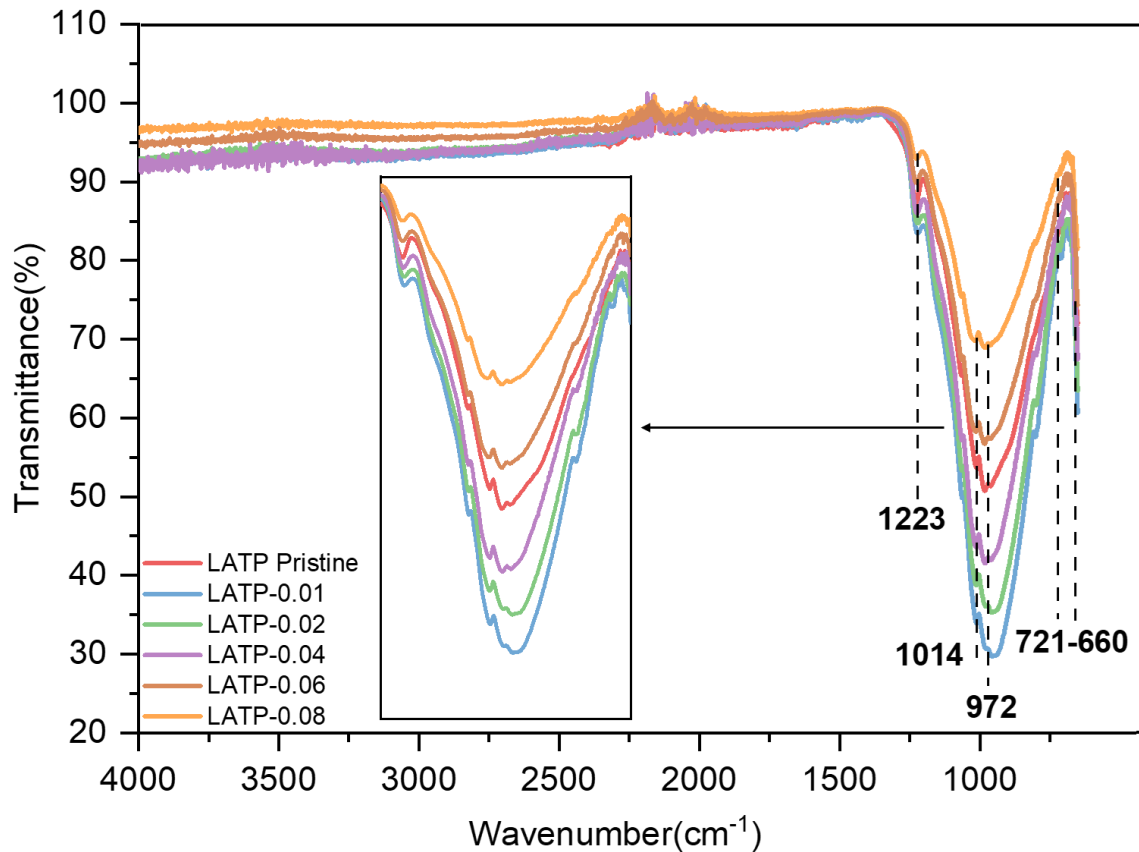

Figure 5.2: FT-IR spectra of pristine LATP and co-doped LATP

5.3. Compositional analysis

We have carried out XPS research to investigate the oxidation state and the elemental contents of the synthesized LATP powders. Firstly the Pristine LATP was analyzed shown in **Error! Reference source not found.** (a) which shows a general spectrum indicating the existence of base elements with respective orbital energy levels Li 1s, Ti 2p, Al 2p, P 2p, and O 1s elements. The peaks in survey spectra of co-doped material LATP-0.04 **Error! Reference source not found.** (a) shows peaks of Li 1s, Al 2p, P 2p, Ti 2p, O 1s and Si 2p, Co 2p confirm the main composition of the sintered sample, which is well consistent with the results of the EDX

78

analysis. **Error! Reference source not found.** (b-h) shows the deconvolution spectrum obtained by XPS of LATP-0.04. The two peaks of Ti 2p3/2 and Ti 2p1/2 at 459.79 and 465.73 eV, respectively, in the high-resolution XPS spectra of Ti 2p can be attributed to Ti^{4+} ions in an oxygen environment[12]. As reported, the observed titanium peaks differ by 2.0 EV[13]. The phenomenon is caused by the ease with which the Ti-O bond can become polarized by the induced effect of the P-O bond present in the LATP-0.04 sample system[14]. The high energy XPS of oxygen reveals that its peak is deconvoluted into two peaks indicating two different chemical environments of oxygen: the non-bridging oxygen (NBO) peak at 531.37 eV and the bridging oxygen (BO) peak at 532.99 eV [2]. Two peaks for Phosphate can also be identified at 133.69 eV and a small shoulder peak at 133.76 eV corresponding to 2P1/2 and 2P3/2 respectively. Cobalt peaks can be seen at 781.67 eV and 797.54 eV, with the peak at 781.67 eV corresponding to the Co 2p3/2 state and the peak at 797.60 eV corresponding to the Co 2p1/2 state which indicates the presence of Co_3O_4. The presence of cobalt peaks in our material confirms that Co has been successfully doped into its lattice structure. At 103.06 eV, a silicon peak was observed, indicating that silicon exists in 2p states and has been successfully doped. Due to the lower aluminum concentration, the aluminum peak seems to be smaller. It can also be seen that the Aluminum peak deconvolutes to only one peak at a binding energy of 74.88 eV, which corresponds to Al^{+3}. This shows that in the LATP spectrum, Al only exists in one valance state[15].
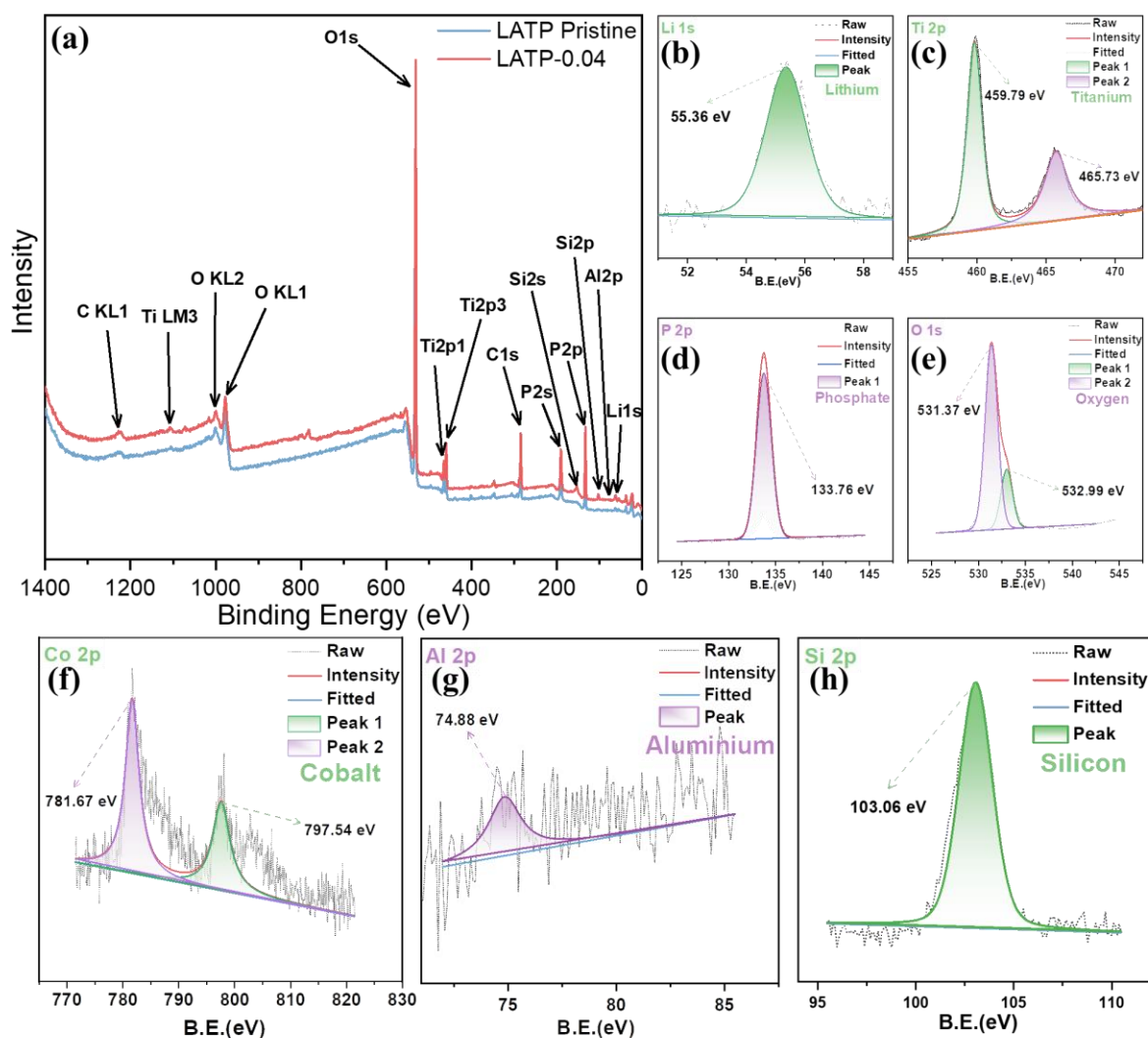
Figure 5.3: **XPS survey spectra (a) LATP Pristine, and LATP-0.04 doped LATP. Deconvoluted Spectra of LATP-0.04 (b) Lithium, (c)Titanium, (d) Phosphate, (e) Oxygen, (f) Cobalt, (g) Aluminum, and (h) Silicon**

5.4. Morphological analysis

5.4.1. SEM Analysis

SEM micrographs were used to analyze the surface morphology of our as prepared powder samples shown in **Error! Reference source not found.** (b, d). The Pristine LATP synthesized via the solid-state technique has a regular cubical structure. In contrast, our doped sample has a slight random cubical pattern, but the particle's strong coalescence of the grains obscures any imperfections or intraparticle pores. Particle size has increased slightly, which can be seen in the histogram **Error! Reference source not found.** (b, d) showing the particle size distribution of the Pristine and LATP-0.04. The existence of agglomerated particles on the surface of our sample can be attributed to the presence of impurities such as $AlPO_4$, $LiTiPO_5$, or pollutants in

80

the electrolyte, which can form small particles on the surface during processing or storage[16]. These agglomerated particles are observed to increase when we dope silicon, which is due to the fact that as we dope silicon into our crystal structure, it creates SiO_2, the existence of which has also been confirmed by XRD[17]. Although SiO_2 is considered an impurity phase, it can fuse the grains during the sintering process, as previously stated, which densifies our pallets[14]. Additionally, the presence of defects in the crystal structure of the electrolyte, such as voids or cracks, can also attract small particles to the surface. It is also possible that these small particles that appear in morphology are secondary particle or debris coming from the sample preparation process and not related to the electrolyte itself. As observed in our SEM photos, debris can accumulate onto the material during the calcination process, in which material is placed in the muffle furnace, which is insulted using refractory brick containing calcium. This is supported by EDX SEM (supplementary data), showing the presence of calcium in our material.

5.4.2. TEM Analysis
We used TEM at low and high resolution to investigate the phases formed further and confirm that they are well aligned with our XRD, as shown in the **Error! Reference source not found.** (a). According to low-resolution TEM, The particle size is around 500 to 600 nm **Error! Reference source not found.** (a). Furthermore, we can examine the phases formed using high-resolution TEM **Error! Reference source not found.** (a), which allows us to see lattice fringes with varying lattice spacing. The fringes with a lattice spacing of 0.42nm correspond to the (104) plane, while the other planes observed had lattice spacings of 0.60 and 0.36 nm, corresponding to the lattice planes (012) and (113), respectively[18]. These planes are perfectly matched with our material's XRD. The selected area electron diffraction (SAED) pattern obtained using TEM of the LATP particle depicts a NASICON-based structure consistent with the XRD pattern[19]. The elements of Co, Si, Al, Ti, O, and P were further confirmed by the EDX spectrum; moreover, as demonstrated by the EDS of the LATP LATP-0.04 particle Figure 5.5: (i-vii), these elements were uniformly dispersed in the nanosheets. **Error! Reference source not found.** is used to demonstrate the atomic composition of elements contained within the sample. Analysis of the concentration reveals that the doping of Cobalt at the Titanium site reduces the atomic percentage of Aluminum. As the concentration of Co is increased, there is a possibility that it may displace Li ions and limit the number of available sites for Al substitution. This can result in a reduction of aluminum in the NASICON phase, and an increase in the $ALPO_4$ phase impurity, which is also evident from XRD analysis where the

intensity of $AlPO_4$ impurity increases slightly with an increase in cobalt doping [20]. This decrease is interpreted as evidence of successful doping of Cobalt at the Titanium site. The decline in the concentration of Phosphorus and Oxygen can also be attributed to the doping of Silicon at the Phosphate site. The reason behind lithium not being detected can be attributed to the fact that lithium has a low atomic number ($Z = 3$) and a relatively small electron cloud, which makes it difficult to detect using EDS. In general, EDS is better suited for elements with higher atomic numbers (e.g. $Z > 6$).
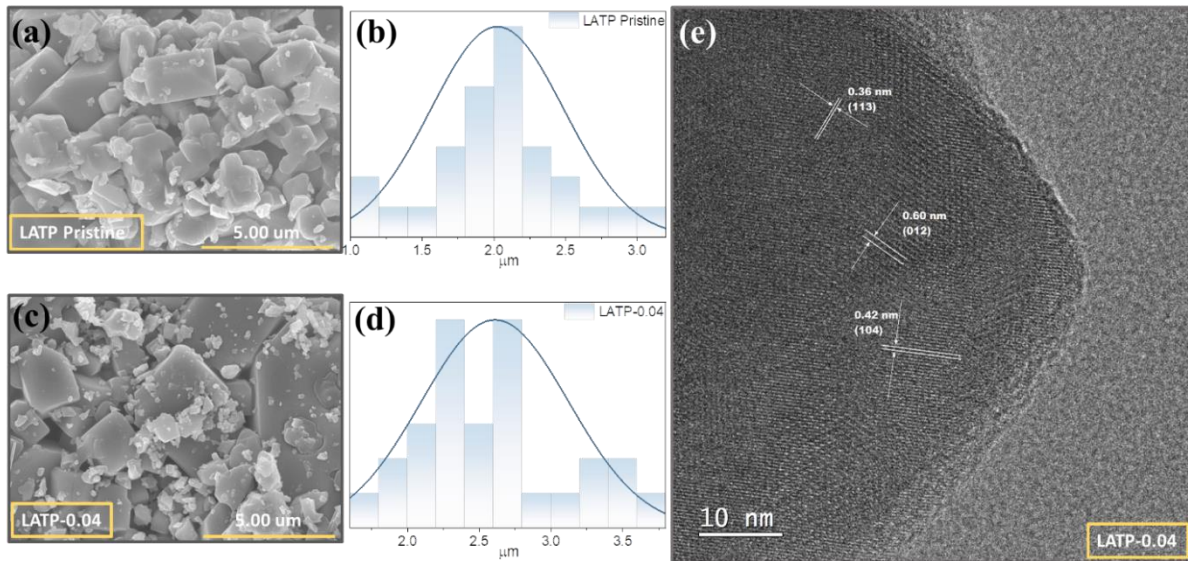

Figure 5.4: **TEM and SEM analysis (a) HRTEM analysis of LATP-0.04 doped LATP, (b) SEM 5 μm resolution image LATP, (i) Particle Size distribution of LATP, (c) SEM 5**
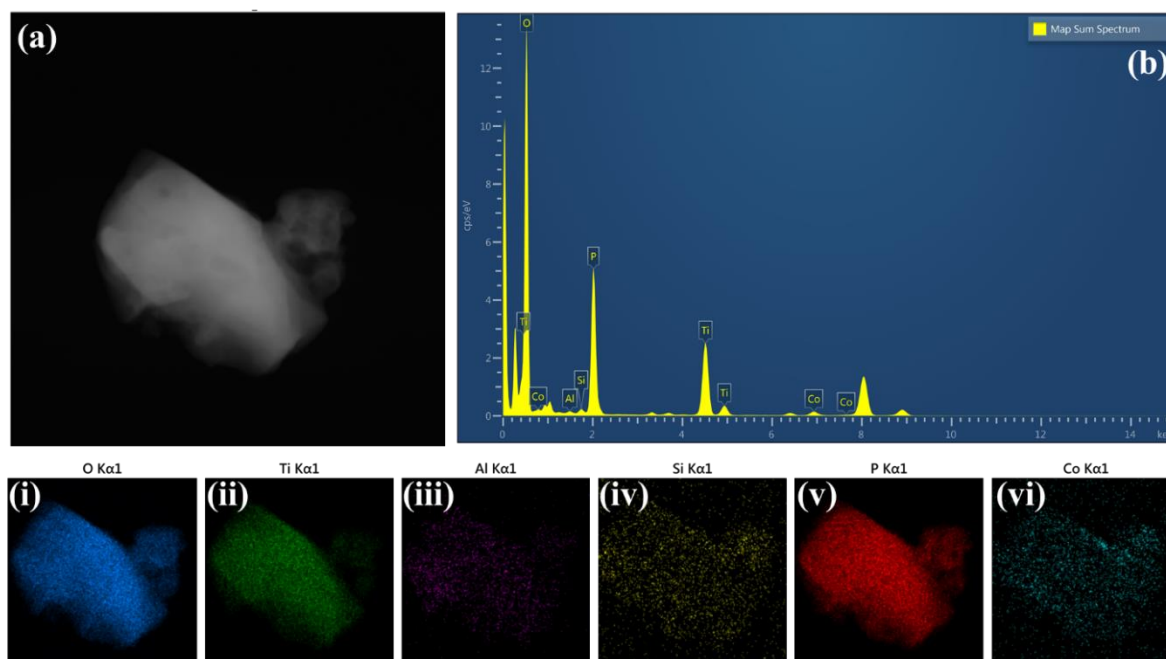
Figure 5.5: **(a) EDX Particle, (b) EDX pattern of LATP-0.04, and corresponding EDX elemental mapping images (i-vi) of LATP-0.04**

Sample	Atomic Percentage %					
	Al	**Ti**	**Co**	**P**	**O**	**Si**
LATP	1.85	4.74	-	15.43	77.98	-
LATP-0.04	0.14	5.42	0.28	11.90	81.92	0.35

Table 5.1: **Atomic Composition from TEM EDS**

5.5. Electrochemical Performance:

To determine the ionic conductivity of the series, we measured the electrochemical impedance spectra (EIS) for both pristine and co-doped LATP shown in the **Error! Reference source not found.**. A semicircle can be seen in the impedance spectra at high frequencies, and an oblique line can be observed at low frequencies. The angled line depicts lithium-ion diffusion through the blocking Au electrodes. The diameter of the semicircle represents charge transfer resistance

in the same way that the left intercept at the high-frequency zone represents grain resistance. Therefore, the overall impedance (R) determined in this study encompasses the resistance within the grains (R_g) and the resistance of charge transfer (R_{ct}), resulting in a total impedance equal to $R = R_g + R_{ct}$ [21]. Due to the limits of the electrochemical workstation test frequency, the grain resistance region at high frequency cannot be exhibited. The resistance values for R_g and R_{ct} measured at room temperature, as presented in the **Error! Reference source not found.**, were acquired through the adjustment of the Nyquist plot to the corresponding circuit diagram found in the supplementary information[22].

	LATP	LATP-0.01	LATP-0.02	LATP-0.04	LATP-0.06	LATP-0.08
Rg(Ω)	1698	2579	3394	1624	2673	3416
Rct(Ω)	9645	1.94×10^4	2.19×10^5	5445	1.28×10^5	1.72×10^5
Ionic Conductivity (S cm⁻¹)	2.19×10^{-5}	1.76×10^{-5}	1.73×10^{-6}	5.45×10^{-5}	2.97×10^{-6}	2.21×10^{-6}

Table 5.2: **Resistance measurements from the circuit fitting (Randall's circuit) of EIS. Grain Resistances (R_g), Charge Transfer Resistances (R_{ct}), and Ionic Conductivities of Pristine LATP and Doped LATP**
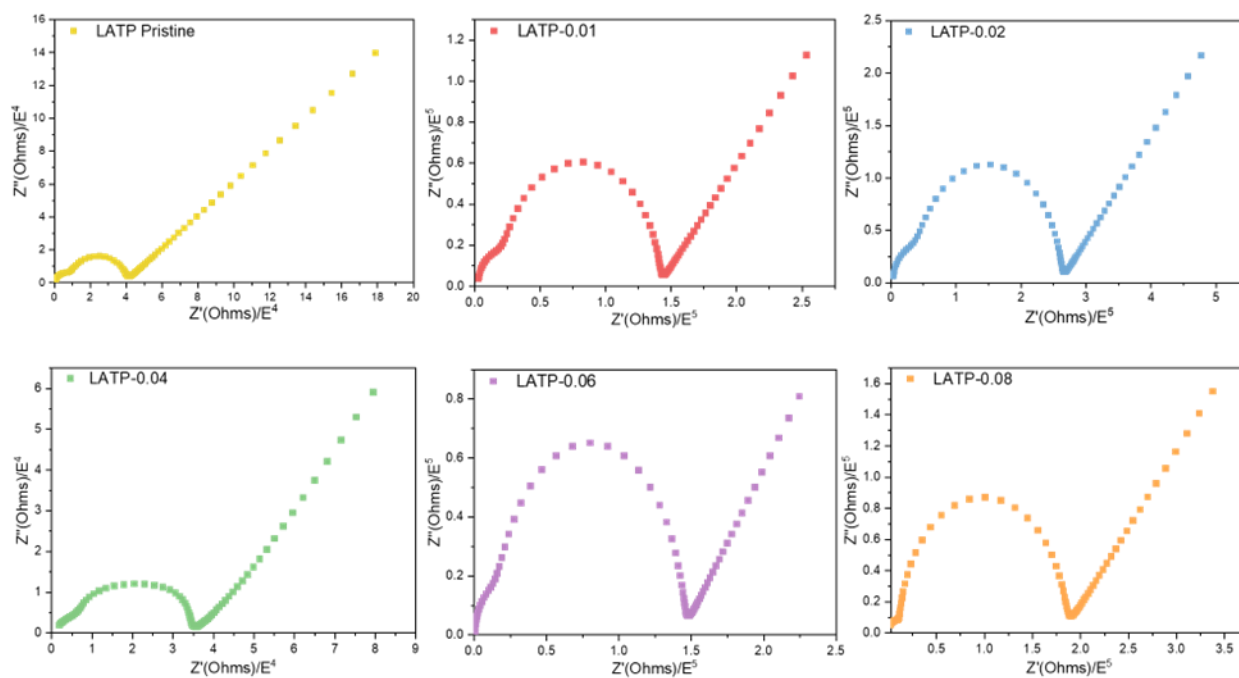
Figure 5.6: **Impedance spectra of LATP prepared with different Co ratios and LATP Pristine.**

The doping of silicon shows a new phase of SiO_2. As mentioned in XRD analysis, the phase of silicon oxide emerging with silicon doping exhibits an increase in ionic conductivity, which several studies have attributed to SiO_2 silicate accumulating at the grain boundary, which may bind the grains together and increase the compaction density of solid electrolyte [23][24]. Additionally, this phase might make it simpler for Li+ ions to travel from the grain core to the grain boundary phases, increasing the ionic conductivity of the grain boundaries. The Nyquist plot is shown in the figure; the table displays the values obtained for R_s, R_{ct}, and the ionic conductivities of LATP with co-doping. The total conductivity is dominated by lithium-ion conduction across the grain boundary, which initially decreased and subsequently rose with the addition of cobalt. The analysis revealed that the maximum value of the measured parameter was observed at a doping concentration of 0.04, but beyond this concentration, a decrease in ionic conductivity was noted as the doping concentration increased. This decrease is due to the accumulation of non-lithium ion conducting excess CoO phases at the grain boundaries, which obstruct lithium ion conduction[25]. Electrochemical impedance spectroscopy reveals that LATP-0.04 has the lowest impendence value of 5.45 x 10^{-5} S cm^{-1}. This can be interpreted due to the fact that the binding force of dopant ions to Li+ ions can be reduced by a lower-valence cation occupying the Ti (Al) site, due to which Li+ ions can easily to move past bottlenecks because they have fewer electrostatic interactions. The XRD analysis results are well aligned

85

with our EIS analysis which suggests that doping with Cobalt can enhance the ionic conductivity of LATP material. However, the degree of doping is critical as indicated by the peak shift observed in the analysis. Cobalt doping at 0.04 showed improved ionic conductivity as demonstrated by the peak shift to the left. Conversely, over-doping is not recommended as it can lead to a decrease in ionic conductivity as demonstrated by the peak shift to the right in LATP-0.02, LATP-0.06, and LATP-0.08. These findings have important implications for optimizing the doping strategy for enhancing the ionic conductivity of LATP material. Therefore, a balanced Cobalt doping concentration is crucial for optimizing the electrochemical properties of the LATP material for potential use as a solid electrolyte. Additionally, the channel size of Li^+ ion migration can be optimized by using the right doping content[26].
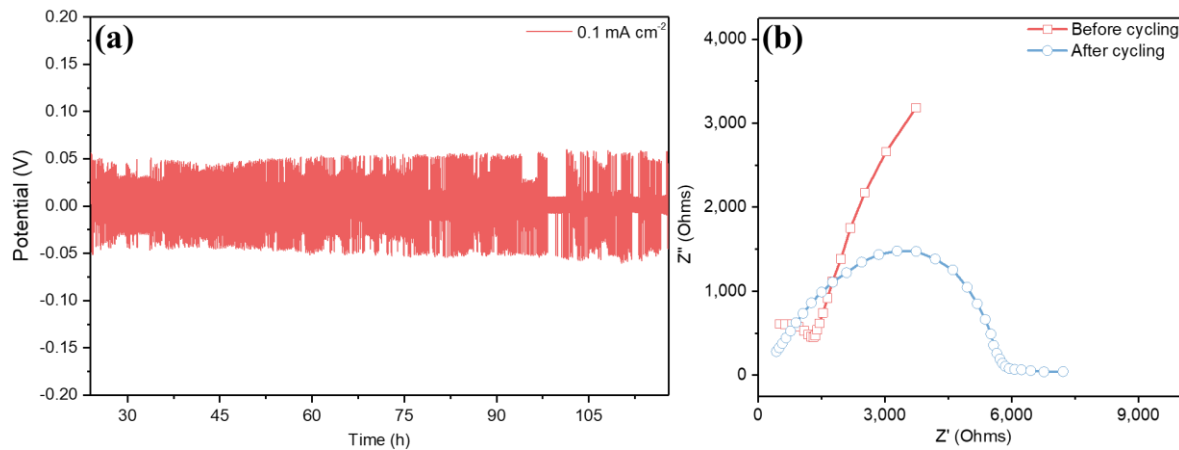
5.6. Cell Testing

Figure 5.7: **(a) Polarization cycling test for 100 hours (b) EIS of LATP-0.04 before and after cycling**

An investigation was conducted on the interfacial stability of a Li|LATP-0.04|Li symmetric cell through polarization testing using a consistent current density of 0.1 mA cm^{-2}. Our results show that Li|LATP-0.04|Li symmetric cell based on LATP demonstrates smaller polarization of 0.05 mV. It was noticeable that there were voltage fluctuations occurring during the processes of Li intercalation and deintercalation. One possible explanation for these voltage fluctuations is the incomplete formation of a solid electrolyte interphase (SEI), which may result in a somewhat unstable interfacial compatibility between the lithium metal electrode and the solid-state electrolyte (SSE) [27], [28].

Summary

In this chapter, a comprehensive discussion is provided regarding the research results. The obtained results of XRD, SEM, TEM, EDS, FTIR, and XPS characterization techniques are presented and justified with reference to previous studies in order to better comprehend the morphology, structure, composition, thermal stability, functional groups, surface area, and porosity of the synthesized materials. Towards the end, the electrochemical and cell testing results of the synthesized electrolytes are discussed. The presented results are compared with literature and analyzed in the context of the properties obtained from characterization techniques.

List of References

[1]   Q. Wang, J. F. Wu, Z. Lu, F. Ciucci, W. K. Pang, and X. Guo, "A New Lithium-Ion Conductor LiTaSiO5: Theoretical Prediction, Materials Synthesis, and Ionic Conductivity," *Adv Funct Mater*, vol. 29, no. 37, Sep. 2019, doi: 10.1002/adfm.201904232.

[2]   Z. Kou, C. Miao, Z. Wang, and W. Xiao, "Novel NASICON-type structural Li1.3Al0.3Ti1.7SixP5(3-0.8x)O12 solid electrolytes with improved ionic conductivity for lithium ion batteries," *Solid State Ion*, vol. 343, Dec. 2019, doi: 10.1016/j.ssi.2019.115090.

[3]   C. R. Mariappan, M. Gellert, C. Yada, F. Rosciano, and B. Roling, "Grain boundary resistance of fast lithium ion conductors: Comparison between a lithium-ion conductive Li-Al-Ti-P-O-type glass ceramic and a Li 1.5Al0.5Ge1.5P3O12 ceramic," *Electrochem commun*, vol. 14, no. 1, pp. 25–28, Jan. 2012, doi: 10.1016/j.elecom.2011.10.022.

[4]   D. H. Kothari and D. K. Kanchan, "Effect of doping of trivalent cations Ga3+, Sc3+, Y3+ in Li1.3Al0.3Ti1.7 (PO4)3 (LATP) system on Li+ ion conductivity," *Physica B Condens Matter*, vol. 501, pp. 90–94, Nov. 2016, doi: 10.1016/j.physb.2016.08.020.

[5]   S. Yu *et al.*, "Influence of microstructure and AlPO4 secondary-phase on the ionic conductivity of Li1.3Al0.3Ti1.7 (PO4)3 solid-state electrolyte," *Functional Materials Letters*, vol. 9, no. 5, Oct. 2016, doi: 10.1142/S1793604716500661.

[6]   A. Kizilaslan, M. Kirkbinar, T. Cetinkaya, and H. Akbulut, "Sulfur doped Li1.3Al0.3Ti1.7(PO4)3solid electrolytes with enhanced ionic conductivity and a

reduced activation energy barrier," *Physical Chemistry Chemical Physics*, vol. 22, no. 30, pp. 17221–17228, Aug. 2020, doi: 10.1039/d0cp03442h.

[7]   Z. Kou, C. Miao, Z. Wang, and W. Xiao, "Novel NASICON-type structural Li1.3Al0.3Ti1.7SixP5(3-0.8x)O12 solid electrolytes with improved ionic conductivity for lithium ion batteries," *Solid State Ion*, vol. 343, Dec. 2019, doi: 10.1016/j.ssi.2019.115090.

[8]   Z. Li, K. Zhu, J. Li, and X. Wang, "Morphological and orientational diversity of LiFePO4 crystallites: Remarkable reaction path dependence in hydrothermal/solvothermal syntheses," *CrystEngComm*, vol. 16, no. 43, pp. 10112–10122, Nov. 2014, doi: 10.1039/c4ce01397b.

[9]   A. Hakiki *et al.*, "Synthesis and characterization of mesoporous silica SBA-15 functionalized by mono-, di-, and tri-amine and its catalytic behavior towards Michael addition," *Mater Chem Phys*, vol. 212, pp. 415–425, Jun. 2018, doi: 10.1016/j.matchemphys.2017.12.039.

[10]   O. Sheng *et al.*, "In Situ Construction of a LiF-Enriched Interface for Stable All-Solid-State Batteries and its Origin Revealed by Cryo-TEM," *Advanced Materials*, vol. 32, no. 34, Aug. 2020, doi: 10.1002/adma.202000223.

[11]   F. Chen *et al.*, "Optimized Ni-rich LiNi0.83Co0.06Mn0.06Al0.05O2 cathode material with a Li1.3Al0.3Ti1.7(PO4)3 fast ion conductor coating for Lithium-ion batteries," *J Alloys Compd*, vol. 923, p. 166277, Nov. 2022, doi: 10.1016/J.JALLCOM.2022.166277.

[12]   C. Miao *et al.*, "LiF-doped Li1.3Al0.3Ti1.7(PO4)3 superionic conductors with enhanced ionic conductivity for all-solid-state lithium-ion batteries," *Ionics (Kiel)*, vol. 28, no. 1, pp. 73–83, Jan. 2022, doi: 10.1007/s11581-021-04324-2.

[13]   P. Bhanja, C. Senthil, A. K. Patra, M. Sasidharan, and A. Bhaumik, "NASICON type ordered mesoporous lithium-aluminum-titanium-phosphate as electrode materials for lithium-ion batteries," *Microporous and Mesoporous Materials*, vol. 240, pp. 57–64, Mar. 2017, doi: 10.1016/j.micromeso.2016.11.005.

[14]   Z. Kou, C. Miao, Z. Wang, and W. Xiao, "Novel NASICON-type structural Li1.3Al0.3Ti1.7SixP5(3-0.8x)O12 solid electrolytes with improved ionic conductivity

for lithium ion batteries," *Solid State Ion*, vol. 343, Dec. 2019, doi: 10.1016/J.SSI.2019.115090.

[15] S. Wang, H. Xu, W. Li, A. Dolocan, and A. Manthiram, "Interfacial Chemistry in Solid-State Batteries: Formation of Interphase and Its Consequences," *J Am Chem Soc*, vol. 140, no. 1, pp. 250–257, Jan. 2018, doi: 10.1021/JACS.7B09531/SUPPL_FILE/JA7B09531_SI_010.AVI.

[16] K. Waetzig, A. Rost, U. Langklotz, B. Matthey, and J. Schilm, "An explanation of the microcrack formation in Li1.3Al0.3Ti1.7(PO4)3 ceramics," *J Eur Ceram Soc*, vol. 36, no. 8, pp. 1995–2001, Jul. 2016, doi: 10.1016/j.jeurceramsoc.2016.02.042.

[17] S. D. Jackman and R. A. Cutler, "Effect of microcracking on ionic conductivity in LATP," *J Power Sources*, vol. 218, pp. 65–72, Nov. 2012, doi: 10.1016/j.jpowsour.2012.06.081.

[18] Z. Yao *et al.*, "Co-precipitation synthesis and electrochemical properties of NASICON-type Li1.3Al0.3Ti1.7(PO4)3 solid electrolytes," *Journal of Materials Science: Materials in Electronics*, vol. 32, no. 20, pp. 24834–24844, Oct. 2021, doi: 10.1007/S10854-021-06943-X.

[19] S. H. Siyal, M. Li, H. Li, J. le Lan, Y. Yu, and X. Yang, "Ultraviolet irradiated PEO/LATP composite gel polymer electrolytes for lithium-metallic batteries (LMBs)," *Appl Surf Sci*, vol. 494, pp. 1119–1126, Nov. 2019, doi: 10.1016/j.apsusc.2019.07.179.

[20] S. Miyoshi, Y. Nishihara, and K. Takada, "Influence of Cobalt Introduction on the Phase Equilibrium and Sintering Behavior of Lithium-Ion Conductor Li1.3Al0.3Ti1.7(PO4)3," *ACS Appl Energy Mater*, Jun. 2022, doi: 10.1021/acsaem.2c00996.

[21] F. Maglia, F. Farina, M. Dapiaggi, I. G. Tredici, and U. Anselmi-Tamburini, "Transport properties in bulk nanocrystalline Sm-doped ceria with doping content between 2 and 30 at.%," in *Solid State Ionics*, Oct. 2012, vol. 225, pp. 412–415. doi: 10.1016/j.ssi.2011.12.015.

[22] J. R. Macdonald, "Impedance spectroscopy," *Ann Biomed Eng*, vol. 20, no. 3, pp. 289–305, 1992, doi: 10.1007/BF02368532.

[23] Z. Kou, C. Miao, Z. Wang, and W. Xiao, "Novel NASICON-type structural Li1.3Al0.3Ti1.7SixP5(3-0.8x)O12 solid electrolytes with improved ionic conductivity for lithium ion batteries," *Solid State Ion*, vol. 343, Dec. 2019, doi: 10.1016/j.ssi.2019.115090.

[24] E. Zhao *et al.*, "High ionic conductivity Y doped Li1.3Al0.3Ti1.7(PO4)3 solid electrolyte," *J Alloys Compd*, vol. 782, pp. 384–391, Apr. 2019, doi: 10.1016/j.jallcom.2018.12.183.

[25] H. Xu, S. Wang, H. Wilson, F. Zhao, and A. Manthiram, "Y-Doped NASICON-type LiZr2(PO4)3 Solid Electrolytes for Lithium-Metal Batteries," *Chemistry of Materials*, vol. 29, no. 17, pp. 7206–7212, Sep. 2017, doi: 10.1021/acs.chemmater.7b01463.

[26] D. Chen, J. Yang, Y. Zhou, H. Xie, H. Zhang, and H. Lai, "Divalent-Doped Li1.3Al0.3Ti1.7(PO4)3 Ceramics with Enhanced Microwave Absorption Properties in the X-band," *J Electron Mater*, vol. 51, no. 5, pp. 2663–2672, May 2022, doi: 10.1007/s11664-022-09522-w.

[27] J. Zhang *et al.*, "Cross-linked nanohybrid polymer electrolytes with POSS cross-linker for solid-state lithium ion batteries," *Front Chem*, vol. 6, no. MAY, May 2018, doi: 10.3389/FCHEM.2018.00186.

[28] R. Pathak *et al.*, "Fluorinated hybrid solid-electrolyte-interphase for dendrite-free lithium deposition," *Nat Commun*, vol. 11, no. 1, Dec. 2020, doi: 10.1038/S41467-019-13774-2.

Chapter 6: Conclusions and Recommendations

6.1. Conclusion

NASICON Type Co/Si doped $Li_{1.3}Al_{0.3}Ti_{1.7}(PO_4)_3$ electrolyte material was successfully synthesized by ball milling assisted solid-state method. XRD patterns indicated the attainment of Rhombohedral structure in space group R-3c, while EDX results showed a slight increase in orthorhombic impurity phase $AlPO_4$ intensity as the concentration of cobalt increased, leading to a decrease in the concentration of Al. High resolution TEM confirmed the phases which were well aligned with the XRD results. XPS analysis demonstrated successful doping of cobalt and silicon, and the co-existence of all oxidation states in LATP. EIS analysis revealed that the doped electrolyte material $Li_{1.3+2x+y}Al_{0.3}Co_xTi_{1.7-x}Si_yP_{3-y}O_{12}$ achieved a higher total ionic conductivity of 5.45×10^{-5} S cm^{-1} at room temperature as compared to the undoped $Li_{1.3}Al_{0.3}Ti_{1.7}(PO_4)_3$. Optimal doping levels can provide a larger channel for the transportation of lithium ions, which can be attributed to the observed improvement in ionic conductivity This study offers a new approach for enhancing the ionic conductivity of LATP through doping, which can help improve the transportation properties and interface characteristics of NASICON solid electrolyte materials.

6.2. Recommendation

To enhance the electrochemical efficiency and performance of ASSLBs, it is suggested to investigate novel combinations of materials that can be used as electrolytes, alongside a careful selection of appropriate electrode materials. The following suggestions are proposed to overcome the limitations in current research on solid electrolyte materials:

- Attaining a high ionic conductivity is heavily reliant on the synthesis of pure LATP. It is advisable to opt for a synthesis route that can yield the purest form of LATP, without any notable impurities.

- Synthesis of hybrid solid-state electrolyte is one of the solutions to the problem of solid-state electrolytes. Hybrid electrolytes can be provide advantages of both liquid and solid-state electrolytes. Where a solid electrolyte is synthesized on which a thin layer of liquid electrolyte is deposited. This will enable the formation of solid electrolyte interphase (SEI) which will help in improving the stability of the solid electrolyte and still providing us with a safe and high energy density batteries.

- Conventional lithium-ion batteries utilize graphite as the anode material, while solid-state electrolytes have the potential to support the use of lithium metal anodes. Lithium metal anodes have a higher theoretical energy density compared to the graphite anodes used in traditional lithium-ion batteries. Therefore, the synthesis of a full cell with lithium as the anode has the potential to yield high energy density solid-state batteries.

Appendix: Publications

Investigation of the Effect of Cobalt and Silicon Co-Doping on the Structural and Electrochemical Properties of LATP Solid State Electrolytes

Hassaan Bin Shahid,[a] Khadija Nasir,[a] Haseeb Ahmed,[a] Ghulam Ali,[a,*]

[a]U.S.-Pakistan Center for Advanced Studies in Energy (USPCASE), National University of Sciences and Technology (NUST), H-12, Islamabad, 44000, Pakistan.

*Corresponding author: ali@uspcase.nust.edu.pk

Abstract

Solid-state electrolytes are a promising alternative to liquid electrolytes in lithium-ion batteries, as they have the potential to improve safety, energy density, and cyclic performance. Solid-state electrolyte can help overcome the challenges associated with traditional liquid electrolytes, thereby paving the way for high-performance batteries to be commercialized. The NASICON-type solid electrolyte $Li_{1.3}Al_{0.3}Ti_{1.7}P_3O_{12}$ (LATP) is a desirable option due to its high ionic conductivity, good stability, and remarkable air stability. In this study, we synthesized a co-doped LATP electrolyte by the solid-state method, with the dopants targeted on the Titanium and Phosphate sites respectively. We investigated the effect of cobalt and silicon on the phase composition, microstructure, and ionic conductivity of the LATP solid-state electrolyte. X-ray photon spectroscopy confirmed the doping of silicon and cobalt, with peaks showing Co in the +2 oxidation state and Silicon in the +4 oxidation state. X-ray diffraction revealed a highly crystalline structure. The optimal dopant content of cobalt and silicon offered an ionic conductivity of 5.45 x 10^{-5} Scm^{-1} at room temperature. These results suggest that an optimal doping of cobalt exhibits better ionic conductivity compared to pristine LATP.